Suspended Particulate Matter Formation And Accumulation In The Delta From Monitoring To Modelling

Safar, Z.

DOI
10.4233/uuid:17d027d9-9667-4afa-89b9-aacd557a41ac

Publication date
2022

Suspended Particulate Matter Formation and Accumulation In The Delta

From monitoring to Modelling

SUSPENDED PARTICULATE MATTER FORMATION AND ACCUMULATION IN THE DELTA

FROM MONITORING TO MODELLING

Proefschrift

ter verkrijging van de graad van doctor
aan de Technische Universiteit Delft,
op gezag van de Rector Magnificus Prof. dr.ir. T.H.J.J. van der Hagen,
voorzitter van het College voor Promoties,

door

Zeinab SAFAR

Delft University of Technology
Master of Science in Earth Sciences, Universiteit Utrecht, Nederland
geboren te Karbala, Irak.

Dit proefschrift is goedgekeurd door de

Promotor: prof. dr. J.D. Pietrzak
Promotor: dr. C. Chassagne

Samenstelling promotiecommissie:

Rector Magnificus,	voorzitter
Prof. dr. J.D. Pietrzak	Technische Universiteit Delft
Dr. C. Chassagne	Technische Universiteit Delft
Onafhankelijke leden:	
Prof. dr. P.M.J. Herman	Technische Universiteit Delft
Prof. dr. A.J. Manning	University of Plymouth, United Kingdom
Dr. M. Fettweis	Royal Belgian Institute of Natural Sciences
Dr. ir. T. van Kessel	Deltares
Prof. Q. He	East China Normal University
Prof. dr. ir. Z. B. Wang	Technische Universiteit Delft (reserve member)

Keywords: Flocculation, Sediment, Organic Matter

Printed by: Preofschrift maken - Utrecht

Front & Back: Beautiful picture of Rhine-ROFI taken during a survey.

ISBN 978-94-6366-579-7

An electronic version of this dissertation is available at
http://repository.tudelft.nl/.

To my lovely Mother

Radiyah Qassem Hassan

CONTENTS

SUMMARY

Modelling fine sediment transport in coastal areas (the Rhine-Meuse delta in particular) is important for dredging management in harbour areas, as well as for morphological and biological studies. Suspended sediments play an important role in terms of water quality, by transporting nutrients and pollutants, and are a key factor in light penetration. Large scale sediment transport models predict suspended sediment concentrations as a function of space and time. However, they do not properly account for particle-particle interactions. In this thesis, several aspects of sediment flocculation and transport are studied, which are connected to in situ monitoring, laboratory experimentation and modelling.

In Chapter 2, we show that the combination of multiple instruments used to visualize in situ suspended particles (LISST 100X, LISST-HOLO, video cameras) enables us to define three classes of particles based on organic matter content, rather than on particle size as is often done. Redefining classes is an important step towards proposing a new flocculation model. We confirm that the shape of the largest particles consisting of algae strains ($> 100\ \mu$m) has an influence on the particle size distribution found by LISST. This could lead to misinterpretations of the data. For further studies we therefore recommend to couple laser diffraction data (obtained from instruments such as LISST) to video microscopy data. This is at present possible, thanks to the technical improvement of underwater video cameras.

In Chapter 3, we describe the new flocculation model, based on logistic growth theory, which is used to study the characteristic timescales associated to flocculation. This is done by modeling the data, obtained by performing a series of laboratory studies, as a function of ionic strength, organic matter type and different organic matter/clay ratio. We show that Population Balance Equations that are currently in use to model flocculation is not the best model to be applied in the case of organic matter induced flocculation, which is the dominant type of flocculation observed in situ (Chapter 2). A logistic growth theory, like the one presented in this thesis is a better candidate as it has the advantage to be easy to implement in numerical models (it is not CPU demanding) and the parameters for the model can be obtained from series of laboratory experiments. The role of salt ions on the flocculation kinetics is highlighted thanks to the study: they promote the aggregation of organic matter to clay. Therefore the transition between fresh and saline water in the ROFI is an important driver for flocculation. From the results of Chapter 3, it was found that aggregation timescales are very short for laboratory conditions. It remains to be investigated whether these timescales are representative for in situ conditions.

In Chapter 4, an extensive in situ data analysis was performed based on data that was collected in the Rhine-ROFI region of the Dutch coast, at 12 meters depth, in the vicin-

ity of the Sand Engine. This data was collected in two different seasons (autumn and winter), and covered at least one spring-neap tidal cycle. The Particle Size Distribution (PSD) analysis shows that elongated algae rich particles were mainly present during strong stratification and low mixing conditions at neap tides especially during the autumn seasons. More spherical particles were present during the well mixed conditions of spring tides especially during the winter season. The presence of these rounder particles correlated with higher bed stress which indicate that they were resuspended from the bed. In contrast, the presence of elongated highly anisotropic particles correlated with low bed stress, indicating that these were advected particles. These organic matter-rich particles were most probably advected by the Rhine freshwater plume and it was found that their mean diameter correlated with the cross-shore velocity (the mean diameter is large when the velocity is onshore directed and vice versa). Two storm periods were captured during both seasons at neap tides. These storms shed light on the presence and dynamics of the 'fluff' layer found at the top of the bed during different seasons.

An existing numerical model that is often used to model sediment transport in Dutch coastal regions has been run for the time period of the monitoring and is described in Chapter 5. This model does not contain flocculation, each fraction is represented by a concentration distribution (in space and time) and constant settling velocity. The fractions have no interaction with each other. In particular, the finer fraction (with a settling velocity of about 0.01 mm/s), in the absence of aggregation, is evenly distributed through the water column. With the two classes proposed in this thesis, Class 1 being composed of mineral sediment and Class 2 of flocs (mineral sediment aggregated with organic matter), the concentration of the particles in each class depend strongly on the availability of organic matter which is a spatial and temporal, as well as seasonal variable. It is therefore proposed to have organic matter content implemented as an input parameter in the model. This organic matter can be measured in situ by recording for instance Chlorophyll-a concentration which is a proxy for algae concentration. Biochemical and ecological models also exist that could be used to define input parameters. Salt concentration should also be an input parameter as it enhances flocculation ability (Chapter 3). By flocculation with organic matter, the concentration of Class 1 particles will be decreasing, while the concentration of Class 2 particles (flocs) will be increasing. While the density of Class 1 particles is constant, the density of Class 2 particles is a function of shear and shear history. The settling velocity representative for Class 2 particles is therefore very dynamic in time and space. Discussion and recommendations for further research are given in Chapter 6.

SAMENVATTING

Het modelleren van fijn sedimenttransport in kustgebieden (met name de Rijn-Maasdelta) is van belang voor het baggerbeheer in havengebieden, maar ook voor morfologische en biologische studies. Gesuspendeerde (sediment) deelties spelen een belangrijke rol voor waterkwaliteit door het transport van nutrienten en verontreinigende stoffen. Ze zijn een sleutelfactor in het vermogen om licht door te laten. Grootschalige sedimenttransportmodellen voorspellen gesuspendeerde sedimentconcentraties als functie van ruimte en tijd. Ze houden echter niet goed rekening met interacties tussen deeltjes. In dit proefschrift worden verschillende aspecten van sedimentflocculatie en transport bestudeerd, die verband houden met in situ monitoring, laboratoriumexperimenten en modellering.

In Hoofdstuk 2 laten we zien dat de combinatie van meerdere instrumenten die worden gebruikt om in situ zwevende deeltjes te visualiseren (LISST 100X, LISST-HOLO, videocamera's) ons in staat stelt drie klassen van deeltjes te definiëren op basis van het gehalte aan organische stof, in plaats van de deeltjesgrootte zoals vaak wordt gedaan. Het herdefiniëren van klassen is een belangrijke stap in de richting van een nieuw flocculatiemodel. We bevestigen dat de vorm van de grootste deeltjes bestaande uit algencellen (> 100 μm) invloed heeft op de door LISST gevonden deeltjesgrootteverdeling. Dit kan leiden tot verkeerde interpretaties van de gemeten data. Voor verdere studies raden we daarom aan om laserdiffractiedata (verkregen van instrumenten zoals LISST) te koppelen aan videomicroscopiedata. Dit is momenteel mogelijk dankzij de technische verbetering van onderwatervideocamera's.

In Hoofdstuk 3 beschrijven we het nieuwe flocculatiemodel, gebaseerd op de 'Logistic Growth Theory', dat gebruikt wordt om de karakteristieke tijdschalen geassocieerd met flocculatie te bestuderen. Dit wordt gedaan door laboratoriumexperimenten te modelleren als functie van de ionsterkte, het type organische stof en verschillende organische stof/klei-verhoudingen. We laten zien dat 'Population Balance Equations' die momenteel worden gebruikt om flocculatie te modelleren, niet het beste presteren in het geval van door organische stof geïnduceerde flocculatie, wat het dominante type flocculatie is dat in situ wordt waargenomen (Hoofdstuk 2). Een 'Logistic Growth Theory', zoals gepresenteerd in dit proefschrift, is een betere kandidaat omdat deze het voordeel heeft dat het gemakkelijk te implementeren is in numerieke modellen (het is niet CPU-veeleisend) en de parameters voor het model kunnen worden verkregen uit een reeks laboratoriumexperimenten. De rol van zoutionen op de flocculatiekinetiek wordt benadrukt dankzij het onderzoek: ze bevorderen de aggregatie van organisch materiaal tot klei. Daarom speelt de overgang tussen zoet en zout water in de ROFI een belangrijke rol voor flocculatie.

In Hoofdstuk 4 is een uitgebreide in situ data-analyse uitgevoerd op basis van data die zijn verzameld in het Rijn-ROFI-gebied van de Nederlandse kust, op 12 meter diepte, in de buurt van de Zandmotor. Deze gegevens zijn verzameld in twee verschillende seizoenen (herfst en winter) en bestrijken ten minste één springtij-doodtij cyclus. De deeltjesgrootteanalyse laat zien dat langwerpige algenrijke deeltjes voornamelijk aanwezig waren tijdens sterke gelaagheid en lage mengcondities bij doodtij, vooral tijdens de herfstseizoenen. Meer bolvormige deeltjes waren aanwezig tijdens de goed gemengde omstandigheden van springtij, vooral tijdens het winterseizoen. De aanwezigheid van deze rondere deeltjes correleerde met hogere bedschuifspanning, wat erop wijst dat ze uit het bed waren geresuspendeerd. Daarentegen correleerde de aanwezigheid van langwerpige sterk anisotrope deeltjes met een lage bedschuifspanning, wat aangeeft dat dit advectiedeeltjes waren. Deze organische materiaal-rijke deeltjes werden hoogstwaarschijnlijk geadvecteerd door de Rijn-zoetwaterpluim en het bleek dat hun gemiddelde diameter correleerde met de cross-shore snelheid (de gemmidelde diameter is groter wanneer de getij in kustwaarde richting is en vice versa). Tijdens beide seizoenen werden bij doodtij twee stormperiodes vastgelegd. Deze stormen werpen licht op de aanwezigheid en dynamiek van de 'fluff' laag die tijdens verschillende seizoenen aan de bovenkant van het bed wordt aangetroffen.

Een bestaand numeriek model dat vaak wordt gebruikt om sedimenttransport in Nederlandse kustgebieden te voorspellen, is gebruikt voor de tijdsperiode van de monitoring, beschreven in Hoofdstuk 5. Dit model bevat geen flocculatie, elke deeltjes fractie wordt weergegeven door een concentratieverdeling (in de ruimte en tijd) en constante bezinkingssnelheid. De fracties hebben geen interactie met elkaar. Met name de fijnere fractie (met een bezinkingssnelheid van ongeveer 0,01 mm/s) wordt bij afwezigheid van aggregatie gelijkmatig over de waterkolom verdeeld. Met de twee klassen die in dit proefschrift worden voorgesteld, waarbij Klasse 1 bestaat uit mineraal sediment en Klasse 2 uit vlokken (mineraal sediment geaggregeerd met organisch materiaal), hangt de concentratie van de deeltjes in elke klasse van de beschikbaarheid van organisch materiaal af, wat een ruimtelijk en temporele, evenals seizoensvariabele valsnelheid geeft. Daarom wordt voorgesteld om het organischestofgehalte als invoerparameter in het model te implementeren. Deze organische stof kan in situ worden gemeten door bijvoorbeeld door chlorofyl-a-concentratie te registreren die een proxy is voor de algenconcentratie. Er bestaan ook biochemische en ecologische modellen die kunnen worden gebruikt om invoerparameters te definiëren. Zoutconcentratie zou ook een invoerparameter moeten zijn omdat zout het uitvlokkingsvermogen verbetert (Hoofdstuk 3). Door uitvlokking met organisch materiaal zal de concentratie van Klasse 1 deeltjes, die horen bij de kleinste maten, afnemen, terwijl de concentratie van Klasse 2 deeltjes (vlokken) zal toenemen. Terwijl de dichtheid van Klasse 1-deeltjes constant is, is de dichtheid van Klasse 2-deeltjes een functie van afschuiving en afschuifgeschiedenis. De bezinkingssnelheid die representatief is voor Klasse 2 deeltjes is daarom zeer dynamisch in tijd en ruimte. Discussie en aanbevelingen voor verder onderzoek worden gegeven in Hoofdstuk 6.

1

INTRODUCTION

1

1.1. CONTEXT

Coastal areas are subjected to major anthropogenic influences, as they are traditionally economically important regions, which is reflected by the presence of harbours, especially at river mouths. The Dutch coastal area is influenced by the discharge of fresh water from the Rhine river that creates the Rhine Region Of Freshwater Influence (Rhine -ROFI). There is also an additional sediment supply by alongshore transport resulting from seabed or coastal erosion.

Anthropogenic activities and climate change affect the sediment supply and flux by modifying the hydrological and sedimentation regimes, influencing the structure and function of the coastal wetlands [1, 2]. Harbour maintenance such as dredging activities cause changes in sediment dynamics which are of great influence on the benthic communities and coastal and estuarine habitats, that mainly depend on nutrient fluxes that are closely linked to sediment fluxes [3, 4].

In order to ensure safe navigation and economic viability of the ports, dredging works are performed routinely and are one of the major costs for port authorities. To optimize these costs, these authorities are investing in new in situ monitoring tools, as at present suspended or settled sediment layers of different densities are difficult to distinguish [5]. The results of the monitoring campaigns can also serve as validation for numerical models. The ultimate goal, shared by stakeholders and scientists alike, is to develop numerical models that enable prediction of the accumulation and transport of sediment in time and space in the ROFI regions.

ROFI's however, do extend far beyond the port areas. River plumes discharging into seas and oceans create brackish water bodies that overlay saline water. These plumes acts as conveyor belts for suspended particles that did not deposit in the river (harbour) area. The front of the river plume is visible at the sea surface from a surveying vessel and is characterized by a rather well-defined interface where fish and birds like to dwell in order to feed on the phytoplankton and other nutrients carried by the front [6].

The river plume influence extends tens of kilometers in the coastal area. For these zones as well, modelling sediment transport is of key importance, as the mouth of the river acts as a sink and source for the sediment within the harbour part of the ROFI. The accumulation or depletion of sediment also leads to morphological changes in shallow water areas (such as the Wadden Sea region in the Netherlands) and influences ecological life. Primary production is dependent on light penetration, which is a function of suspended sediment concentration, and mineral suspended particles acts as nutrient (and pollutant) carriers. The need for a robust sediment transport model therefore extends beyond dredging management interests.

1.2. HYDRODYNAMICS IN THE RHINE-ROFI

The transport of sediment is primarily driven by hydrodynamics. The hydrodynamics in ROFI's are complex. A good overview of the principle mechanisms of the river plume

discharge is given by [7]. The Dutch coastal area, which is the area of study of this thesis, is dominated by the region of Rhine and Meuse rivers freshwater influence. This freshwater is passing through the Rhine Delta estuary with an annual average discharge of 2500 $m^3 s^{-1}$ into the North Sea. This freshwater outflow is then directed to the right and northwards by Earth rotation (Coriolis) and maintains the Rhine Region Of Freshwater Influence (Rhine-ROFI) along the Dutch coast from Hoek van Holland to IJmuiden.

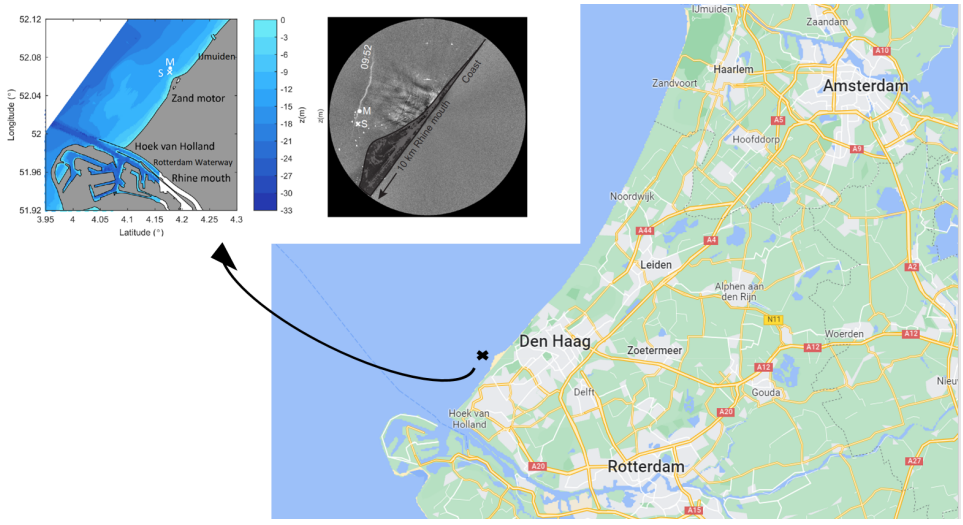

Figure 1.1: Map showing the study region, left: the location of the mooring (M) and the survey (S), Right: Radar image showing the front arrival at the mooring location.

The freshwater discharge input by the Rhine river is the driving force for both the water column stability and the dynamics and it influences the density field near the coast significantly [8–10]. This river discharge stays as a freshwater layer above the saline seawater that does not mix easily due to difference in density and creates a salinity based stratified water column [11]. Figure 1.1 shows a radar image of this freshwater layer, and highlights the precise study location.

The salinity difference between the layers can increase from 0.1 PSU (Practical Salinity Unit) to 4.0 PSU in the vertical direction. This is because a new freshwater tidal plume front can arrive while the previous one is still not fully mixed. This leads to a water column with water layers of different salinities. The surface freshwater layer has a typical depth of 2 to 5 m [11, 12]. This surface layer of low salinity flows along-shore during a short period around the high tide, whereas during a complete tidal cycle, the bottom layer is cross-shore directed, see Figure 1.2 upper panel [9, 12]. Salinity of this bottom layer is 28-30 PSU and it does not show large fluctuations over tidal periods nor does it vary much between periods of high and low discharge. This counter-directed surface and bottom layers are resulting in a cyclonic near bottom flow that is cross-shore di-

rected and an anti-cyclonic near surface flow that is directed off-shore, Figure 1.2 lower panel [9].

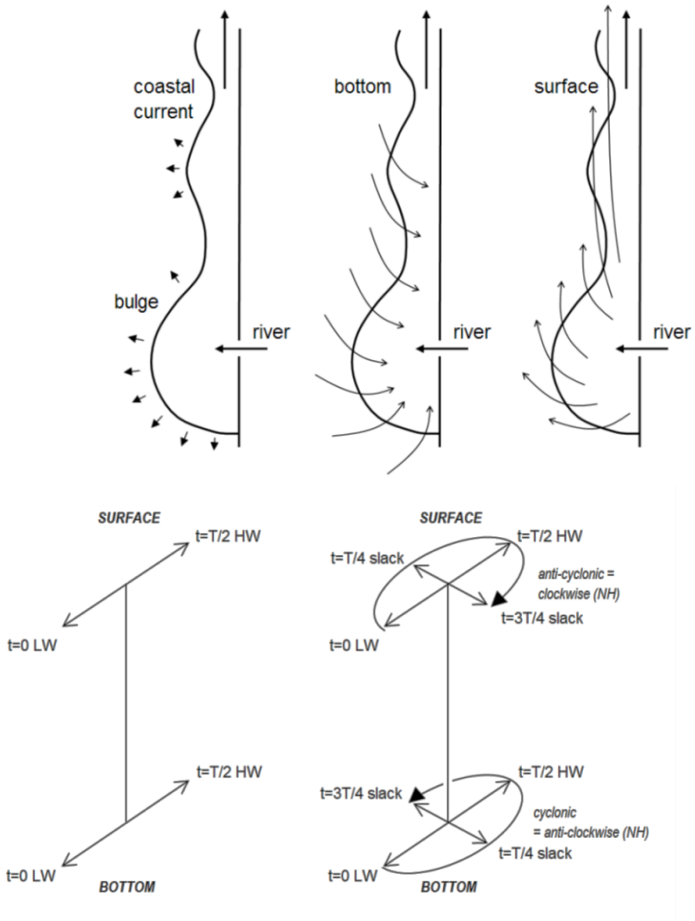

Figure 1.2: upper panel Left: Sketch defining river plume and the cross shore velocity component, taken from [13]. Lower panel: The vertical variation of horizontal tidal velocities in the Rhine-ROFI during the well mixed condition (left) and stratified condition (right), taken from [13].

River plumes are semi-diurnal tidal currents that stratify the water column. The cross shore density gradients compete with tidal/wind mixing to maintain the stratification, which acts on a short timescale (about 1 day). The long timescale is a function of neap-spring tidal cycle (about 14 days). The short term semi-diurnal stratification is causing also a semi-diurnal cross-shore velocity signal, which was identified as tidal straining by Simpson and Souza [14]. Tidal straining is the effect of differential advection by vertical velocity shear acting on a horizontal density gradient. In the Rhine- ROFI the tidal

straining consists of the episodic cross-shore velocity shear interacting with the average cross-shore density gradients [9, 14].

At longer times scales, on spring tides, long-shore tidal currents are found while on the neap tides significant cross-shore currents and tidal straining are dominant. The tidal straining results in temperature-related upwelling which has a significant influence on the local circulation and transport of nutrients and sediment through the water column every tidal cycle [9, 10, 15, 16].

During the neap tides the fronts stratify the water column for long periods, as tidal mixing is weak and turbulence is damped. Current induced bed stresses are too low to resuspend the bed material [17]. A schematic representation of the hydrodynamics during front arrival is given in Figure 1.3. During the spring tides, in contrast, the water column is mixed by tidal forcing and the front arrivals stratify the water column for shorter periods causing a near-bottom turbulent peak that can resuspend bed material [17]. During storm periods the water column is well-mixed, as illustrated in the right panel of Figure 1.3.

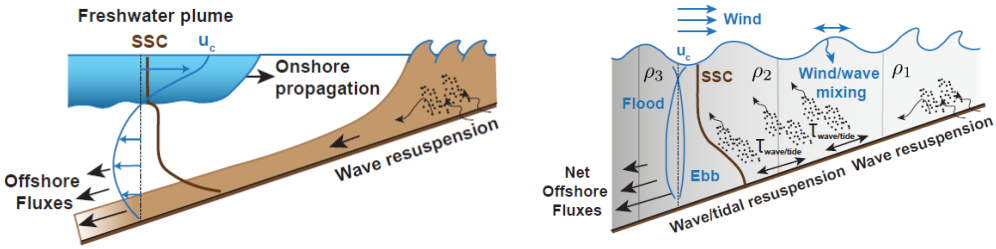

Figure 1.3: Schematic illustration of freshwater plume stratification (left panel) and storm mixing hydrodynamics (right panel). These illustrations were adapted from [17].

1.3. FINE SEDIMENT TRANSPORT MODELS

Fine sediment transport models have as output sediment concentration as function of space and time. These models make use of hydrodynamic models to compute the transport (advection and diffusion) of suspended matter in the water column. Quite often, the sediment is decomposed into a few fractions with an associated settling velocity. The models are calibrated using in-situ observations, whereby suspended mass concentrations are measured at given locations in time. The settling velocities are estimated from (bulk) in-situ observations. To give an order of magnitude, it is generally found that using 3 classes of particles, with settling velocities of the order of < 0.01 mm/s, 0.1 mm/s and > 1 mm/s enables to correctly predict the Suspended Particulate Matter (SPM) in space and time for a large number of situations in coastal areas [18–21]. However, changes in particle properties by flocculation and exposure to shear result in a change in settling velocity over time for a given sediment fraction. These changes are currently not ac-

counted for in sediment transport models and lead to erroneous predictions in coastal regions where these changes are triggered. Several studies have therefore concentrated on implementing flocculation in sediment transport models [22–25]. These models are however non-predictive as they contain adjustable parameters that are fitted to the data, and more importantly, they do not account for specific physical processes such as organic matter induced flocculation or the coiling of particles under shear.

The models used up to present to describe flocculation are based on so-called Population Balance Equation (PBE) models, whereby flocculation is represented by aggregation and break-up of similar colloidal particles, as in salt induced flocculation. Even though these models may mathematically capture the features of particle size evolution over time, it is doubtful whether they capture the key physical processes [26].

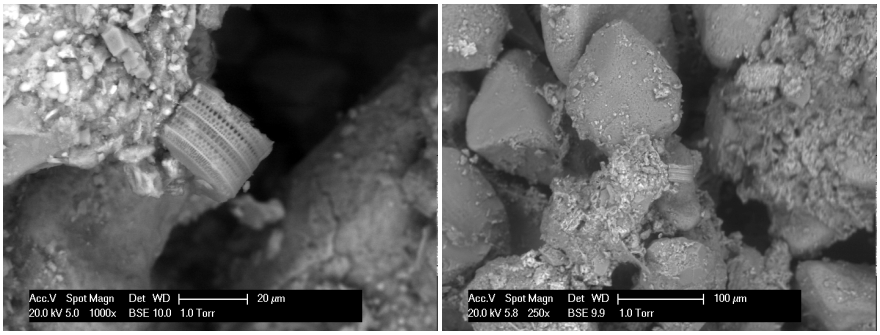

Figure 1.4: Right: Environmental Scanning Electron Microscope (ESEM) picture of a centric diatom attached to sediment. Left: the centric diatom enlarged.
These ESEM pictures are obtained from the analysis of grab samples at 18m depth in the Dutch coastal area of Rhine-ROFI.

INFLUENCE OF FLOCCULATION

The transition zone between fresh and saline waters is a scientifically interesting region to investigate, from sediment transport perspective. The change in suspending medium (the 'water') in terms of ionic strength and organic matter composition leads to changes in particle-particle interactions. The composition of the clay and silt size fractions can be quite heterogeneous and mixed with microorganisms that produce organic matter [27], as illustrated in Figure 1.4. This raises the question: how different is organic matter induced flocculation compared to salt induced flocculation? Does salt play a role in organic matter induced flocculation? How does the type of organic matter (microorganisms, Extra-Polymeric Substances) influence flocculation?

Flocculation is greatly promoted in saline environment, and sediment particles are thereby more prone to flocculate in coastal regions, leading to different transport, settling, deposition and erosion dynamics as compared to freshwater conditions. The exposure to different shearing condition over time alters the suspended particle structure. It has been shown that in general the floc size is inversely proportional to shear stress [28, 29].

Salinity stratification forms a halocline between the fresh and saline water which are of different density. At slack water, the production of large flocs is enhanced [30, 31]. The SPM transported with the freshwater can be temporally trapped above the halocline, where they can flocculate and settle by gravity [32–36]. As the stratification damps the turbulence [32–36], it favours differential settling resulting in formation of elongated particles, especially in the presence of algae cells.

After deposition on the sea floor, the accumulated flocs form a 'fluff' layer with time-dependent properties, as the organic matter contained in the fluff will degrade over time. This leads to changes in the physical characteristics of the bed, such as its density and cohesiveness, which are linked to its erosion properties. The role of organic matter in bed erosion is an on-going research topic [37–39].

1.4. SPM FORMATION AND DYNAMICS

Suspended Particulate Matter (SPM) is defined as a suspension of microscopic particles consisting of clay minerals (sediment) aggregated or not with organic matter. Aggregated particles (flocs) are composed of different fractions of inorganic and organic parts. The inorganic part consists of clay minerals, non-clay minerals such as (hydro)oxides, carbonates or phosphate, salt ions and the organic part contains microbial cells, organic detritus and Exo-Polymeric Substances (EPS) with pore space [40]. The pore space is filled with either water or gas. SPM accumulates in coastal areas where freshwater runoff from rivers meets the sea, passing through deltas and estuaries. This suspended matter can be of fluvial or coastal origin [41, 42].

River plumes that pass the estuaries reaching the coastal areas play an important role in terms of SPM formation and transport, especially in ROFI regions. These systems enhance the aggregation probability at slack water resulting in production of large flocs [32, 35]. The water composition plays a key role in the formation of flocs. Aggregation is for instance promoted by the presence of cations in the water column [28] and the presence of polymeric substances [43]. This is the reason why flocculation and consequently deposition of sediment (siltation) is likely to occur in delta regions where fresh and salt water meet. Additionally, delta regions are rich in biogenic organic matter, where microorganisms (bacteria and microbial cells, see Figure 1.4) can find light and nutrients. These organisms enrich the delta regions with organic matter that acts as flocculation agent due to its high stickiness [44–46, 46–49].

Hydrodynamic conditions are also of prime importance to understand the flocculation dynamics. On one hand hydrodynamics can enhance the formation of aggregates by mixing, hereby promoting the flocculation process [42, 44, 50–54]. On the other hand, flocs can be disrupted by hydrodynamic shearing [55–58]. In addition, hydrodynamic conditions are responsible for resuspension of sediments and flocs deposited at the bottom, where they form a so-called 'fluff' layer during hydrodynamically calm conditions.

1

1.5. IN SITU MONITORING

Most sediment transport models are calibrated using in situ data, based on particle concentration and particle size measurements. From these measurements, the mean density of particles is estimated and their settling is deduced using Stokes' law. The characteristic timescales for in situ flocculation are unknown, as only video microscopy can without ambiguity enable quantification of particle-particle aggregation.

Video microscopy is currently limited in use and cannot track particles smaller than 10 μm. The reason is associated with particle scattering and field of view. The most common in situ particle size measurement devices are based on laser diffraction techniques, of which LISST (Laser In situ Scattering and Transmissometry) is an example. The LISST 100X used in this study measures particle size in the range of 2.5-500 μm [59, 60]. In addition the digital holographic method of LISST-HOLO (Submersible Digital Holographic Camera), also used in this study, is becoming a widely used technique that provides both particle size and 2D images of SPM captured by the holographic camera. However these techniques have their limitations [61]. The suspended sediment concentration and the corresponding particle size distribution measured by LISST 100X for instance, is influenced by the so called 'schlieren' effect [62–64]. 'Schlieren' can cause a peak to appear in the measured spectrum that is not attributed to the particles, but is caused by salinity stratification in the water column. The data affected by this effect can however be discarded by comparing the particle concentration from the LISST data with Optical Back Scatter (OBS) data, which is a technique not sensitive to schlieren. A greater problem associated with the LISST 100X data is caused by the shape of particles. Non-spherical large particles particles lead to non-trustworthy Particle Size Distribution (PSD), as the instrument software which converts raw data in PSD's is based on the assumption of spherical particles with a given density [65, 66]. For instance in the presence of phytoplanktonic particles, the LISST 100X shows an extra peak caused by the shape of the species [67].

Due to these limitations the LISST 100X data cannot be used alone and it needs to be compared with additional measurements performed by OBS or ADCP (Acoustic Doppler Current Profiler) [68, 69], LISST-HOLO [66, 70] and underwater camera system [71]. The advantage of LISST 100X however, is that it enables to detect clay particles < 10 μm, a range which is not accessible to camera. As particles within this range are usually mainly solid minerals with known densities and reasonably spherical shapes, it is expected that the PSD's estimated by LISST in the 2.5-10 μm range are accurate.

LABORATORY STUDIES

Numerous laboratory studies have focused on flocculation of interest for sanitary engineering purposes, where dewatering of slurries is a key issue [72–74]. At present, a small number of laboratory studies are performed in the context of mimicking in situ SPM flocculation dynamics [28, 75, 76]. However, all these studies have demonstrated their added value to in situ monitoring. System investigation in the laboratory enables to understand key processes, such as the role of shear in flocculation dynamics [29, 77], the characteristics of salt induced flocculation [28] or the influence of organic matter type

and concentration [29, 43].

It has recently been demonstrated that combining in situ monitoring and laboratory work can help to study the limiting factors in algae mineral sediment flocculation [78]. Moreover, laboratory flocculation studies have the great advantages to enable the study of a confined sample, where sediment sink and source are not present, and the sediment concentration is constant over time. This can be of great help where the calibration of numerical models is concerned.

1.6. RESEARCH OBJECTIVES AND THESIS OUTLINE

The general aim of this thesis is to present a flocculation model that properly predicts SPM formation by flocculation in space and time that can easily be implemented in numerical sediment transport models. The model could then be parameterized with laboratory experiments. Ideally, such a model should capture the essential physico-biochemical processes occurring in the case of organic matter-induced flocculation, but clearly these processes are complex and cannot be properly assessed, even in laboratory conditions (for example it is impossible to control and monitor the production of EPS by living algae in a flocculation experiment).

It was therefore decided that a more pragmatic approach would be used that is also used in the description of biological systems which are similarly complex. The chosen model is based on logistic growth theory, which was originally meant to describe the time evolution of the population of Belgium [79]. It has been successfully used to mimic auto-catalysis rate in chemical reactions [80] or growth rate of bacteria [81]. The model should be adapted to reflect the behavior of the in situ particles. A first step is therefore to identify these particles and ensure that their properties are well assessed. The first research questions to be answered are hence:

1. What are the types of particles that are found in situ (in the Rhine ROFI)? what are their properties (size, effective density, shape/ composition and settling velocity)?

2. How do particle shape and composition affect light scattering measurements? How reliable is the obtained in-situ data?

These questions are addressed in Chapter 2. To answer them, the data obtained from a one-day boat survey with multiple instruments (LISST,LISST-HOLO, LabsFloc camera and underwater camera) is analysed and interpreted. Subsequently, the observed SPM is divided in classes based on their size, effective density and composition. This classification is used for Chapter 3 where the new model, based on logistic growth theory is presented. The results of laboratory experiments are analysed in order to answer the third research question:

3. What are the flocculation timescales and how are these associated with different flocculation mechanisms?

Experiments where conducted to investigate the interactions between clay minerals, algae and natural organic matter in detail. The experiments were performed under controlled conditions to achieve optimum flocculation which enable to find the required characteristic timescales for flocculation.

The laboratory experiments were performed for constant conditions (constant shear and constant sediment concentration). The temporal and spatial distribution of SPM is addressed in Chapter 4, where two data sets obtained from monitoring campaigns called STRAINS I and STRAINS II were analysed. This data consists of Particle Size Distribution (PSD) measured by LISST 100X and LISST-HOLO in winter 2013 and autumn 2014 respectively. In this Chapter correlations between the SPM particle size and the hydrodynamics and salinity stratification are given. Hypothesis about the origin of SPM in terms of advection and resuspension during the neap and spring tidal cycles are discussed for both seasons. The research questions addressed in Chapter 4 are:

4. How do the SPM concentration and size correlate with water column hydrodynamic conditions (when are they advected, and when resuspended)?

5. How do the seasonal changes in hydrodynamics and organic matter availability determine the composition and shape of the SPM particles and fluff layer development and depletion?

In Chapter 5 of this thesis, the in situ data is compared to the data obtained from the numerical sediment transport model Delft3D. The Suspended Sediment Concentration (SSC) at the measurement location was calculated with the so called ZUNO-DD model, which does not include flocculation [82, 83]. A detailed analysis of particle structure in correlation with the hydrodynamics is performed, based on the long timescale in situ measurements, studied in Chapter 4 and the laboratory studies presented in Chapter 3. From this analysis and the comparison between the model data and in situ data, a conceptual model is developed and presented in this chapter. This model is discussed in terms of mass transfer between classes. In this chapter, the following research questions are addressed:

6. What are the main features of a flocculation model that could be implemented in sediment transport models?

In the last chapter (Chapter 6) the main findings and conclusions are summarized, and some recommendations for further work are proposed.

2

CHARACTERIZATION AND CLASSIFICATION OF SUSPENDED PARTICULATE MATTER (SPM) PARTICLES BASED ON SIZE AND COMPOSITION

Measurements were conducted during a 13h survey in the Rhine region of Freshwater Influence (Rhine-ROFI) about 10 km downstream of the mouth of the Rotterdam Waterway. This data set is used to analyze the characteristics of suspended particulate matter (SPM) near the seabed during a full tidal cycle, at neap tide, during calm weather conditions. Characterization of SPM is important for understanding SPM dynamics in longer time series. Therefore, several optical techniques were used in combination to analyse the SPM particles properties in detail and categorize them in classes. A large range of settling velocities (0.1 - 10 mm/s) and aspect ratios between 1 and 10 were recorded by video microscopy (LabSFLOC-2) in quiescent water for samples taken during the survey period. This spreading in settling velocities and aspect ratio is due to the different nature of the particles in the water column, as identified from the underwater video recording and LISST-HOLO. Some particles were bare algae particles, which are thin, very elongated particles whereas others were sediment-algae flocs in different states of coiling. We identify different types of particles: mineral sediment based particles in the range size 5 - 10 µm, small aggregates and algae 20 - 50 µm, organic and inorganic aggregates 50 - 350 µm and chain like algae of equivalent diameter 100 - 500 µm from which three classes are defined, based on composition (inorganic sediment, inorganic-organic flocs, organic particles). In addition flocculation laboratory experiments were conducted with natural sediment obtained from Port of Rotterdam harbour and living algae. The results of these experiments show a shift in effective density and clustering in particle size upon addition of living algae to the natural sediment, which confirm the flocculation ability between sediment and algae.

This chapter is submitted to *Frontiers in Marine Science, section Coastal Ocean Processes* and is under review.

Coastal waters are nutrient-rich and suitable environments for microorganisms such as diatoms, bacteria, dinoflagellates, phytoplankton and zoo-plankton [42, 50, 84–87]. These microorganisms are important in the formation of aggregates (flocs); they influence floc characteristics, such as size, shape, density and settling velocity, by colonizing and growing on the nutrient-rich sediment particles [48].

A wide variety of diatoms, dinoflagellates and flagellates are found in the Dutch coastal area of the North Sea. Most abundant are *Skeletonema Costatum, Rhizosolenia delicatula, Chaetoceros* and *Paralia* [88–90]. These diatoms and other biological species generally present in the water column, along with corresponding organic matter, influence the Suspended Particulate Matter (SPM) properties by flocculating with clay mineral particles. This produces different types of aggregates that have a dynamic size, density and settling velocity [30, 91, 92]. The floc properties are also depending on other elements present in the water column, such as salinity [35], pH [77], and hydrodynamic shear [55].

The floc history (in which conditions the floc was formed and which shear stress it did experience) is an equally important parameter that determines floc structure and composition. Therefore in order to study flocs dynamics, floc properties and dependency on the environmental conditions need to be analysed.

A previous study has shown that in the Rhine freshwater plume, at the top of the water column, the SPM concentration, in terms of clay minerals, is much lower than in the ambient coastal water during stratified water column conditions with calm weather at neap tides [93]. However, algal species and organic debris, i.e. organic particles can be advected by the freshwater plume which is of great influence on the SPM particles properties as they can lead to flocculation [84, 94, 95]. The near-bottom water flow transports (in)organic matter and microorganisms and is a driving mechanism for sediment transport along many coasts, where both advection and resuspension occur [96].

The aim of this chapter is to study the properties of particles in the Rhine ROFI (size, shape,composition, density and settling velocity) and categorize those particles accordingly. Samples were taken during a 13 hour boat survey, measurements on SPM characteristics were performed capturing a complete tidal cycle. This field survey is part of a large field campaign that was conducted in September-October 2014 in the mid-field region of the Rhine ROFI [17], close to the Sand Engine [97]. A mooring and two frames were deployed at 12 m depth as part of the Stratification Impact on Near-shore Sediment Transport (STRAINS II) experiment [17, 98, 99].

A one day field-survey has been devoted to study the SPM in the near bed part of the water column. Several in situ instruments, based on optical techniques, have been used simultaneously during this one day boat survey in the Rhine-ROFI to perform this analysis. These instruments are: LISST 100X (Laser In Situ Scattering and Transmissometry), which is based on laser scattering and estimates particle size in the range of 2.5 - 500 μm; LISST-HOLO (Submersible Digital Holographic Camera), which provides both particle size and 2D images of SPM; an underwater camera; and an onboard camera

(LabSFLOC-2) which provides both Particle Size Distribution (PSD), aspect ratio and settling velocities of particles in quiescent water. Both LISST 100X and LISST-HOLO were part of a mooring that had been placed in the vicinity of the survey vessel, while the underwater camera and LabSFLOC-2 were used in water and on board respectively during the boat survey.

The use of underwater cameras was long limited to size analysis of objects larger than hundreds of microns [76, 100]. Due to the latest development in camera specifications, it is nowadays possible to use underwater cameras with a much better resolution and light sensitivity [101–103], which enables to assess particles larger than 10 μm and estimate particle densities based on grey-scale analysis.

Combining the particle size distribution obtained from the LISST 100X and LISST-HOLO with the data from LabSFLOC-2 camera system and underwater camera, the types and properties of particles in the Rhine ROFI are identified. Additional laboratory experiments were conducted to study the interactions between the microorganisms (algae) and sediment in more detail, under controlled conditions for optimal flocculation.

2.1. MATERIALS AND METHODS

2.1.1. MOORING

In the present study, the LISST 100X and LISST-HOLO data of the mooring was used, in addition to the survey data. The mooring was located in the coast 10 km from the Rhine mouth and at 2 km distance from the coastline in the vicinity of Sand Engine were the water depth is 12m (see Figure 1.2). All times are referenced to GMT.

LISST 100X

LISST 100X uses laser diffraction to determine the volume concentrations of particles in 32 logarithmically spaced effective spherical diameter classes (PSD) ranging for the 100X type from 2.7 to 460 μm [59, 60]. The LISST 100X was placed on the bottom frame, 1.65 m above the bed (mab) on the frame, and measurements were taken every 10 seconds. The data was averaged on 10 minutes bursts.

LISST-HOLO

LISST- HOLO is an in situ digital holographic technology that uses solid state diode laser at 658 nm and 4.4 μm pixel size digital camera (1600 × 1200 pixels). It measures equivalent spherical diameters in the size range of 25- 2500 μm, within 50 log spaced size classes. The LISST- HOLO was placed at 1.40 mab on the frame and took a picture every 5 minutes.

The LISST - HOLO software was tuned to find the most appropriate values for *clean stack* and *threshold* parameters [66]. *Clean Stack* 3 and default *threshold* of 0.15 was found to give the most clear pictures and was used to process the raw data [104]. The density of the particles can be estimated from the calculated *solidity* by the LISST- HOLO software. The *solidity* is defined as the solid fraction of a given particle, and can be related to the

porosity of that particle [105]. A fully solid particle will have a *solidity* of 1, whereas a *solidity* close to 0 will indicate a very porous particle. The *solidity* is obtained by dividing the black area ($A_B = N \times r^2$ where r^2 is the area of a black pixel and N the number of black pixels within a particle) of a particle by the total area (A) of that particle. We assume that the volume of the particle is given by $V = A \times c$, where c is the dimension of the particle perpendicular to the field of view of the camera, and $V_B = A_B \times c$ is the volume of the black area. Assuming that the particles properties do not change along the direction indicated by c, we can express *solidity* as function of the volume of the particle by:

$$S = \frac{A_B \times c}{A \times c} = \frac{V_B}{V} \tag{2.1}$$

The density ρ_p of a particle is given by:

$$\rho_p = \rho_s \frac{V_B}{V} + \frac{(V - V_B)}{V} \rho_w \tag{2.2}$$

where ρ_s is the absolute density of the solid part and ρ_w is the absolute density of water (that fills the voids). It is assumed that no air is trapped in the flocs. From this we can deduce that the effective density of a floc $\rho_e = \rho_p - \rho_w$ is given by:

$$\rho_e = (\rho_s - \rho_w) S \tag{2.3}$$

The density of the solid fraction ρ_s (represented by black pixels) is at this stage unknown. For mineral sediment flocs it can be expected to be close to 2600 $kg.m^{-3}$ and for organic rich particles, it is expected to be much lower (1016-1600 $kg.m^{-3}$). Note that the assumption that the particle's properties do not change along the direction indicated by c can lead to erroneous estimations.

2.1.2. FIELD SURVEY

The survey was performed in the proximity of the 12 m mooring on the 17^{th} of September 2014. The study was carried out from the research vessel Navicula during a full tidal cycle. The measurement day was chosen such that, the hydrodynamic conditions were energetically low to ensure that particles mostly settle by gravity and re-suspension would not play a major role in the observation of SPM during this tidal cycle [17]. During the 13 hours survey (6:00 - 17:00 GMT), 26 water samples were taken with a van Dorn sampler at 0.6 meters above bed (mab), every 1/2 hour, in vicinity of the mooring.

CTD

CTD measurements were performed during the boat survey. Every 1/2 hour a CTD cast was made to measure the salinity profile and determine the water column stratification state.

LABSFLOC-2 SETTLING COLUMN CAMERA SYSTEM

The water samples were taken at 0.6 mab depth and were analysed using the (INSSEV_LF) LabSFLOC-2 camera system (Laboratory Spectral Flocculation Characteristics, version 2) that recorded the settling velocity of particles from a pipetted amount of sample.

The particle size, shape and effective density were estimated from the settling velocity [106–108].

LabSFLOC-2, see Figure 2.1 was developed by Manning et al. [107, 109, 110], and it utilizes a high magnification 2.0 MP Grasshopper monochrome digital video camera [110] to observe individual flocs as they settle in a 350 mm high by 100 mm square Perspex settling column. The video camera, positioned nominally 75 mm above the base of the column, views all particles in the center of the column that pass within a 1 mm depth of field, 45 mm from the Sill TZM 1560 Telecentric (maximum pixel distortion of 0.6%), 0.66 (1:1.5) magnification, F4, macro lens fitted behind a 5 mm thick glass face-plate.

During sampling, a modified pipette is used to carefully extract a floc sub-sample from the Van Dorn chamber and is filled to produce a fluid head of 50 mm, which results in a video image control sample volume nominally of 400 mm^3 (1 mm image depth and 8 mm nominal video image width, with a nominal 50 mm high suspension extracted with a modified pipette). This controlled volume permits in principle LabSFLOC-2 calculated floc mass to be compared and calibrated directly to ambient SSC. The pipette sub-sample is immediately transferred to the LabSFLOC-2 settling chamber, whereby the aperture of the pipette was brought into contact with the LabSFLOC-2 settling column water surface and permitted the flocs to pass from the vertically held pipette to the chamber and settle solely under gravity, i.e. naturally and unassisted. Thus, the flocs allowed to pass into the settling column were naturally segregated as they fell by the process of differential settling; i.e. the fastest falling aggregates would be observed first.

Settling flocs are viewed as silhouettes (to reduce image smearing) resulting from a CCS LDL-TP-43/35-BL, 43 x 35 mm, homogeneous blue (470 nm) back-illumination LED panel, located at the rear of the settling column. The video images are streamed in real time as AVI files to a laptop PC via a FireWire-B PCI card interface. The digital floc images are captured at a frame rate of 7.5 Hz (one frame is 0.04 s), at a resolution of 1600 × 1200 pixels, with an individual pixel nominally representing 5 μm (confirmed by independent calibration). The AVI files are not Codec compressed, so they could be analysed with MatLab software routines. During post-processing, the HR Wallingford Ltd DigiFloc software - version 1.0 [107, 109], is then used to semi-automatically process the digital recordings to obtain floc size and settling velocity spectra.

The sphere-equivalent floc diameter, D, was calculated by measuring both major-axis and minor-axis of each observed two-dimensional floc image [111]:

$$D = (D_{major} \times D_{minor})^{0.5} \tag{2.4}$$

Each floc settling velocity was determined by measuring the vertical distance that the floc travels between a sequence of frames. Stokes' law then enables an estimation of individual floc effective density [111],

$$\rho_e = \rho_p - \rho_w = \frac{18 W_s \mu}{g D^2} \tag{2.5}$$

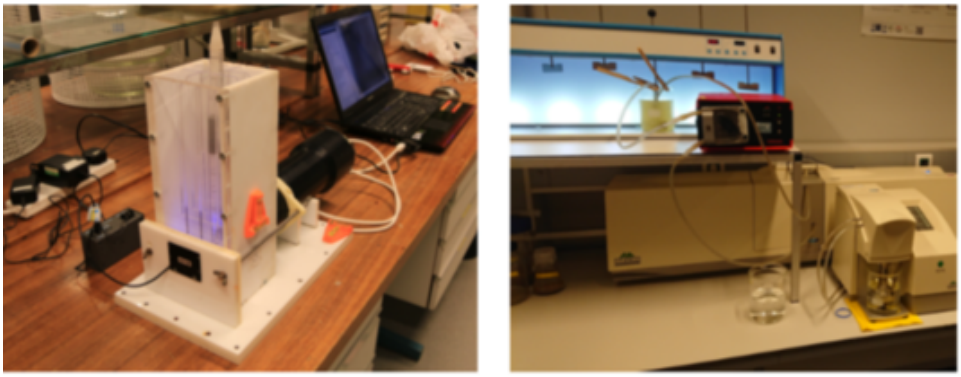

Figure 2.1: Malvern MasterSizer 2000 instrument (right) and LabSFLOC-2 settling column (left). Pictures were taken at the Deltares laboratory

where W_s is the settling velocity, μ is the water viscosity, g is the gravitational acceleration, and D is the particle diameter.

UNDERWATER VIDEO CAMERA:

In addition to the LabSFLOC-2 system, a video camera mounted under the Van Dorn sampler (Figure 2.2 a and b) was lowered at the sampling time, to take videos of the particles at the sample location. This was an Imaging source GigE color camera, I/O Aptina CMOS MT9P031, with a maximum resolution of 2592 × 1944. The pixel size is $2\mu m \times 2\mu m$.

The use of underwater cameras was long limited to size analysis of objects larger than hundreds of microns [76, 100]. Due to the latest development in camera specifications, it is nowadays possible to use underwater cameras with a much better resolution and light sensitivity [101–103], which enables to assess particles larger than 10 μm.
The video's taken with the underwater camera were used for qualitative analysis of the flocs and not for quantitative size analysis. The size analysis was done with the LISST 100X, LISST-HOLO and LabSFLOC-2 system.

2.1.3. WEATHER CONDITIONS AND HYDRODYNAMICS

The 17^{th} of September 2014, was a calm weather day during neap tide. The tidal elevation at Hoek van Holland was between 0.85 m and -0.62 m, and the wind speed stayed below 6 m/s coming from the east. In addition, the significant wave height was below 0.5 m, which was retrieved from a wave rider buoy 1 km south from the survey site. The total river discharge from the Rhine and Meuse River was about 1500 m^3/s, for that day.

Figure 2.2: a) The underwater camera, mounted under the van Dorn sampler, b) The set-up is lowered into the water, c) The Seabird CTD

The boat survey started at flood tide, before the flood peak. The water column was weakly stratified with a salinity difference of 2 PSU (Practical Salinity Unit) between surface and bottom. The water column was however divided into different salinity layers after a front arrival 2 hours later. The stratification prevailed almost the whole day as it was a neap tide day with low energetic mixing conditions. Note that the salinity close to the bottom remained close to 30 PSU.

2.1.4. LABORATORY MEASUREMENTS

Based on the observed field results, additional laboratory experiments were conducted to produce flocs of different composition and analyse the impact of composition on their temporal evolution.

SEDIMENT

The experiments were conducted with sediment taken from the Port of Rotterdam (PoR). The dry weight was 33.2 % - 34.2 % as assessed by the provider (Port of Rotterdam) and the mineralogical composition of this sediments are summarized in table 2.1. In each jar test 7 grams of this untreated sediment was diluted, which results in a end concentration of 0.2 g/L in the Jar. Seawater (sieved through a 5 μm filter) was used as suspending medium.

ALGAE

The algae *Skeletonema Costatum* was chosen in the study, as being one of the most predominant algae species in the coastal area [88]. The algae was obtained from the hatchery Roem van Yerseke B.V. The concentration of the algae stock suspension was about

5.10^6 cells/mL and was kept in dark to avoid photosynthesis and change in concentration. The algae suspension was refreshed every two weeks to ensure that the concentration used in the experiments was constant.

Table 2.1: Mineralogy of PoR sediment used in the laboratory experiments

Mineral	**% Weight content**
Quartz	26.8
Alkali Feldspar	3.4
Plagioclase	3.5
Illite	21.1
Chlorite	2.4
Dioctahedral Smectite	20.2
Interstratified Illite/ Semctite Reichweite	50.4
Carbonates	**% Weight content**
Calcite	14.5
Mg-Calcite	4.1
Aragonite	2.2
Dolomite	0.3
Ankerite	0.8

PARTICLE SIZE MEASUREMENTS

The Particle Size Distribution (PSD) of samples were obtained by Static Light Scattering (SLS) using a Malvern masterSizer 2000 which provides a full PSD every 30 s. The size range of the SLS device is 0.01-2000 μm in 100 logarithmic-spaced bins. The samples are stirred in a 1L-jar at constant rate of 35 rpm (30 s^{-1}), and pumped through pipes to and from the SLS device at constant rate of 10 rpm (about 12 s^{-1}). The set-up is the same as the one used by Ibanez et al. [43]. The shear rates used are usually higher than those observed in the field (which are of the order of 0-10 s^{-1}), especially at neap. However, these rates were determined in preliminary experiments to ensure a minimal breakage of the aggregated fractions and avoid settling in the pipes. When the steady state size was reached for a given algae concentration, the concentration of the algae was adjusted to a higher content. The percentage of algae content was increased in steps to reach concentration 5, 20 and 30 volume %. This percentage corresponds to volumes taken from stock suspension divided by the total volume in the jar. At steady state, some subsamples have been pipetted and studied with the LabSFLOC-2 camera system that was mounted in the laboratory. The description of the LabSFLOC-2 camera system is given in section 2.1.2. In order to obtain a good signal to noise ratio by SLS we used sediment and algae concentrations that are 100 times more concentrated than the ones observed in situ during our one-day survey. The algae to clay ratio is however the same. The time scale of aggregation will of course be different.

2.2. RESULTS AND DISCUSSION

The SPM was studied using two camera systems, the underwater camera and the LabSFLOC-2 camera, on-board during the survey. With these instruments, and the photos obtained from the LISST- HOLO, the shape and settling velocity of the SPM particles could be recorded and their density estimated. The low energetic conditions (neap tide) during the campaign day led to the presence of very anisotropic particles in the water column and low SPM concentrations, which makes the interpretation of the in situ data with respect to particle size distribution challenging. Studying the particles characteristics during these conditions is however interesting because at higher energetic conditions, mineral sediment particles dominate the PSD. This does not allow the study of organic matter-based particles which have typically a low concentration but play an important role in the flocculation and resuspension processes.

FLOC SIZE, SETTLING VELOCITY AND SHAPE

From the underwater camera records and the LISST-HOLO pictures, different types of particles could be identified, as shown in Figures 2.3 and 2.4. The floc structure depends on the Organic Matter (OM), present in the water column, which is a temporal and spatial variable [39, 112–114]. This OM can be composed of living or dead microorganisms (algae, bacteria) or exo-polymers, secreted by these organisms. As these particles can have variety of shapes, aspect ratio can be used to obtain an estimation of the shape. Aspect ratio provides information about the anisotropy of particles and seems to be a suitable parameter to differentiate between algae like *Skeletonema Costatum*, which are known to form elongated strings and other particles. [115, 116].

Based on the LabSFLOC-2 measurements and the underwater camera snapshots, the particles are divided into three major types. One type corresponds to (mineral) sediment-rich flocs, having an effective density close to 1600 kg/m^3 with settling velocity of 1 - 10 mm/s. These particles have compact form and dark color (high density). An other particle type corresponds to algae-rich particles having an effective density between 16 - 160 kg/m^3 with a settling velocity of 0.1 - 1 mm/s. These particles display an open or anisotropic structure and have a lighter color (low density). They are likely composed of inorganic and organic particles such as Transparent Exopolymer Particles (TEP) [117, 118]. For some of these flocs, the elongated algae structure is still recognizable, although the algae is coated with (in)organic debris and can be in some state of coiling (Figures 2.3 and 2.4). The third type corresponds to bare algae, or algae bound to very little amount of sediment, which have a very low density of about 16 kg/m^3 with low settling velocity, mostly around 0.1 - 0.5 mm/s.

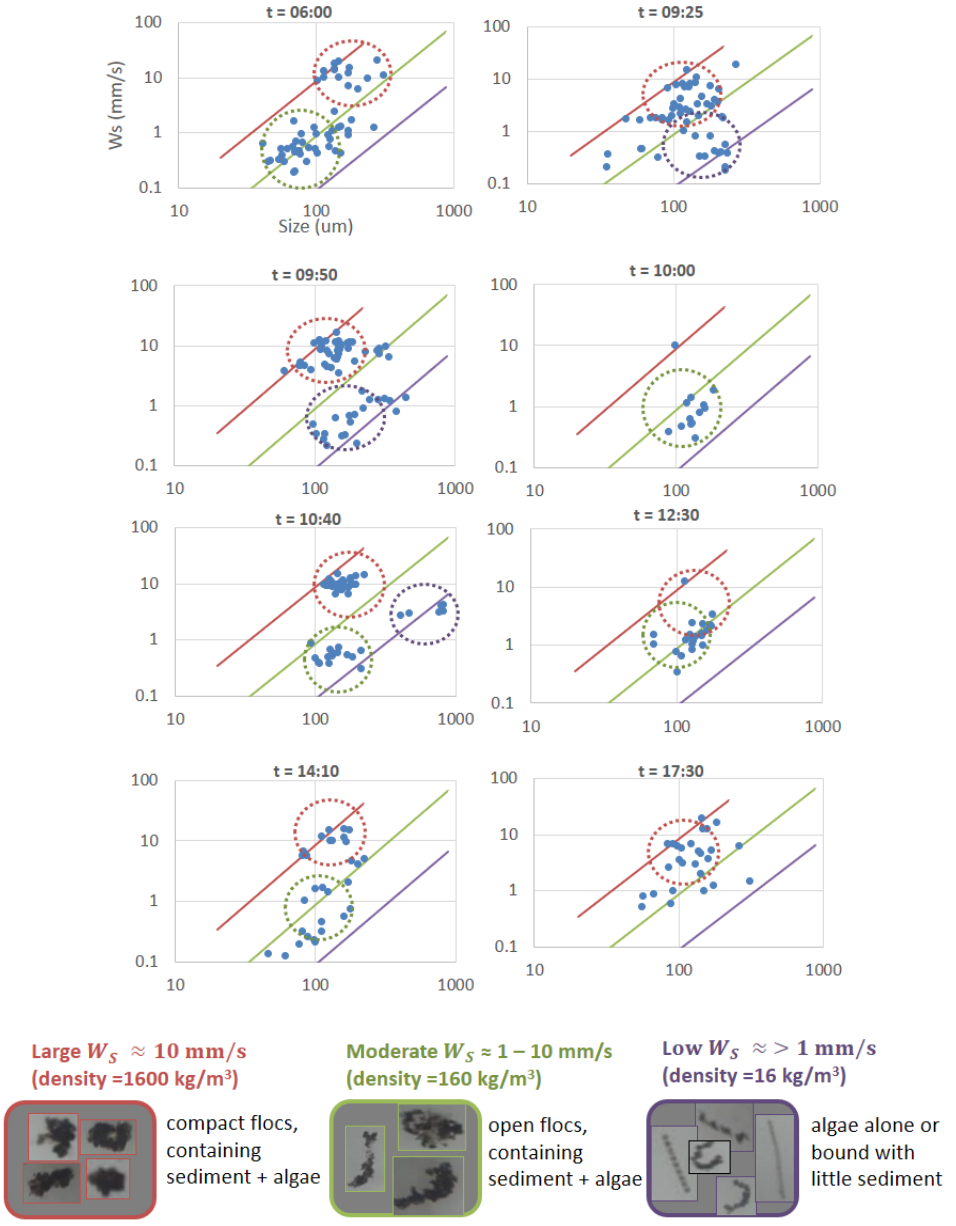

Figure 2.3: Results from the LabSFLOC-2 camera experiments: settling velocity as function of particle size. The 3 lines represent constant effective density lines, in red 1600 kg/m^3, in green 160 kg/m^3 and in purple 16 kg/m^3. The floc pictures are snapshots obtained from the underwater camera.

The results, in Figure 2.5, are given in terms of D10, D50 and D90, where Dk represents the k% particles having a mean size smaller than Dk. A special class > D90 was created which corresponds to the mean size of all particles larger than the D90 size. Specific LISST - HOLO measurements at the sampling times are also divided into these classes and displayed so that they can be compared with the LabSFLOC-2 camera data. The aspect ratios $AR = D_{major}/D_{minor}$ were evaluated using the same classes for both methods (Figure 2.5 a and b). We used the aspect ratio in combination with the density and settling velocity obtained from the LabSFLOC-2 to evaluate the relationship between particles shape and their settling velocity. Comparing Figure 2.5b and c with 2.5d, it can be seen at t = 9:36 (between 9:00 - 10:00), the particles have high aspect ratio and relatively low settling velocity. These highly anisotropic particles with low density have a lower settling velocity than spherical particles (from 10:00 to 15:00), with high density and low anisotropy (close to unity). These low density particles can have an increase in mass in time by aggregating with clay minerals.

High aspect ratio particles have large sizes (> 100 μm) but their concentration is lower than particles with higher density. Studies have shown that the algal mucous secretion and cell protuberance lead to entanglement and aggregate formation of algae during sinking, and these 'sticky' aggregates scavenge minerals and other particles during settling, which further increases the settling velocity [119–122]. Even small-celled diatoms such as *Skeletonema Costatum*, which is probably the observed algae species with the underwater camera and the LISST- HOLO, attain high settling velocities due to their formation in chains and their ability to aggregate [107, 123, 124].

Dead algae cells can on the other hand, accumulate as particulate organic matter. This organic matter will be a source of sticky material that also scavenge clay minerals and sediment particles and form flocs (see Chapter 3). Some of the particulate organic matter will be microbially decomposed into dissolved organic matter in the water column as well as in the sediment bed [125].

The density of flocs decreases with the size, as expected [126–130]. The comparison between the density obtained by LabSFLOC-2 camera of the particles from the sample taken at 08:04 with the density calculated from the LISST-HOLO picture taken at the same time is shown in Figure 2.6a. For this Figure, we took ρ_s = 2600 $kg.m^{-3}$ in eq.(2.3).

The LabSFLOC-2 does not measure sizes below 10 μm, a range that is accessible to the LISST-HOLO. On the other hand, with the LabSFLOC-2 technique, more large particles (> 100 μm) are observed. This can partially be due to the fact that differential settling is occurring while particles are left to settle after being pipetted into the settling column. Nonetheless, both data-sets (LabSFLOC-2 and LISST-HOLO) confirm that density is a decreasing function of size and that for a given size there can be a large spread in density. This was also observed in the study of Manning and Schoelhamer [111, 131].

As the camera and LISST-HOLO pictures show (Figure 2.6b), this spreading in density for a given size can be attributed to two factors: first, the composition of a floc (the amount

of mineral and organic matter within) and second, a raw data conversation artifact due to the shape of a floc. For highly anisotropic particles such as algae, the equivalent diameter will be estimated by:

$$D_{equivalent} = D_{minor} \times \sqrt{AR} \tag{2.6}$$

where the AR the aspect ratio. For a 1 mm long algae, with AR = 10, this gives an equivalent diameter of about 100 μm, which is the size that many flocs of aspect ratio close to 1 also have. Plotting the major axis as function of density provides therefore, a better size and density trend for the algae particles (Figure 2.7). We used eq.(2.3) to check the influence of ρ_s on the density trend. From Figure 2.7a and 2.7b it is found that the smallest particles have densities comparable to the ones found using the LabSFLOC-2 data when $\rho_s = 2600\ kg/m^3$ while the largest particles have densities comparable to the ones found using LabSFLOC-2 data when $\rho_s = 1016\ kg/m^3$. This implies that a black/white scale to estimate the solidity as proposed in section 2.1 is not appropriate to estimate densities and that a proper greyscale analysis should be performed. This can not be done at present, as this analysis requires a proper calibration of the greyscale colours based on more extended research.

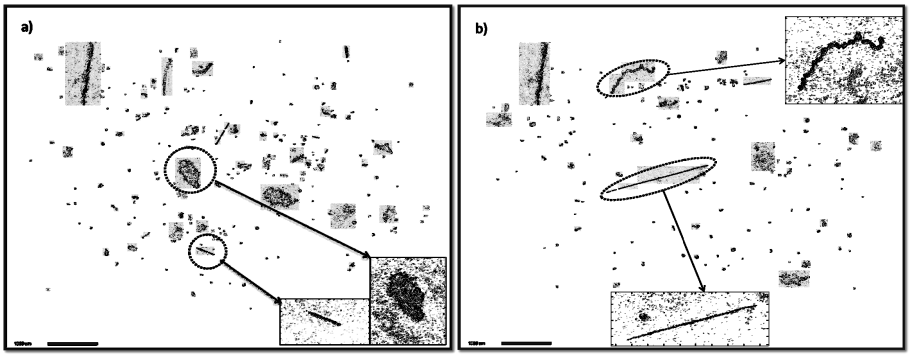

Figure 2.4: LISST- HOLO photo's: a) two differently shaped particles are chosen, an anisotropic particle (probably bare algae) with AR of about 5-6, and a spherical particle (floc) with an AR of 1-2 b) bare and slightly coated elongated algae particles. The bars are representing 1000 μm scale.

PARTICLE SIZE DISTRIBUTION (PSD) WITH VARIOUS TECHNIQUES

As the size of the particles did not change significantly during the whole day, the PSD data from the LISST 100X and the LISST-HOLO and the LabSFLOC-2 camera system were averaged over the entire day for each instrument. This also enabled to have a statistically significant data set, as the amount of particles detected was low during the day. Figure 2.8 shows the day average particle size distributions estimated by the three techniques, the LISST 100X, LISST-HOLO and the LabSFLOC-2 camera system. Although the LabSFLOC-2 camera data are not directly comparable with the LISST data due to

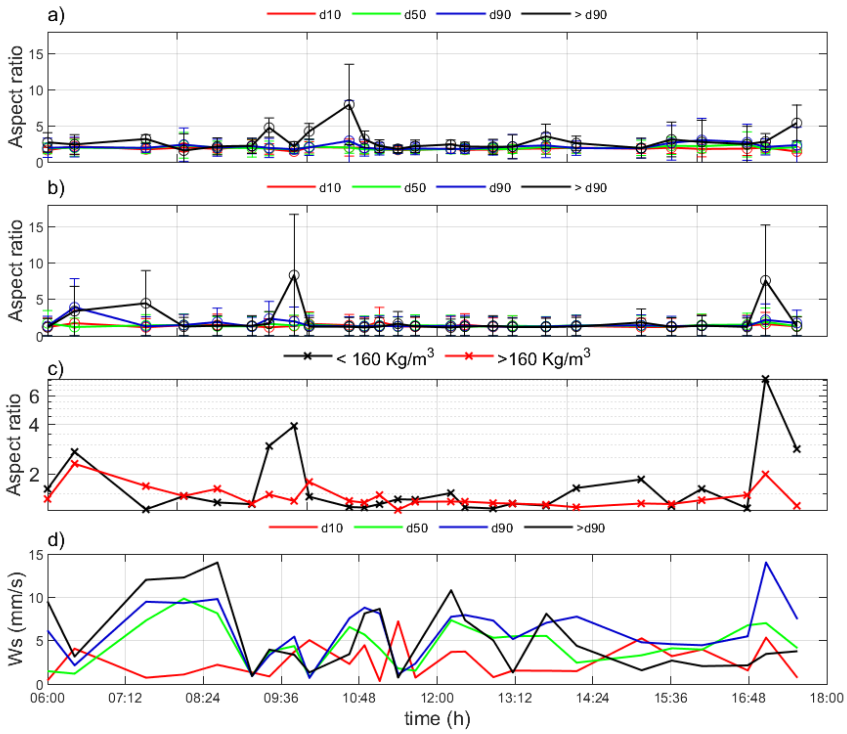

Figure 2.5: Results of the LabSFLOC-2 camera study and the LISST - HOLO. a) Mean aspect ratio of each class, as function of time for LISST - HOLO data (at the survey sampling times) from the 12m mooring. b) measured mean aspect ratio of each class, as function of time for LabSFLOC-2 camera samples taken during the survey. c) measured aspect ratio per density as function of time for the LabSFLOC-2 data. d) Settling velocity corresponding to the particles, measured with LabSFLOC-2 camera.

discrepancies between the two techniques [132], the overall mean size of the particles obtained from the LabSFLOC-2 camera correlates with the mean particle size obtained from the LISST data and fluctuates between 150 and 220 μm. The averaged PSD measured by LISST 100X is trimodal with peak particle sizes being 300, 200 and 70 μm for the whole day, whereas the LISST-HOLO displays two peaks which overlap the LISST- 100X 200 μm and 300 μm size peaks.

The LabSFLOC-2 data on the other hand displays one wide peak that tends to be bimodal, overlapping mainly the 200 μm peak and slightly the 300 μm peak. The larger sizes correspond to elongated bare algae whereas the peak in the range of 100-200 μm corresponds to flocculated organic rich particles. The clay size fraction (< 10 micron) is however observed only by the LISST 100X, which is out of the LISST-HOLO and LabSFLOC-

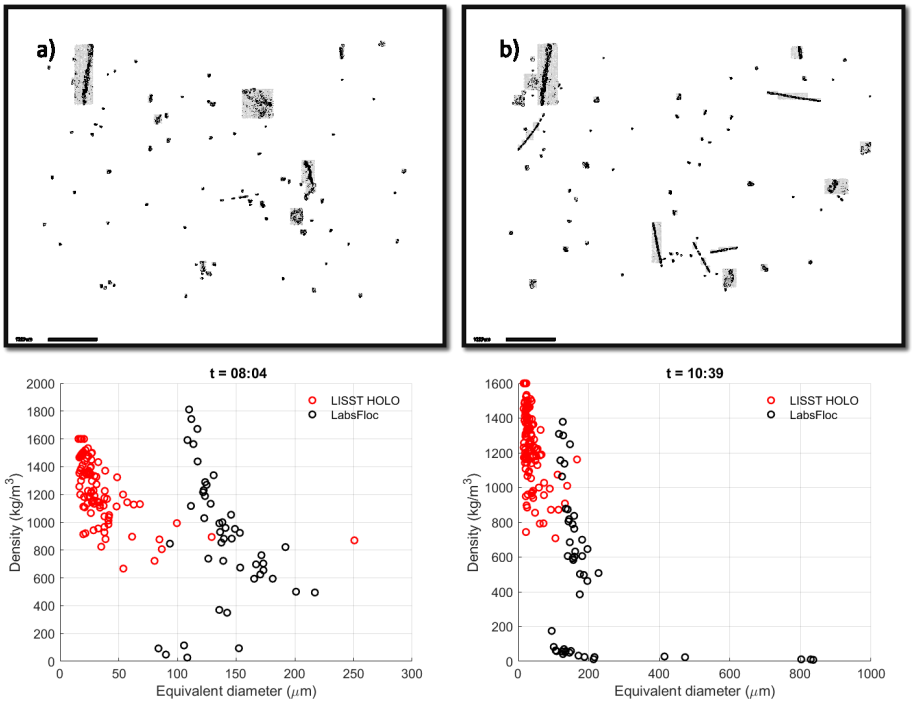

Figure 2.6: Comparison of density trend for two samples: a) Sample at t = 8:04 h where a low amount of algae particles are detected and the sample contains mostly sediment mineral particles. b) Sample at t = 10:39 where low sediment mineral content is present and significant amount of algae species are present (bar represents 1000 μm). LISST-HOLO density was evaluated according to eq 2.3 using ρ_s = 2600 $kg.m^{-3}$, LabSFLOC-2 density was evaluated according to eq 2.5.

2 range, since they are both camera based techniques. Graham et al.[133] similarly showed that the PSD produced by LISST-HOLO overlap with the PSD of LISST 100X in sizes 20-500 μm. They also observed that the LISST 100X reports a larger number of particles in the same size range, and that the LISST 100X enables to measure the smallest size classes in the suspension i.e. below 20 μm [133].

Graham and Nimmo Smith [134], who compared the LISST-HOLO PSD with the Malvern Hydro 2000G PSD, have found that the LISST-HOLO PSD showed multiple modes as compared to the monodal PSD produced by the Malvern Hydro 2000G, which were attributed to overlapping large particles in the field of view of the holographic system. In our case, the presence of highly anisotropic particles leads to same kind of effect. It was shown by Karp-Boss et al. that biological species cause trimodal distributions due to their shape effects [115].

Agrawal et al. inverted the data found by LISST 100X using different kernel matrix to produce particle size distribution for non-spherical particles [135]. However their method

does not cover very anisotropic particles such as bare algae and flocculated algae as are present in our observations. This is why a combination of holographic pictures and/ or other video or camera recording, are necessary to interpret the LISST 100X PSD as was also concluded by Graham et al. [133].

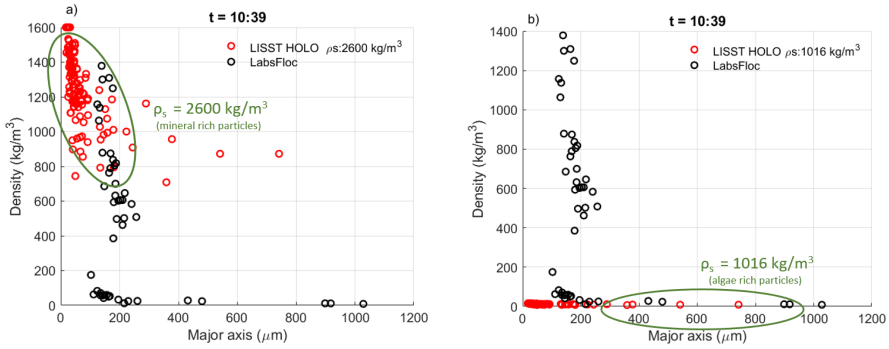

Figure 2.7: Influence of particle density ρ_s on the estimation of floc density (given on the y-axis). The density is calculated using eq 2.3 from LISST HOLO particle size data. Density of the particles as function of major axis for the sample taken at t = 10:39, with a) ρ_s = 2600 $kg.m^{-3}$. b) ρ_s = 1016 $kg.m^{-3}$

LABORATORY EXPERIMENTS RESULTS

The untreated PoR sediment was suspended in seawater as described in Materials and Methods section, the PSD was measured during flocculation. Figure 2.9, upper panel shows the SLS (Malvern 2000) measurements of particles size evolution in time. PoR sediment particles do flocculate with each other, 2.9a, as the water is saline. The samples have been disturbed during sampling, and therefore the particles are re-flocculating during the jar test. It has been shown that salt-induced flocs are extremely fragile, and that their (fully reversible), growth/break-up is proportional to shear shear stress [26]. The organic matter in the PoR samples is dead organic matter that could be decayed, as the sample has been stored for long time in a fridge. It is unclear at this stage whether the organic matter plays a role in the flocculation process. According to [136] fresh TEP is one of the most important constituent controlling the settling of the particles in coastal waters.

The floc growth in the jar is different from in-situ as the sample is continuously stirred and pumped though the device. This results in flocs having a low anisotropy. Moreover, the raw data processing by the Mastersizer software results in smoothed particle size distributions which hide possible multiple peaks [43]. After reaching steady state, Living Algae (LA) is added to produce 5% LA + 0.2 g/L suspension. After reaching a steady state, the LA content is increased to reach 20% LA + 0.17 g/L clay. Note that the suspension is slightly diluted and the PoR sediment concentration is lower. This procedure is repeated

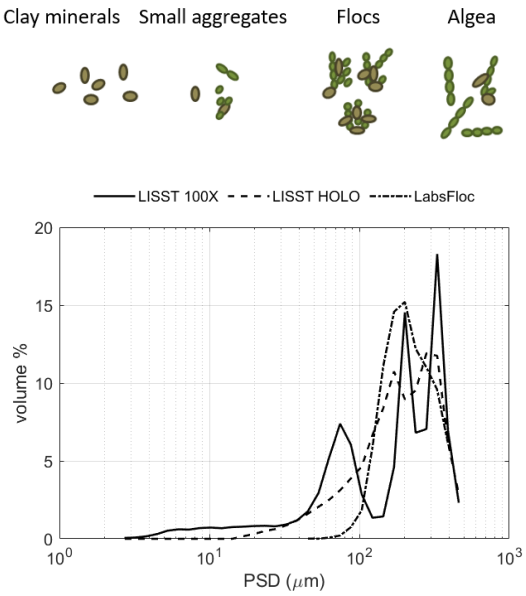

Figure 2.8: Comparison of particle size distribution measured by the LISST 100X (full line), the LISST-HOLO (dashed line) and LabSFLOC-2 (dashed dotted line). Clay minerals: < 10 μm, small aggregates: 70 μm, flocs (large aggregates): 200 μm and algae: 300 μm

for the 30% LA + 0.15 g/L clay suspension. The SLS data show a small shift in D50 over time upon increase in LA concentration. A tail is observed in the distribution between 1 and 10 μm (clearly visible in d). This tail exists for all LA concentrations, and the PoR sample (0% LA). This size range is attributed to the fine size class that will not necessarily aggregate. After reaching steady state a sample was taken to be analysed with the LabSFLOC-2 camera system. The settling velocity and the diameter were estimated and the density was calculated according to Stokes' law.

The LabSFLOC-2 measurement of PoR sediment sample (Figure 2.9a) shows that the sample consists of a wide range of particle in the size range 20-200 μm with a wide range of settling velocities and densities. In the sample with 5% LA content (Figure 2.9b), the particles have grown such to form roughly uniform settling velocity clusters of between 0.1 mm/s and 0.5 mm/s with a wide size range (10-200 μm.). One large cluster with density of about 160 kg/m^3 is found in the size range of 10 - 100 μm, indicating flocculated sediment with algae, and a smaller cluster with a density between 160 kg/m^3 and 16 kg/m^3 is found in the size range < 100 μm. These low density particles are algae particles.

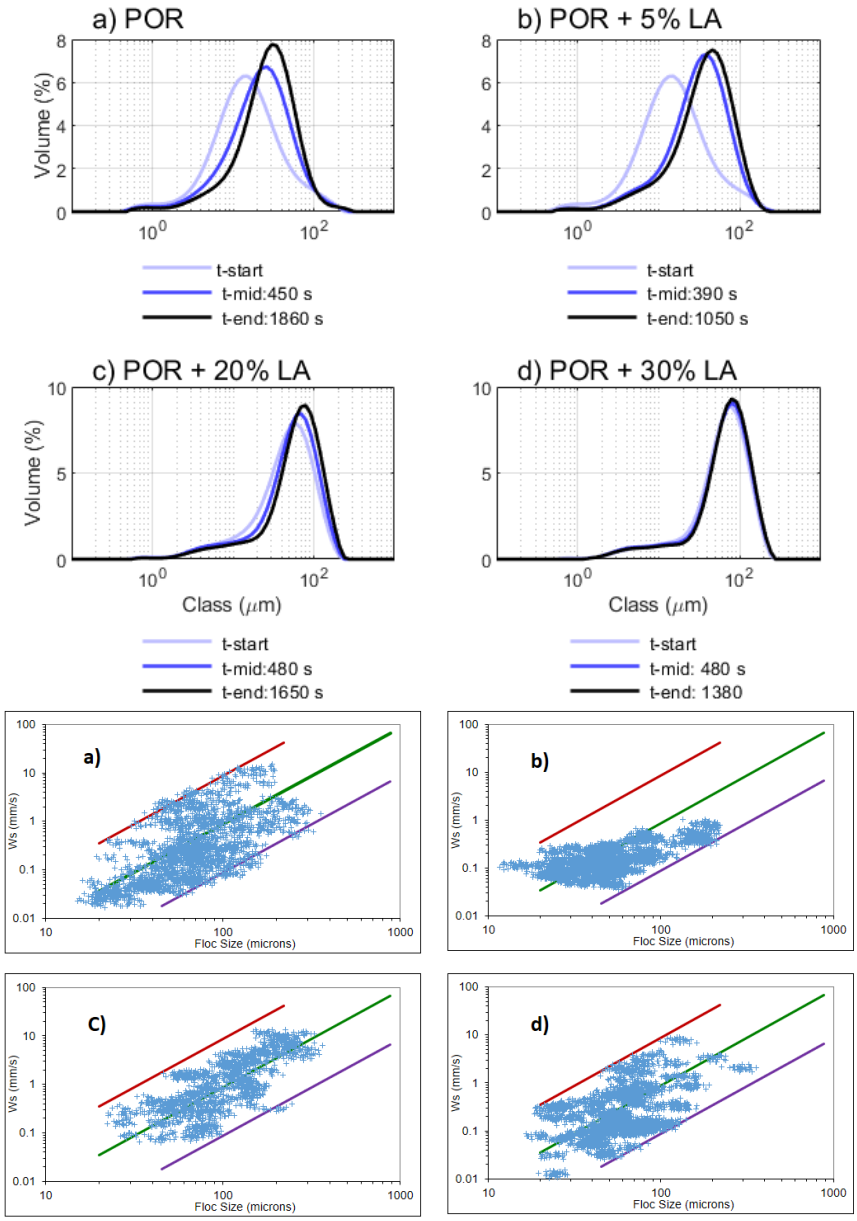

Figure 2.9: Flocculation experiments PoR sediment with Living Algae (LA), left panel: SLS particle size measurements, right panel: LabSFLOC-2 measurements of the same samples after reaching equilibrium size, a) PoR sediment without algae, b) POR sediment with 5% LA, c), POR sediment with 20% LA, d) PoR sediment with 30% LA. The 3 lines represent constant effective density lines, in magenta 1600 kg/m^3, in green 160 kg/m^3 and in red 16 kg/m^3.

The sample with 20% of LA (Figure 2.9c), shows a cluster of roughly uniform density of 160 kg/m^3, with wide range of settling velocities between 0.05 - 10 mm/s and wide size range (50-300 μm). Some of the particles however, have densities of 16 kg/m^3, which are probably bare unflocculated algae particles.

The sample with 30% LA (Figure 2.9d), shows a spreading in clusters, while the settling velocity remains large (0.01 - 10 mm/s). A large amount of particles are found in the density range 160 - 16 kg/m^3 and sizes > 100 μm, which indicates that these particles are algae-reach.

The aspect ratio of PoR sediment sample did not show a significant difference compared to the samples with LA. The AR was measured to be between 1-3 for all samples. This is due to the fact that the samples were taken after the flocs had reached steady state and that the flocs could not grow anisotropically, due to the shear imposed in the jar. This condition is most probably different in situ, where the shear is different and differential settling can occur, whereby particles can "catch-up" with each other. Lab experiments could be designed to study the change in AR of sample in different shear conditions, but this is beyond the scope of this thesis. The Aspect Ratio (AR) and densities of PoR and PoR +5% LA and PoR + 30% LA are shown as examples in Figure 2.10. Dividing the samples into two clusters based on their density (Figure 2.10 upper panel), shows that lower density particles have higher aspect ratio in the PoR + 5% LA and the PoR + 30% LA samples, while the PoR sample shows uniform AR for both densities.

It is worthy to mention the sampling method could possibly had an influence on the aspect ratio of the particles. The jar stirrer had to be stopped prior sampling, and the flocs could settle to the bottom of the jar. This can cause a change in size and shape of flocs resulting in higher AR.
In Figure 2.10 lower panel, the density is plotted as function of size for the size classes D10 - > D90 for the same samples. It is clear that every size class consists of a wide range of densities. Upon addition of LA, the density/size profile changed and an exponential decreasing function density is found as function of size, as it is usually observed in estuarine conditions [111]. It seems that sediment and dead organic matter (PoR sample) has a much wider spread in density for a given particle size compared with sediment and living algae. The Dk% of the sizes found in situ and lab is given in table 2.2. The sizes of the > D90 class is quite similar in the lab and in situ, indicating that very large particles (algae) are not very sensitive to shear. All the other classes have sizes that are smaller in the lab as compared to in situ, as by shearing the particles get denser and smaller.

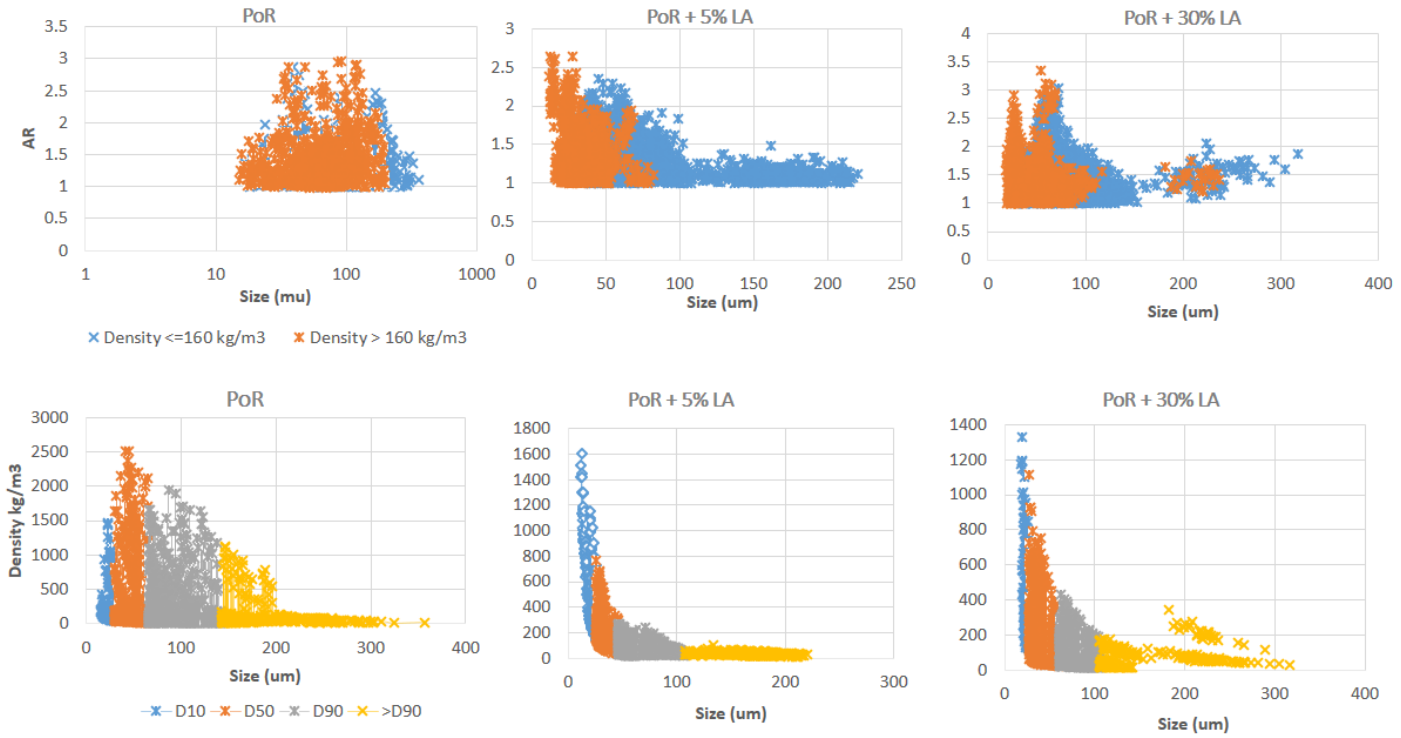

Figure 2.10: Left panel: Aspect Ratio as function of size for PoR (upper graph) separated based on low and high effective density particles (see legend), and density as function of size (lower graph). Mid panel: Similar graphs for PoR + 5 % sample and PoR + 30% sample in the right panel. Note: these results are obtained from LabSFLOC-2 measurements.

Table 2.2: The D10, D50, D90 and > D90 based on LabSFLOC2 measurements for in-situ and laboratory samples

In-situ				
sample	*D10*	*D50*	*D90*	*> D90*
t = 6.00	56.09	114.48	183.42	310.52
t = 9:25	61.16	128.47	223.11	269.12
t = 9:50	85.80	149.73	292.28	449.75
t = 10:00	89.38	99.09	130.39	163
t = 10:40	115.63	154.15	414.55	836.21
t = 12:30	70.69	130.24	171.27	179.15
t = 14:10	81.92	113.6	185.25	225.759
t = 17:30	67.60	131.87	175.89	311.79
Lab experiments				
PoR	29.7	65.66	142.63	357. 15
PoR + 5% LA	25.89	46.27	107.38	220.77
PoR + 20% LA	20.17	58.77	110.91	358.17
PoR + 30% LA	27	60.81	105.28	317.1

2.3. CONCLUSION

In this study, the results of a one-day field survey in the Rhine ROFI region, during neap tide calm weather conditions were presented. The SPM characteristics for these typical neap tide conditions were analyzed with a variety of optical and camera techniques.

Videos from the underwater camera and LISST-HOLO data, show the presence of many algae particles in the bottom water layer. These particles can be found in the form of elongated chains, or bound to debris and mineral particles in different degrees of coiling. From sample analysis done on board with a LabSFLOC-2 camera, the aspect ratio of the particles could be quantified and was found to be close to 2 for the lightest particles (relative density < 160 kg/m^3) and at given moments in time, aspect ratios between 3 and 8 were observed for this class of particles. According to their density estimations, and confirmed visually from the LISST-HOLO and underwater camera video recordings, these lightest particles were algae-rich flocs or bare algae particles. All the other particles have an aspect ratio close to 1 for any condition.

In the laboratory experiments, no floc or algae strain had an AR larger than 3, suggesting that the creation of highly anisotropic particles (as observed in the field data), requires environmental conditions that are different from the lab.

The particle density was estimated using Stokes' law from the LabSFLOC-2 data. It could in principle also be estimated from the solidity derived from the LISST-HOLO data, however due to presence of organic rich particles, the conversion is not straightforward, as the density of organic and inorganic particles are very different. Further research is required to find a proper calibration between the gray-scale recorded from LISST-HOLO

and density.

The fact that particles are highly anisotropic leads to multiple peaks in the PSD found using the LISST 100X. This fact has to be accounted for when longer time series will be analysed, solely based on LISST 100X data from the mooring (chapter 4). The mean particle size obtained by LISST 100X for the larger flocs is in agreement with the mean particle size obtained with the LISST-HOLO and LabSFLOC-2 camera system.

The use of different measurement techniques provide a full spectrum of particle size distribution: LISST 100X detects the fine fraction (< 20 μm) properly, while from the LabSFLOC-2, LISST-HOLO and underwater camera information about the coarser fraction, the flocs, their shape, settling velocity and density can be obtained.

Based on these findings the SPM particles are categorized into three classes, in view of creation of a flocculation model (chapter 3). In contrast to what is currently the practice, it is proposed that the particles classification is done based on their composition rather than their size. These classes are defined as follows:

Class 1: Sediment inorganic particles (clay minerals): the particles in this class have high effective density and small anisotropy. These can flocculate with organic matter (including algae) for the non-sand fraction.

Class 2: Flocculated particles: these class have a wide range of sizes, effective densities and settling velocity based on availability of the other classes, the floc history and hydrodynamic conditions.

Class 3: Bare algae and/or bare organic matter: particles in this class have low effective density (and an anisotropic shape) and can flocculate with sediment particles.

It is expected that these three classes are also present during spring tide and storm conditions, however in different relative ratios. For instance, during storm a large amount of Class 1 is expected to be in the water column.

3

APPLYING LOGISTIC GROWTH THEORY TO MODEL FLOCCULATION

In the present Chapter we are aiming to parameterize a new flocculation model by conducting different types of experiments in the laboratory. The suspension constituents are chosen such that they mimic the natural floc composition as much as possible based on the particles identified in the previous chapter and literature [40]. In addition these flocculation experiments will strengthen our understanding of sediment / algae and sediment / organic matter flocculation process whereby the aggregate size exceeds the Kolmogorov length scale in natural waters [137]. In addition these flocculation experiments will strengthen our understanding of sediment / algae and sediment / organic matter flocculation process whereby the aggregate size exceeds the Kolmogorov length scale in natural waters [26].
The model can be used to study either the evolution of a class volume concentration as function of time, or the change in size of a given class as function of time. It will be shown that the data can be used to parameterize the model. Different flocculation characteristic time scales are found for different constituents. The flocculating agents cover a wide range of constituents starting from monovalent and divalent salts to natural organic matter and living algae species. Divalent salts are shown to promote flocculation of clay and sediment and play a crucial role in flocculating the organic matter to the sediment particles. A discussion about the mass balance between the two classes is given.

Parts of this chapter have been published in *Marine Geology* (2020) [26].

The particle identification performed in the previous chapter showed that the flocs are composed of clay minerals, transparent organic matter structures, algae and other microorganisms. Organic matter such as polysaccharides and proteins fall under generic name of Extracellular Polymeric Substances (EPS) which are complex high molecular-weight mixtures of polymers. These particles have a wide size range of < 3 up to > 100 μm. As these substances are mostly excreted by diatoms and phytoplankton's, their concentrations and abundance are seasonal dependent. Because of their large size and high stickiness they facilitate or enhance flocculation of solids [30, 31, 138–140]. The size evolution and effective density of flocs are depending on these constituents as well as on the dissolved salts that are naturally present in seawater, and shear stresses.

Many studies have been conducted to model flocculation using Population Balance Equation (PBE) models [28, 141–146]. The earliest and simplest PBE originates from Smoluchowski (1917). It describes the rate of early aggregation and it contains two general growth (K_A) and break-up (K_B) terms. The generic form of a PBE is given by:

$$\frac{dN}{dt} = K_A(t) - K_B(t) \tag{3.1}$$

where N represents the number of particles in a given size class and t is the time. Most models assume that the particles are hard spheres and that the flocs maintain their shape during the flocculation process. Some studies use a time varying floc size, which introduce new parameters in the PBE model [147]. The general break-up term in PBE usually accounts for binary break-up by shear, which results in the 'birth' of two small particles by the 'death' of a large one. [145, 146, 148, 149].

The Smoluchowski model has been successfully applied to salt-induced flocculation [77, 147, 150]. However, when polymers are involved in the flocculation process, decrease in size is predominantly caused by reorientation of the polymer and by aggregate restructuring and densification [148] rather than breakage, due to the elasticity of the polymers. Modifying the PBE to account for this effect would introduce new variables that cannot properly be measured, and therefore this step would not add to the system understanding. Modifying the PBE to account for organic matter induced flocculation requires for instance the inclusion of parameters such as the sticking probability of a specific EPS or its reconformation under shear. Additionally, there is a problem in defining the properties of a particle within a given size class, as each particle in a size class may have a different composition. This implies that particles of same size can have a different settling velocity as they have different effective densities. For this reason, the PBE cannot be used for numerical modeling purposes, whereby a size class is associated with a settling velocity.

In view of simplification, other researchers model flocculation using a single equation that represents the change in size of the average particle size (the D50) [37, 75, 145, 151]. This approach has the advantage to be easy to implement in large-scale models, but the disadvantage to not properly account for the sediment (mineral) mass conservation. The

model proposed by Chassagne and Safar [26], makes use of mass conservation and is as easy to implement as the D50 models.

Open questions thus remain: How to parameterize and calibrate this new model? How are the flocculation dynamics, in particular timescales, associated to different flocculation mechanisms?
To answer these questions, the interactions between sediment, EPS and microorganisms are analysed trough flocculation experiments conducted under controlled laboratory conditions. The size class evolution in time with different constituents is then used to parameterize the flocculation model as was proposed in [26].

After briefly describing logistic growth theory, the relevant materials and methods will be presented. The flocculation behaviour and the modelling results for different suspension composition and environmental conditions will be discussed.

3.1. LOGISTIC GROWTH THEORY FOR FLOCCULATION

The analytical model used in this chapter is derived from logistic growth theory, that is used to describe the time evolution of a living population [37, 152–154], with 'birth' and 'decay' parameters. Every class in a flocculating suspension can be seen as a 'living' population that is growing or decaying in time depending on other classes and external parameters. Standard logistic growth models account for either growth of population, until steady state is reached, or decay of a population, until a steady state is reached. For populations that experience first a growth and then a decay, specific growth and decay functions should be given. These functions are depending on parameters that should be studied as function of suspension composition and environmental conditions.

During flocculation each class has a number of individuals (N) which is changing in time (t). The decrease of number of particles with time is associated to the decay function $d(t)$ and their increase with the birth function $b(t)$. The functions $b(t)$ and $d(t)$ should be chosen such that they best mimic the time evolution of all classes. In Chassagne and Safar [26], the following model is proposed:

$$\frac{dN}{dt} = [b(t) - d(t)]N \tag{3.2}$$

The production (birth) rate and the decay rate are given by:

$$b(t) = \frac{1}{tb}\frac{a_b \exp(-\frac{t}{t_b})}{1 + a_b \exp(-\frac{t}{t_b})} \tag{3.3}$$

$$d(t) = \frac{1}{td}\frac{a_d \exp(-\frac{t}{t_d})}{1 + a_d \exp(-\frac{t}{t_d})} \tag{3.4}$$

where a_b, a_d, t_b and t_d are parameters to be fitted. The analytical solution for this differential equation is:

$$N(t) = \frac{N_\infty}{1 + a_b \exp(-\frac{t}{t_b})}[1 + a_d \exp(-\frac{t}{t_d})] \tag{3.5}$$

For a full discussion about the model, see [26]. In this chapter, the logistic growth model is used to fit either the time evolution of the particle size or the volume % concentration of a size class, measured by static light scattering as it was done in [26]. In the last case the variable N then represents the relative volume occupied by particles in a size class. The volumes are normalized to volume %, such that by summing all of the volumes over all the classes a 100% volume is obtained.

3.2. MATERIALS AND METHODS

3.2.1. MATERIALS

SEDIMENT

Two different sediments were used in the experiments. One is a clay referenced K-10.000, which was purchased from the company VE-KA (The Netherlands). The original clay lump has a water content of 35.7% and a sand content of 21%. The clay was dispersed in demineralized water, the obtained suspension having conductivity less then 0.005 mS/cm. The other one was a natural sediment that was obtained from Port of Rotterdam (PoR), that was used as such.

Clay Composition: X-Ray Powder Diffraction (XRPD) patterns were recorded in a Bragg-Brentano geometry in a Bruker D5005 diffractometer equipped with Huber incident-beam monochromator and Baraun Particle Size Detector (PSD) detector. The samples of about 20 milligrams were deposited on a Si 510 wafer and were rotated during measurement. Data collection was carried out at room temperature using monochromatic CuK $\alpha 1$ radiation ($\lambda = 0.154056nm$) in the 2θ region between 5Å and 90Å, step size 0.038 degrees 2θ. Data evolution was done with the ruker program EVA. From X-Ray Diffraction (XRD) measurement the composition of the clay sample is found to be: quartz, calcite, anorthite and muscovite.

ESEM Measurements: The clay was analysed with a Phillips XL30 Environmental Scanning Electron Microscope (ESEM), from Microlab in the Faculty of Civil Engineering and Geosciences, TU Delft. The ESEM image of PoR sediment is shown in Figure 3.1, right panel. The sample description and PoR sediment mineralogy are given in Chapter 2 (table 2.1). During the ESEM measurement the sample was under vacuum, with a beam acceleration voltage of 20 kV, with back-scattered electrons imaging mode and a spot size of 4 (Figure 3.1, left panel). Note that these clay characterization analysis were done in [43] and they are not repeated for this study.

SUSPENDING MEDIUM

Demineralized water and filtered seawater were used separately as suspending medium. For salt flocculation, monovalent NaCl and divalent $CaCl_2$ and $MgCl_2$ were used in different concentrations in demineralized water.

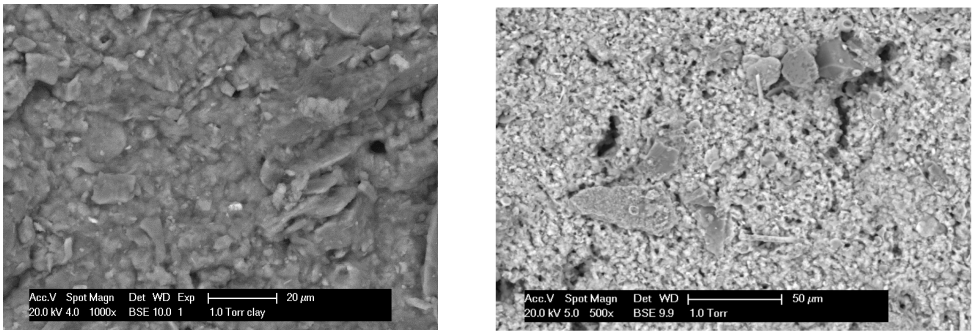

Figure 3.1: ESEM pictures of clay (left panel) and PoR sediment (right panel)

DEAD ORGANIC MATTER

Extracellular Polymeric Substances (EPS) and Frozen Dried Algae (FDA) were used as dead organic matter. The EPS was obtained from the municipal waste water extractions and contained: proteins: 200 mg/L, humic acids: 40 mg/L and polysaccharides: 110 mg/L. Note that the proteins and humic substances are negatively charged whereas the polysaccharides are positively charged [155]. The FDA was obtained from NIOZ (Royal Netherlands Institute for Sea Research). This FDA was analyzed by ESEM to identify its composition. The ESEM analysis is shown in Figure and table 3.2.

LIVING ORGANIC MATTER

Living algae *Skeletonema Costatum* was chosen because it is a common algae species in coastal waters. The living algae was obtained from Roem van Yerseke company for algae and oysters cultivation. The algae bulk concentrations was 5×10^6 cells/L, and every two weeks a fresh batch of this algae was used to keep the bulk concentration constant. The suspending medium was filtered seawater, to keep the living algae in good condition.

3.2.2. EXPERIMENTAL SET-UP AND PHYSICAL CONDITIONS

Flocculation experiments were carried out in a jar that was connected with tubes to the Malvern MasterSizer 2000 for measuring Particle Size Distribution (PSD). The physical conditions, such as shear rate, clay concentration and the jar size were kept constant for all of the experiments. The flocculation experiments were performed in a JLT6 jar test set-up from VELP scientific. The dimensions of the jar are 95 mm for the inner diameter and 110 mm for the height of the fluid. The suspension is stirred using a single rectangular paddle at 30 rpm. The paddle is 25 mm high and 75 mm in diameter. It is placed 10 mm above the bottom of the jar. The suspensions were pumped through the Malvern MasterSizer 2000 in which the SLS measurements are performed, with the help of a peristaltic pump from the mixing-jar to the MasterSizer and back again to the mixing-jar. This set-up allowed us to control independently the speed of the pump and the paddle of the mixing-jar. The internal diameter of the connecting tubes is 6 mm and the shortest total length allowed by the geometry of the set-up (2400 mm from the jar back to the jar). The shear rate was optimized and chosen as the best shear rate for optimal flocculation

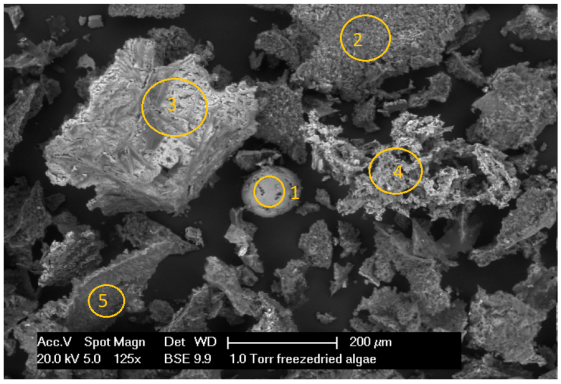

Spot nr	C	Na	Cl	Ca	Si	O
1	18.8	2.49	3.10	-	0.34	46.30
2	39.32	8.37	17.58	27.90	2.75	27.27
3	32.03	17.40	23.46	0.55	0.28	24.64
4	30.46	16.91	23.37	0.58	0.67	20.70
5	42.96	6.17	15.22	1.25	1.78	29.11

Figure 3.2: FDA ESEM analysis: The elemental concentration in weight % in the table correspond to the cirkeld spots in the FDA image.

with this setup. It was found to be 10 rpm pump rate and it corresponds to about 12 s^{-1}. The clay concentration was 0.7 g/L and the PoR sediment concentration was 0.2 g/L.

SALT FLOCCULATION

In these experiments clay and three most dominant salts in seawater were used, the monovalent salt NaCl, and two divalent salts, $CaCl_2$ and $MgCl_2$. Three concentrations were used for each salt. These concentrations were chosen as below, same as and above the concentration they have in seawater.

DEAD ORGANIC MATTER FLOCCULATION

In these experiments two types of organic matter, EPS and FDA were used without salts, and in combination with salts and either clay or PoR sediment. These organic matter represent the excreted 'dead' organic matter debris present in the natural waters.

LIVING ALGAE FLOCCULATION

Living algae *Skeletonema Costatum* was used in this experiments with either clay or PoR sediment. For these experiments the medium was filtered seawater, which was used to keep the living algae in good condition. There were no salts used for these experiments. Additional experiments were performed for algae without any clay or PoR sediment. This was done by suspending different volume % concentrations of algae in seawater. A general overview is given in table 3.1.

Table 3.1: Experimental set-up: constituents and their concentrations

Salt flocculation						
Salt type	Concentration (M)	Medium	sediment type	concentration (g/L)	OM type	Concentration
NaCl	0.1 0.2 0.3	Demi-water	clay	0.7	-	-
$CaCl_2$	0.005 0.01 0.02	Demi-water	clay	0.7	-	-
$Mgcl_2$	0.01 0.05 0.1	Demi-water	clay	0.7	-	-
Natural OM flocculation						
NaCl	0.2	Demi-water	clay	0.7	EPS	10 mg/g
$CaCl_2$	0.005	Demi-water	clay	0.7	EPS	10 mg/g
$Mgcl_2$	0.01	Demi-water	clay	0.7	EPS	10 mg/g
-	-	seawater	PoR sediment	0.2	EPS	2 mg/g
NaCl	0.3	Demi-water	clay	0.7	FDA	0.05 g/L
$CaCl_2$	0.005	Demi-water	clay	0.7	FDA	0.05 g/L
$Mgcl_2$	0.01	Demi-water	clay	0.7	FDA	0.05 g/L
-	-	seawater	PoR sediment	0.2	FDA	0.05 g/L
Flocculation with LA: Skeletonema Costatum						
-	-	seawater	clay	0.7	LA	10 % (v/v)
-	-	seawater	clay	0.7	LA	30 % (v/v)
-	-	seawater	clay	0.7	LA	50 % (v/v)
-	-	seawater	PoR	0.2	LA	10 % (v/v)
-	-	seawater	PoR	0.2	LA	30 % (v/v)
-	-	seawater	PoR	0.2	LA	50 % (v/v)

3.3. RESULTS

The experiments performed with the clay in suspension are presented first in this section. The experiments with PoR suspensions are presented in a second subsection. After these experimental observations, the model fittings results will be presented in the context of large-scale modeling. For each experiment the flocculating agent (salt and/or organic matter) was added at the time defined arbitrary to be 1s (as at t = 0, the curve represents the unflocculated clay or PoR sediment).

3.3.1. CLAY SUSPENSION

SALT FLOCCULATION

The Particle Size Distribution (PSD) of the experiments performed with three different salts at different salt concentrations are shown in Figure 3.3. In the first panel flocculation by the monovalent salt NaCl is presented and in the middle and last panels the flocculation by the divalent salts $CaCl_2$ and $MgCl_2$. As it can be seen the D50 does not exceed 20 μm at equilibrium. This equilibrium size is in agreement with study of Mietta [77] who showed that the equilibrium particle size obtained by salt flocculation can not exceed the Kolmogorov length scale. The Kolmogorov microscale was calculated to be between 8 and 23 μm for the conditions used in the experiments.
The difference however is in the time needed to reach an equilibrium size. The characteristic time t-eq is defined as the time for which the full PSD reach steady state, see Figure 3.3. Flocculation with NaCl takes much more time than with $CaCl_2$ and $MgCl_2$. This confirms the efficiency of divalent salt in the flocculation of clay [156]. The t-eq was in the range ≈ 150-400 s for divalent salts and ≈ 600-1000 s for monovalent salt, for the concentrations used. The way that t-eq is linked to the 'birth' and 'decay' times t_b and t_d will be shown in the modelling section.

FREEZE DRIED ALGAE (FDA) FLOCCULATION

The experiments with clay and added FDA (dead organic matter) in demi-water are displayed in Figure 3.5. The first PSD (t-start) represents the clay monomodal PSD without addition of any EPS or FDA. The EPS, (upper pane)l and the FDA (Lower panel) is added immediately in after the first 30s (t-start). After injecting EPS no change in the PSD was observed until 240 s after injection, indicating that there was no flocculation between the EPS and the clay. Clay in presence of FDA displays a similar behaviour, see the lower panel of Figure 3.5, where the bimodal distribution is caused by the elongated shape of the strings made by the algae cells. The absence of flocculation in both cases is expected as both EPS and FDA are negatively charged and electrostatic repulsion forces prevent flocculation.
Flocculation with anionic (negatively charged) polymers is possible in case cations can act as bridging agents [29]. After addition of salt to the clay and organic matter suspensions, flocculation takes place, see Figure 3.5, and the D50 increases eventually exceeding the Kolmogorov microscale of the system. The divalent salts ($CaCl_2$ and $MgCl_2$) produce larger flocs in shorter times, compared to NaCl. The D50 decreases after reaching its maximum size D_{max}. At this stage the flocs coil under shear and become denser, hereby decreasing in size. At the end of the experiment (t-end) the D50 is therefore lower

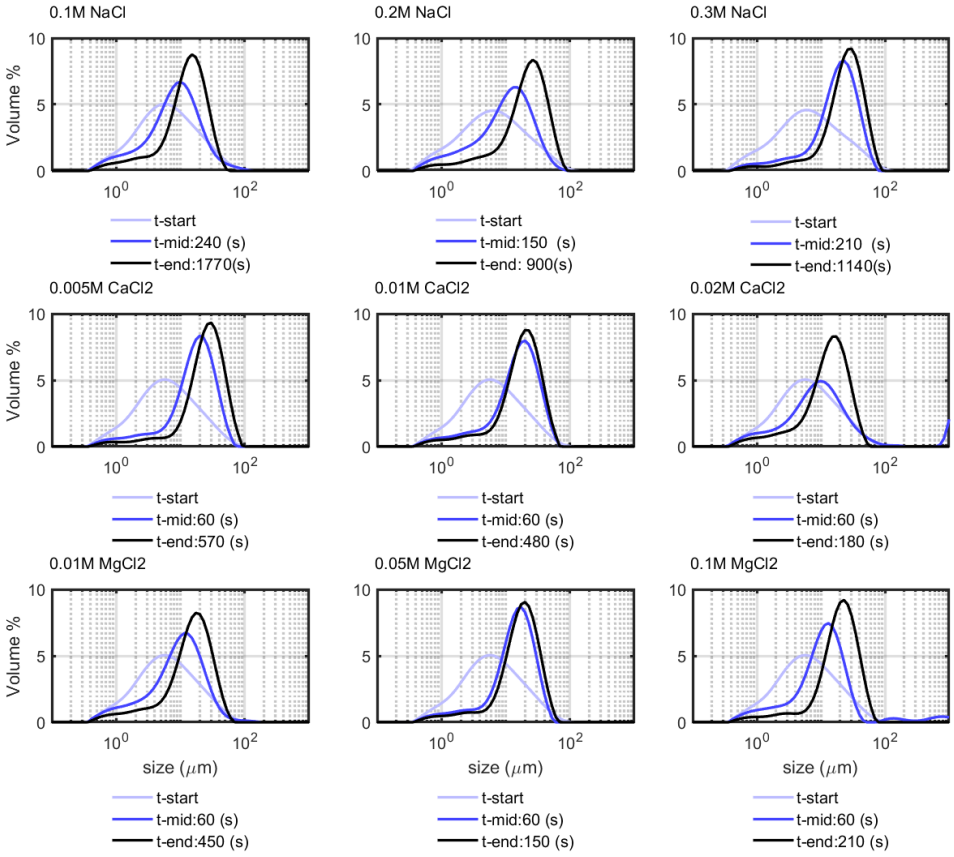

Figure 3.3: flocculation of clay (0.7 g/L) with salt, t-start and t-end correspond to the start of experiment and t-end corresponds to the time at which the D_{50} achieved equilibrium.

than at t-D_{max}.

LIVING ALGAE FLOCCULATION

Living algae in seawater at different volume percentages were studied to check whether the algae cells would flocculate over time. The corresponding PSD's are shown in the first panel of Figure 3.6. The PSD's are multimodal for every algae concentration and do not vary significantly over time, which indicates that the algae kept their elongated structure over time. After addition of clay to the suspensions, see lower panel of Figure 3.6, flocculation takes place gradually and the PSD's reached an equilibrium size. The flocculation time (time to reach t-eq, i.e the time for which the full PSD reach steady state) was observed to increase with algae concentration.

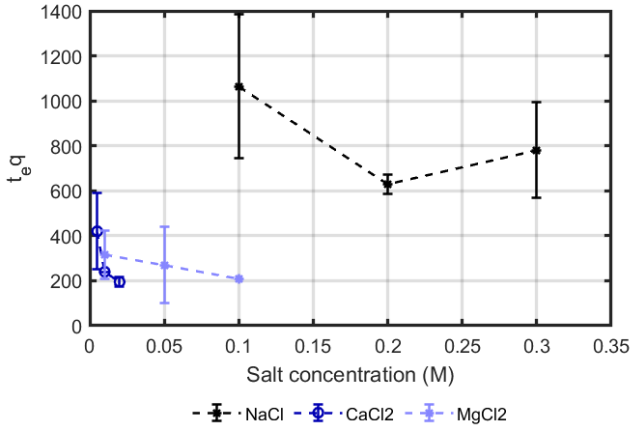

Figure 3.4: Salt flocculation: time needed to reach equilibrium size (t-eq) as function of salt concentration, the error bars indicate the deviation between the duplicate samples.

3.3.2. SEDIMENT FROM PORT OF ROTTERDAM (POR)

Natural sediment obtained from Port of Rotterdam (PoR), was suspended in filtered seawater and left to flocculate without addition of any flocculating agent. The left panel of Figure 3.7 shows the PSD of PoR sediment, that reaches an equilibrium PSD, with a D50 of about 30 μm after 2040 seconds under constant shear. This equilibrium size is larger than the Kolmogorov microscale of the system, which indicates that the natural PoR sediment might contain some organic matter, or large silt particles.
PoR samples in combination with EPS and FDA are displayed in the mid and right panel of Figure 3.7. With EPS an equilibrium D50 of about 31 μm is achieved in 1830 seconds, which is virtually the same as when no EPS was added. With FDA the achieved equilibrium D50 is about 107 μm at 2010 seconds.

3.3.3. MODEL RESULTS

The flocculation results obtained from the experiments were used to parameterize the flocculation model given by eq.(3.5). The model enables to fit both the concentration (in % volume) of a given size class as well as the evolution of D10, D50 and D90 sizes as function of time. In [26], it was shown that the equation 3.2 can also be used to model the particle size evolution as a function of time for any size class. The concentrations of 7, 15, 45 and 60 μm as function of time and the size evolution of the D10, D50 and D90 are displayed in Figure 3.9. The class of 7 μm was chosen because it is representative for the D50 of the unflocculated clay. In addition to this class, 15 μm class was chosen to represent the first flocculated class, which can occur by aggregation of two 7 μm particles. The 45 and 60 μm, represent the coarse classes that are formed during the flocculation process by consumption of the fines. The 45 μm can be compared with the D50, as it shows a similar behaviour in most of the experiments. The D10 however does

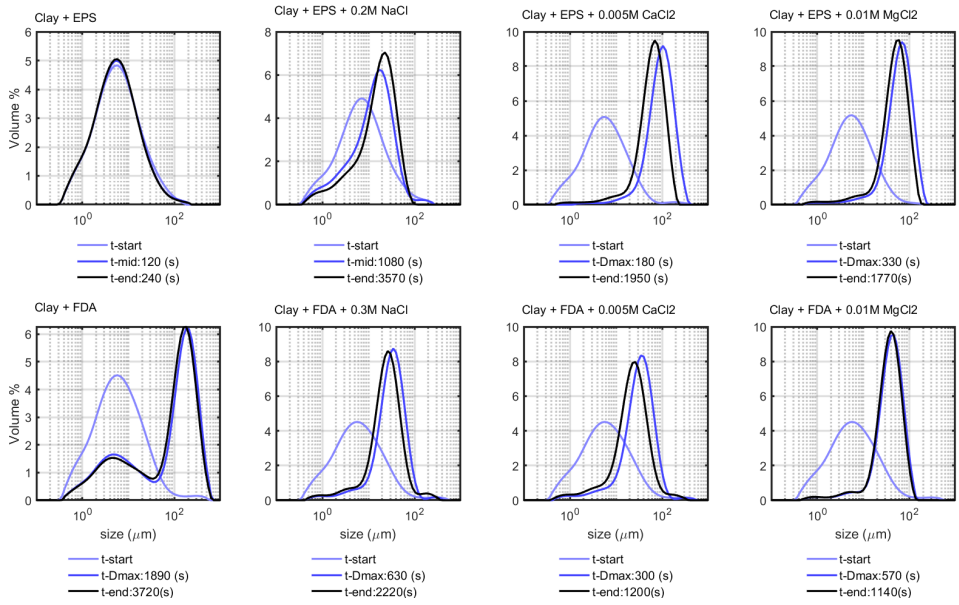

Figure 3.5: Flocculation of clay (0.7 g/L) with EPS and FDA (natural organic matter) in demi-water, t-start and t-end represent start and end time of the experiment respectively, t-Dmax represents the time at which D50-max is achieved and after this the D50 decreases. This does not apply for the 'Clay + EPS + 0.2M NaCl' sample as it grows very slowly in time until the end of experiment. Note that the FDA (the lower panel, the three figures on the right) was added to the sample when it was already flocculated with salt, therefore the t-start is not the pure clay PSD.

not represent the fines, as it displays a behaviour that is different from the 7 and 15 μm.

SALT FLOCCULATION

The curves with values obtained from the model and corresponding experimental data are plotted in Figure 3.9 for one concentration of each of the three salts. From these figures it can be seen that salt type influences the flocculation timescales (t_b and t_d).
As it can be seen the model can be used to fit the experimental results quite accurately for salt flocculation. Most of the size classes especially for flocculation by NaCl, are fitted with values of t_b and t_d which are very close to each other. It has been demonstrated in [26] that having $t_b = t_d$ is mathematically equivalent to set $a_d = 0$ (equivently $d(t) = 0$) and hence to consider only a birth term. This has been done for all the D50 classes in Figure 3.9. Let us define $\tau = t_b = t_d$. Eq.(3.5) then results in:

$$\frac{N(t) - N_\infty a_d/a_b}{1 - a_d/a_b} = \frac{N_\infty}{1 + a_b \exp(t/\tau)} \tag{3.6}$$

Setting $a_d = 0$ (and using $\tau = t_b$) in eq.(3.5) gives

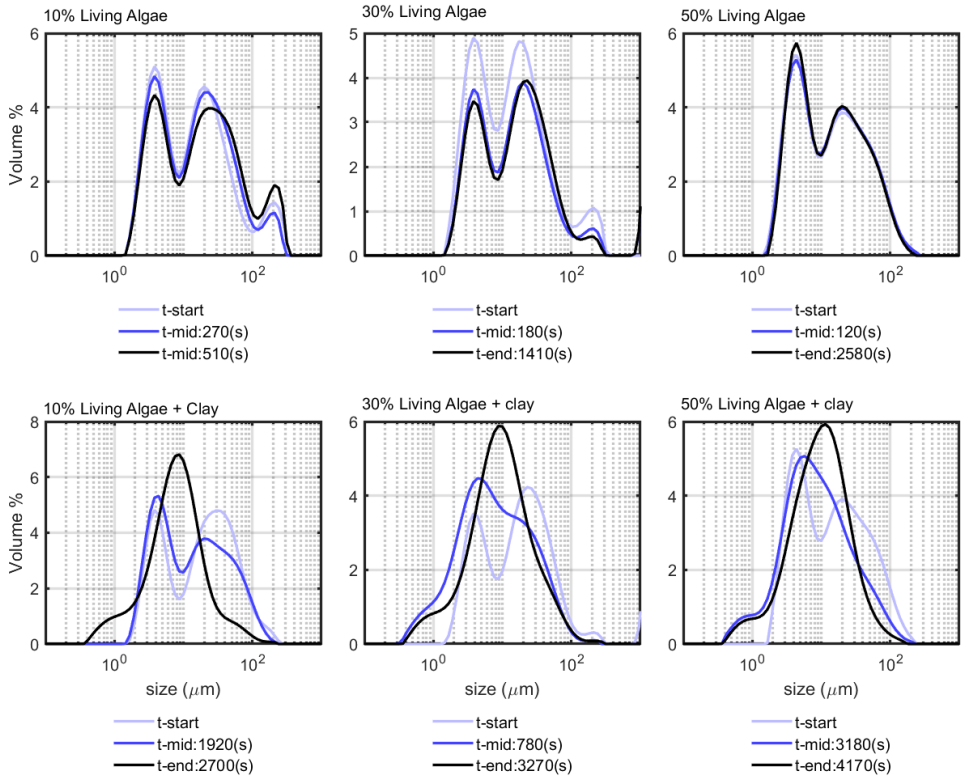

Figure 3.6: Living algae flocculation, the times are given in the legend

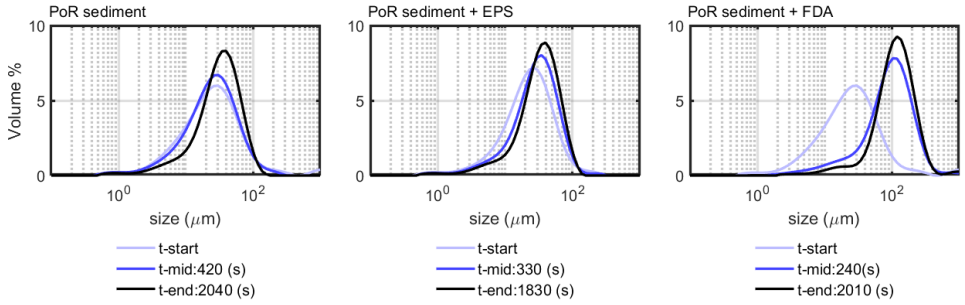

Figure 3.7: PSD of POR sediment (0.2 g/L) without and with natural organic matter flocculation

$$N(t) = \frac{N_\infty}{1 + a_b \exp(-t/\tau)} \tag{3.7}$$

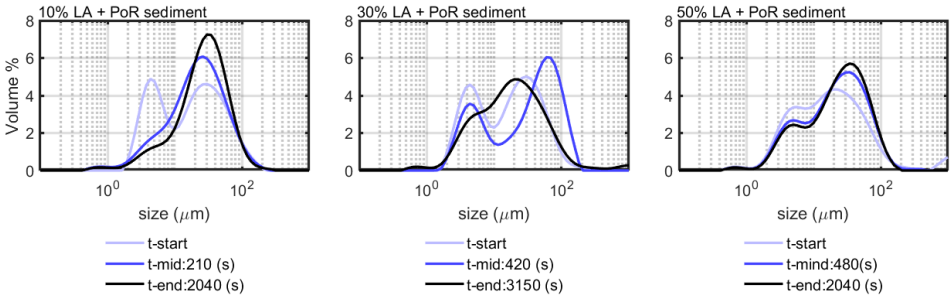

Figure 3.8: PSD of PoR sediment without and with living flocculation

Both eq.(3.6) and eq.(3.7) are sigmoidal funtions and display the same time-dependent behaviour.

The reason why the $d(t)$ term is not necessary here is due to the fact that the flocs do not grow larger than the Kolmogorov microscale and are therefore not prone to coil, which would lead to a size decrease in time. As the shear is constant, neither do the flocs break. The behaviour of the smaller classes in Figure 3.9, reveal pair-wise aggregation, as when the 7 μm concentrations starts to decrease, the 15 μm starts to rise. The characteristic time t-eq defined in the previous section is the largest of the times t_b and t_d found from fitting the size class concentrations.

FLOCCULATION WITH ORGANIC MATTER (EPS)

The experiments of clay with EPS and salts were fitted with the model equation, and the obtained model results are plotted in Figure 3.10, with the corresponding experimental data. The evolution of each size class in time differs significantly from that of the salt flocculation, which highlights the impact of EPS on the flocculation process. The t_b and t_d are different as the floc size does not reach a steady state as discussed in the previous section. The fine classes experience some 'birth' at the start of the experiment, due to the aggregation of smaller classes and are thereafter consumed.

The coarse classes on the other hand show two phases of 'birth'. One is at start of the experiment and is very fast especially in the case of $CaCl_2$, (see Figure 3.10 mid panel, 45 and 60 μm). This 'birth' is well captured in the $MgCl_2$ experiment (Figure 3.10, last row, mid panel: 45 and 60 μm), as the flocculation with $MgCl_2$ is slightly slower than in $CaCl_2$ experiment. After reaching their maximum possible volume concentration the volume concentration decreases again experiencing 'decay'. After several hundreds of seconds, the concentration increases again which can be seen as second 'birth' which is slower than the first one.

This second birth is only fitted for the $CaCl2_2$ case, for which the first birth is not visible (the volume concentrations of the 45 and 60 μm classes do not start at 0) implying that the first birth occurs before the first measurement, within 30 seconds. Both births

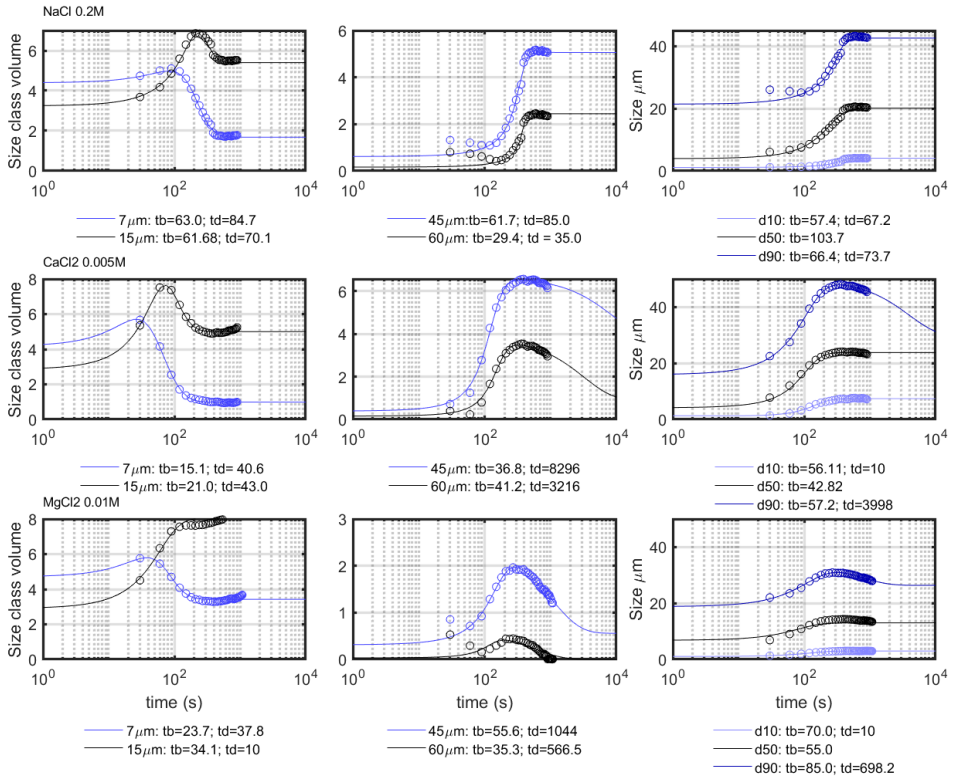

Figure 3.9: Flocculation with different salts as indicated above each graph in the first column. Comparison between the model results (full lines) and the experimental results (circles), for the fines (left panel), coarse (mid panel) and the d10-d90 (right panel).

(as they appear for the $MgCl_2$ case) could be simultaneously fitted without problem by adding a second b(t) function to the equation. While the first birth is related to the aggregation of organic matter with clay, the second birth is related to the coiling of particles of large size into smaller size particles. Breakage and new aggregation are excluded in this case as the shear is kept constant and coiling of elastic organic matter is an established fact [43]. The experimental data for the PoR sediment were also fitted with the model. The model data is compared with the corresponding experimental data in Figure 3.11. The obtained t_b and t_d for most classes differ significantly for the PoR sediment samples, and PoR with EPS samples.

FLOCCULATION WITH LIVING AND FREEZE DRIED ALGAE

Living Algae (LA) flocculation with clay or PoR sediment was fitted, even though the PSD's were bi-modal. The fitted classes for the 30 % LA suspension with PoR and clay are shown in Figure 3.12. The discontinuities in the class volume concentrations are artefacts due to the overlap of two size peaks (since the PSD's are bimodal). The D90

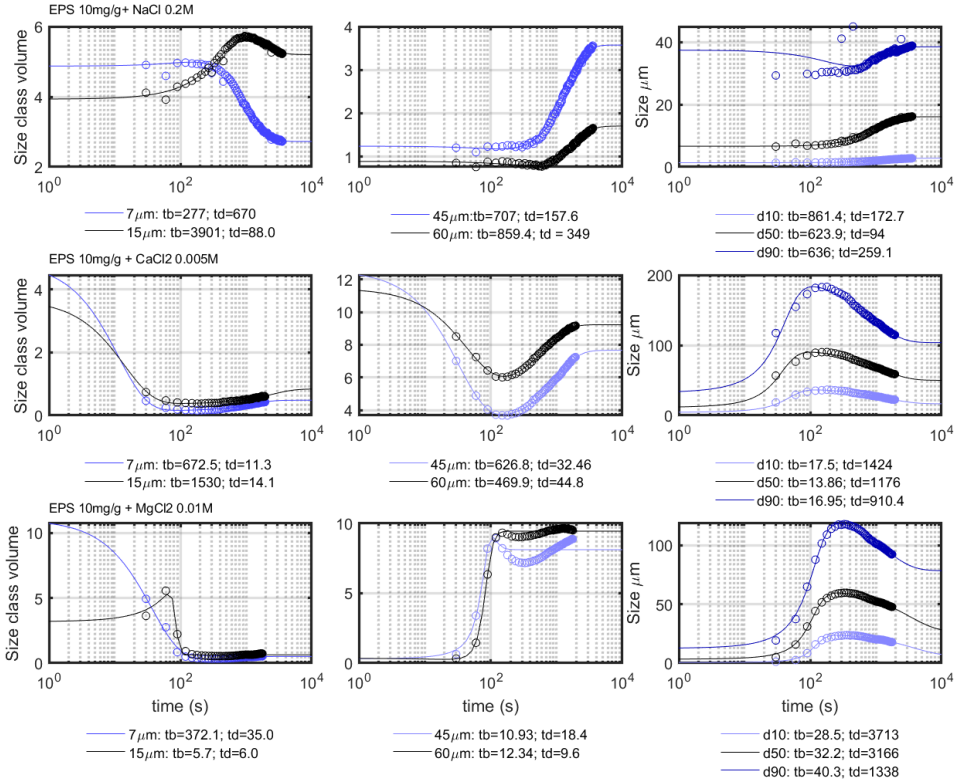

Figure 3.10: Flocculation with EPS and different salts as indicated above the graphs in the first columns. Comparison between the model results (full lines) and the experimental results (circles), for the fines (left panel), coarse (mid panel) and the d10-d90 (right panel).

curves are excluded from the figures as the D90 class is associated with extremely high sizes caused by the fact that the algae particles are very anisotropic. From the behavior of 7 and 15 μm classes, it can be concluded that the flocculation mechanism is different from the salt induced flocculation, as particles do not flocculate in pairs at the onset of flocculation. The small clay particles aggregate with the large algae particles,resulting in the production of large particles. A similar behavior is found for the experiments with FDA, as can be deduced from Figure 3.5.

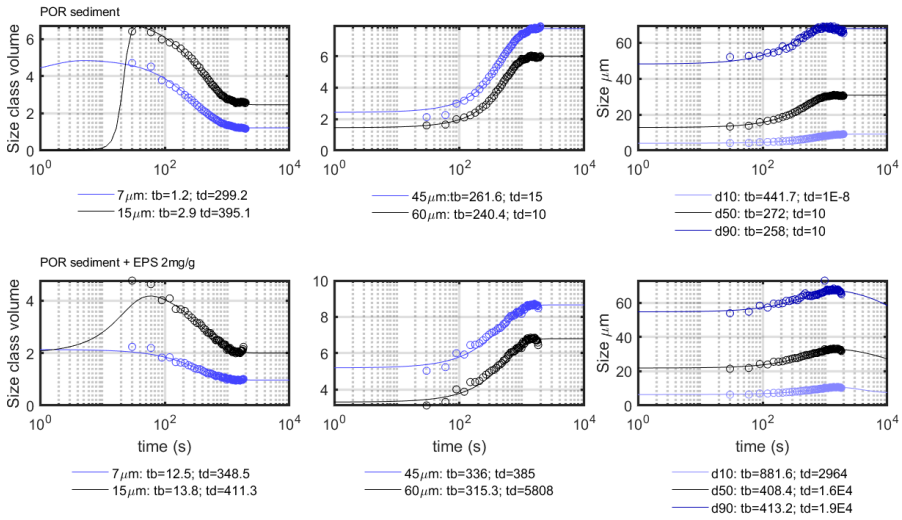

Figure 3.11: Flocculation of PoR sediment with and without EPS, as indicated above the graphs of the first column. Comparison between the model results (full lines) and the experimental results (circles), for the fines (left panel), coarse (mid panel) and the d10-d90 (right panel).

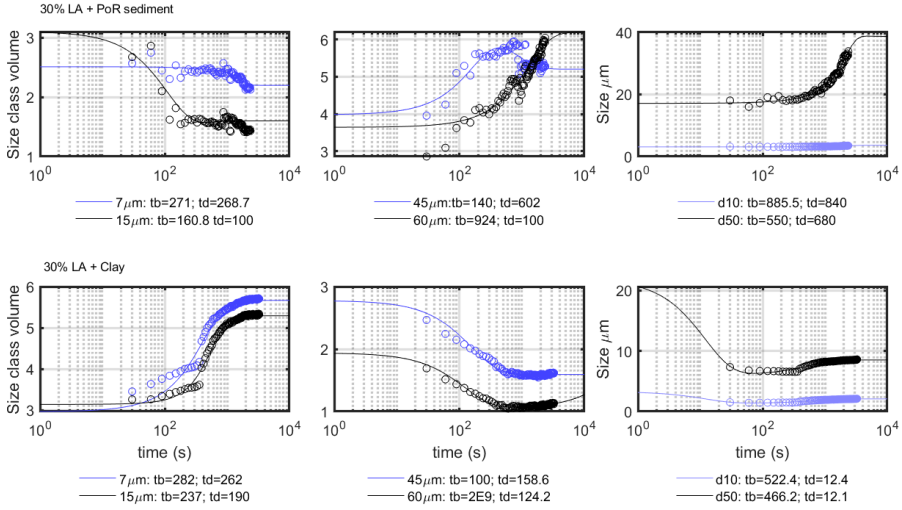

Figure 3.12: Flocculation of PoR sediment with 30 % Living Algae (LA) and flocculation of clay with 30 % LA. Comparison between the model results (full lines) and the experimental results (circles), for the fines (left panel), coarse (mid panel) and the d10-d90 (right panel) for 30 % living algae with PoR (upper panel) and with clay (lower panel).

3.4. DISCUSSION

SALT VERSUS ORGANIC MATTER FLOCCULATION

The flocculation experiments show that with salt flocculation the system achieves an equilibrium size, which can be fitted using only the birth function b(t). This is also a case where the PBE model is known to work perfectly, as it was derived for this case [26]. Flocs are spherical in shape and their density decreases with increasing size (see Figure 2.10). The flocculation mechanism in presence of organic matter differs fundamentally from that of salt-induced one. In salt-induced flocculation, at the onset of aggregation, two fine particles form a pair creating a large particle by electrostatic attraction. The created flocs are fragile and can break or erode by small shear differences to produce the fines. In the case of a time-dependent shear both $b(t)$ and $d(t)$ would therefore be required to fit the data. Both (t) and $d(t)$ are required to fit the organic matter mediated flocculation at constant shear. Indeed the D50 starts to decrease after achieving a maximum size. This decrease is attributed to restructuring and recoiling of the polymer chain that results in densification of the particle after flocculation. Flocs can have different shapes depending on the coiling degree of the long chains high molecular weight polymers and algae strains. For this reason the PBE model coupled with fractal dimension theory [146, 157] do not provide physically meaningful parameters as the flocs can not be treated as self-similar entities.

In presence of organic matter, long polymer chains [28] scavenge a large amount of fines at the onset of aggregation. The flocs are much stronger than the salt-induced ones due to the elasticity of the polymer chain which can coil under shear. Therefore a particle break-up (under very high shear differences) does not produce fines, but smaller flocs [29]. In table 3.2, the characteristics of both flocculation mechanisms are summarized.

Table 3.2: Summary of salt versus organic matter induced flocculation characteristics

Salt-induced	Organic matter-induced
spherical flocs (monomodal PSD)	non-spherical flocs (multimodal PSD)
< Kolmogorov microscale	> Kolmogorov microscale
pair formation mechanism	particles scavenging mechanism
break-up into fines	coiling or break-up into smaller flocs

In view of modeling the mass transfer between classes, two major classes of particles are proposed:

Class 1: Inorganic particles that can be clay, silt and/or sand particles. In theory, salt flocculated particles also belong to this class, because they do not grow beyond the Kolmogorov microscale and they can easily break-up, but for the purpose of the present study, salt induced flocs belong to Class 2. This will be done when salt-induced flocculation is studied in the absence of organic matter.

Class 2: Organic-matter flocculated particles (in the presence of salt). These flocs can grow larger than Kolmogorov microscale, coil and eventually break-up. Inorganic sed-

iment particles are not released from this class, because organic matter will always remain aggregated to the sediment.

These classes can be compared to the classes defined at the end of Chapter 2. There, a Class 3 was defined, which contained only organic matter. This Class 3 plays an indirect role in the (inorganic) sediment balance as its availability will determine whether or not Class 2 will be formed.

Most studies on phytoplankton flocculation [30, 121, 142, 158] do not take the presence of salt in natural waters into account when studying phytoplankton flocculation dynamics. Laboratory studies on salt and organic matter flocculation have used salts and organic matter in separate experiments [159, 160]. In a study that used natural seawater and NaCl-supplemented tap water as control, better flocculation was found in seawater where low density particles of larger size (therefore containing a lot of organic matter) were formed compared to the NaCl-supplement tap water control samples [161]. The transitions between the fresh to saline water in the estuaries and ROFI systems is therefore an important physical condition [162] promoting flocculation of organic matter and sediment particles. This will result in high concentrations of SPM which accumulates near the bed close to the estuary mouth or deltas [163, 164].

INFLUENCE OF THE COMPOSITION ON THE FLOCCULATION RATE

Figure 3.13 shows the 'birth' rate b(t), 'decay' rate d(t) and the total evolution of a size class ($dN/dt = b(t)N - d(t)N$) as function of time for the classes used for three different compositions. This Figure shows clearly that different sample composition results in different flocculation mechanisms.

For the clay and salt flocculation (upper panel of Figure 3.13) for instance the pair forming flocculation mechanism is clear, the fines (7 μm) show first a positive flocculation rate dN/dt for 70s, their volume concentration starts from positive values and go to negative values in less than 500s. The coarse classes functions in contrast, start from positive values taking up the fines, growing through a maximum (the peak of the maximum shifts in time as function of size). After 600s all flocculation rates are zero, indicating that the system has reached steady state.

This is different in presence of EPS where the b(t) and d(t) go through a faster time evolution. The total volume evolution in time for this sample, (the mid panel of Figure 3.13) is also different, the fines show a fast decrease from positive to negative in their volume concentrations. The coarse particles are formed and decayed very fast, therefore their total evolution in time remains close to 0, as they can be taken into larger particles classes. For PoR and LA (lower panel of Figure 3.13), the flocculation rates are different as well. This is due to the bimodal PSD that causes the 7 μm and 60 μm to be constant in time. The flocculation does not take place gradually as it is the case for the clay and salt and salt and EPS flocculation.

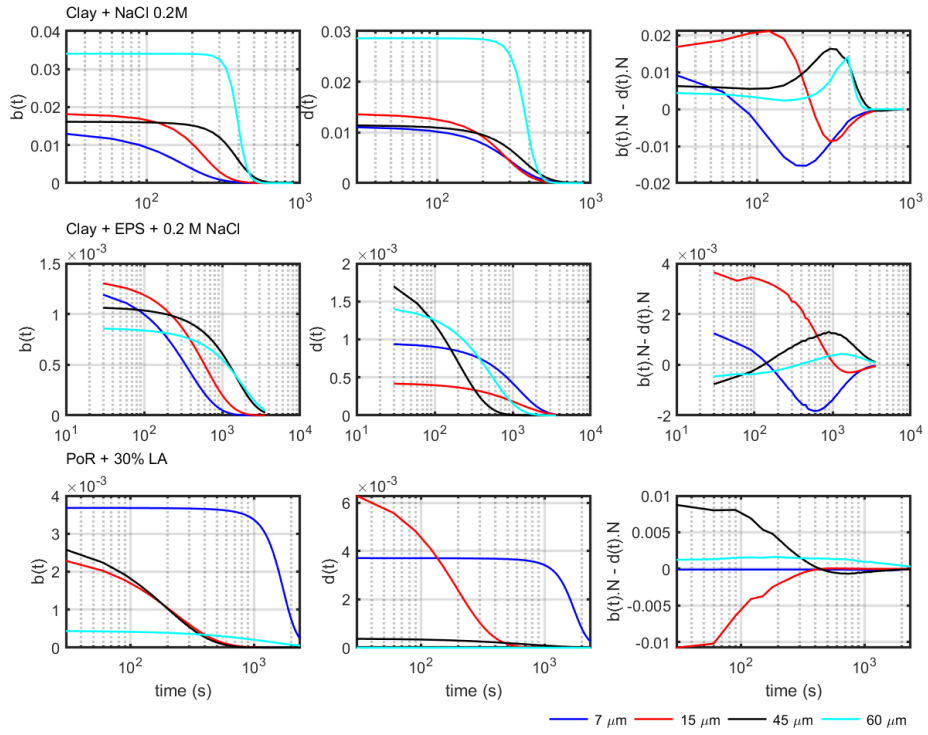

Figure 3.13: The 'birth' rate b(t) (left panel), decay rate d(t) (middle panel) and the total evolution of a class in time: $dN/dt = b(t)N - d(t)N$ (right panel) for three different sample compositions.

COMPARISON BETWEEN MODELS

As has been discussed in [26], the equations 3.1 and 3.2 can also be used to model the particle size evolution as a function of time for any size class. This implies that the equations can be written as:

$$\frac{dL}{dt} = K_A(t) - K_B(t) \tag{3.8}$$

$$\frac{dL}{dt} = [b(t) - d(t)]L \tag{3.9}$$

where K_A and K_B are aggregation and breakup parameters and L a characteristic size. The functions b_t and d_t are given by eqs. 3.3 and 3.4 respectively.

In 1998, Winterwerp proposed the following equation for the time evolution of a size class, with characteristic size L:

$$\frac{dL}{dt} = k_A c G L^2 - k_B G^{(3/2)}(L - L_p)L^2 \tag{3.10}$$

where c is the clay concentration, G the shear rate, L_p the size of the primary particle and k_A and k_B are constants. From eq.3.10 and eq. 3.8 it can be deduced that:

$$K_A = k_A c G L \tag{3.11}$$

$$K_B = k_B G^{(3/2)} L \tag{3.12}$$

The b(t) and d(t) can be compared to the (K_A) and (K_B) in the model proposed by Winterwerp et al. [145, 146]. The difference with our model is that in the Winterwerp model a size $L = L_{eq}$ is obtained when $K_A = K_B$. In our model the b(t) and d(t) are time-dependent functions and decay to zero at very long times, implying that the system, provided that all parameters (concentration, shear, salinity, etc.) are constant over time will always reach a steady state irrespective of the relative values of b(t) and d(t).
In particular, in the case that the characteristic size L is only increasing as function of time, eq. 3.9 reduces to:

$$\frac{dL}{dt} = b(t)L \tag{3.13}$$

the solution of which is:

$$L(t) = \frac{L_{eq}}{1 + a_b \exp(-\frac{t}{t_b})} \tag{3.14}$$

This is the sigmoid function that is used in many research fields, like in biochemistry and pharmacology to model the binding of ligands to macromolecules (Hill-Langmuir equation). Even though, $L(t)$ depends only on the birth function $b(t)$ (no decay), the growth of L is limited in time. In practice this limitation is a result of the depletion in flocculating agent (or ligand in the Hill-Langmuir equation).

Lee et al. used a two-class PBE to model the bimodal particle size distributions measured for marine and estuarine sediments [141]. This model relies on fitted parameters such as collision efficiency for aggregation and breakup, fraction of microflocs created by breakage and fractal dimension of macroflocs, but no parameter is depending on flocculating agent or does account for the fact that particles could change size and shape over time. As it is shown in Chapter 2 bimodality can especially be due to the fact that the composition of microflocs and macroflocs is very different: microflocs are usually composed of clay minerals whereas macroflocs are composed of clay minerals aggregated with organic matter. It is shown in this chapter that aggregation can be limited by the supply and type of flocculating agent which means that the relative ratio between microflocs and macroflocs as well as the floc size are functions of both flocculating agent type and concentration. Shear rate will also limit floc growth. This has not been explicitly studied in this thesis, but general results can be found in [28, 29]. For salt-induced flocculation the floc size will be limited by the Kolmogorov microscale whereas for organic matter-induced flocculation flocs can grow larger than the Kolmogorov microscale but will get denser over time due to recoiling of the polymeric ends. The two-class PBE of Lee et al. has been refined into a three-class PBE by Shen et al. [71].

MASS TRANSFER BETWEEN CLASSES

In this section only the case studied in the laboratory will be discussed whereby no sink and source terms are present. To set-up the mass balance, we make use of the 2 Classes defined in previous subsection. This implies that at start:

$$m_{clay} = m_1(t=0), m_2(t=0) = 0$$

Over time, the clay is aggregating and Class 2 is formed:

$$m_{clay} = m_1(t) + m_2(t)$$

where m_1 and m_2 are the mass of clay within Class 1 and Class 2 per unit of total volume respectively. It follows that:

$$\frac{dm_2}{dt} = -\frac{dm_1}{dt}$$

This is because the m_{clay} does not change in time. The mass transfer between Class 1 and Class 2 can be expressed as the decrease in mass of fine size classes as function of time with a rate:

$$\frac{dm_1}{dt} = -d_1(t) \times m_1 \tag{3.15}$$

$$\frac{dm_2}{dt} = b_2(t) \times m_2 \tag{3.16}$$

Using the clay density and the volumes obtained from the MasterSizer an estimation for m_1 can be done:

$$m_1 = C_1 \times \rho_{clay} \tag{3.17}$$

where ρ_{clay} is the absolute density of clay (2600 kg/m^3). We have:

$$C_1 = \frac{V_1}{V_{tot}} \tag{3.18}$$

where V_1 is the volume occupied by Class 1 (fine particles) and V_{tot} is the total volume. The static light scattering device expresses concentrations in volume % of the total volume of classes V_{class}, which is the sum of all the volumes of all the size classes. The total concentration (the total volume of particles detected by the MasterSizer divided by the total volume of fluid) is given by:

$$C_{tot} = \frac{V_{class}}{V_{tot}} \tag{3.19}$$

The MasterSizer software gives the relative volume of each class i.e. V_1/V_{class} in % volume and the total volume concentration C_{tot} (mL/L).

In Figure 3.14, the dm_1/dt for the fine classes is plotted. The curves indicated by $< 5\mu$, $< 7\mu$m and $< 15\mu$m represent the masses evaluated according to eq.3.17 whereby V_1 is the

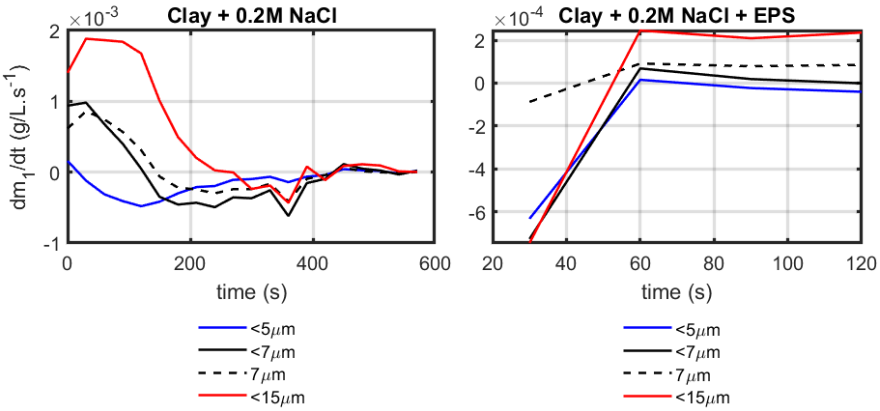

Figure 3.14: Decay rate of the fine classes (dm_1/dt) as function of time for salt-induce (0.7 g/L clay + 0.2 M NaCl), left panel and organic matter induced (with EPS), the right panel.

sum of all the detected volumes smaller than 5, 7 or 15 μm respectively. The dashed curve 7 μm represents the mass corresponding to the volume detected for the 7 μm class. The difference in decay behaviour of salt-induced and organic matter-induced flocculation is clear. The 7 μm class is in good approximation representative of the time evolution of the mass of the finer classes (< 7 μm) for salt induced flocculation. The < 5 μm in that case displays only decay as the fines smaller than 5μm are mainly consumed leading to $dm_1/dt < 0$ for all times. As expected, the < 7 μm class is depleted before the < 15 μm class shifting from $dm_1/dt > 0$ (accumulation by aggregation of small particles into < 7μm particles) to $dm_1/dt < 0$ (depletion by aggregation of < 7μm particles into larger flocs).

In the sample with EPS in contrast, the flocculation mechanism is completely different. At onset of the experiment (t = 30s), all of the fine classes are depleted and large flocs are produced. The particles size changes due to recoiling during the rest of the experiment. The estimation of dm_2/dt is complicated, as it requires to have an estimation of the density $\rho(t)$ and $V_2(t)$ of Class 2, which can be time dependent due to recoiling of the particles. For the present investigation, it was decided to use:

$$m_2 = C_2 \times \rho \tag{3.20}$$

$$C_2 = \frac{V_2}{V_{tot}} \tag{3.21}$$

where V_2 represents the volume of the D50 class. The density ρ was kept constant with a value of 2600 kg/m^3 (clay mineral). Figure 3.15 shows the m_1 (mass of the fines), m_2 (mass of the D50) and the total mass, which is obtained by $m_1 + m_2$ as function of time for both clay + 0.2M Nacl and with EPS samples.

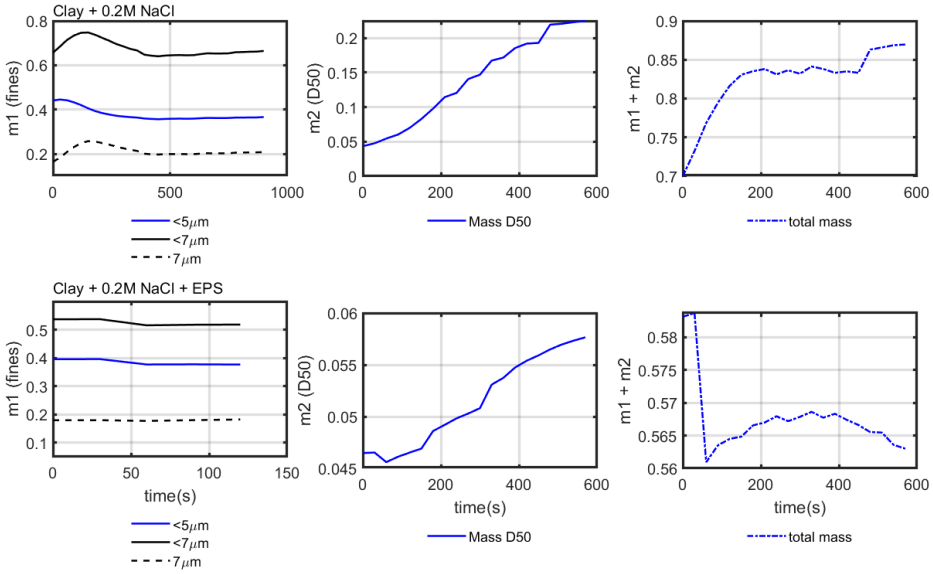

Figure 3.15: Mass balance for two samples: 0.7 g/L clay + 0.2M NaCl, the upper panel and clay 0.7 g/L + 0.2 M NaCl + EPS (10 mg/L), the lower panel. The total mass is calculated using the < 7 μm particles.

The total mass should remain constant as the clay concentration does not change in the system. It can be seen that defining the <7 μm class as 'Class 1' and the D50 as 'Class 2' leads to a relatively constant $(m_1 + m_2)$ over time.

TOWARDS IN SITU FLOCCULATION MODELING

One important process in flocculation is the mass transfer between Class 1 and Class 2. This transfer occurs in timescales that are short compared to the numerical timescales in sediment transport models, in the case of organic matter based flocculation which is the most important flocculation, in situ. In order to calibrate the model with in situ data, the following parameters are required:

1. The mass of primary particles in the system. This mass can be assessed by sampling in situ, removing the OM and weighting. Note that the calibration of the OBS is most often done on the total (organic and inorganic) suspended sediment concentration.

2. The relative volume concentration of Class 1 and 2 and the total volume of measured particles per unit of volume (C_{tot}), this can be obtained from the LISST and OBS data.

3. The concentration and type of organic material (Class 3 in Chapter 2). Quite some in-

formation can be obtained from Chlorophyl-a measurements [78], but the link between organic matter models and sediment flocculation models remains an open topic of research.

This calibration does not give the flocculation rate. In order to estimate flocculation time scales, one can only rely on size time series determined by lab measurements. The important parameter lacking for numerical transport models is the average Stockes' settling velocity which can at present only be estimated on board by settling equipment.

3.5. CONCLUSION

In this chapter flocculation experiments were presented and modeled. These experiments aimed to mimic the natural water flocculation process as much as possible, using natural organic matter EPS and FDA and living algae, *Skeletonema Costatum*, in seawater. The D50 did not exceed the Kolmogorov microscale, in salt-induced flocculation experiments in agreement with other studies [28, 146]. Divalent salts flocculated the clay more efficiently than monovalent salts at short timescales. There was no breakage as the shear was kept constant, and this caused the system to achieve a steady state condition.

The flocs with natural organic matter reach higher sizes than the Kolmogorov microscale also in agreement with other studies [137]. Flocculation experiments with EPS and FDA resulted in high D50 of about 70-100 μm and it was demonstrated that the floc size is strongly composition dependent. Therefore for modeling flocculation in situ, the availability of organic matter has to be known. This should be done by analyzing the water column composition in the laboratory as constituents such as EPS and FDA can not be visualized by in situ techniques. Living organic matter content and its availability are depending on the different biological species that are variable on seasonal basis.

The natural EPS and FDA, however do not flocculate easily with the clay, despite their high stickiness and large sizes [140]. This has to do with the fact that these polymers are mostly negatively charged particles and hence experience an electrostatic repulsion with the negatively charged clay. For this reason the presence of salts, and in particular cations is crucial, as these cations will help bridging the polymer and clay [165]. This is why the divalent salts, having two charged sites are more efficient in the flocculation process. Therefore estimating salt concentrations and identifying salt types is important for modeling flocculation in situ. Combinations of organic matter and salt provide the most efficient flocculation by shortening the flocculation timescales. Model fitting results have shown strong dependency of flocculation timescales (specially t_b) on suspension composition.

For sediment transport models the particles can be divided into two major classes. The first class (Class 1) contains the fine particles which can only flocculate (not break or recoil). Salt induced flocs can belong to this class because they do not grow beyond the Kolmogorov microscale and their breakage returns the fines into Class 1. The effective density of Class 1 can be assumed to be equal to the one of sediment minerals (about

2600 kg/m^3). The second class (Class 2) contains organic matter induced flocs with a size and effective density range. This range can be large as shown in Chapter 2. The breakage of these flocs does not return Class 1 mineral fine particles but microflocs, belonging to Class 2.

Knowing the source and concentration of the primary particles (Class 1) in the system, and flocculation agents such as organic matter and/or algae species and salts, a mass balance could be established whereby the mass concentration of the fines decrease in time by uptake, and the mass concentration of the mean size (D50 class), increases as function of time. The model parameterization showed that the flocculation time-scales are too short (in order of seconds to minutes), to be relevant in large-scale sediment transport models. These timescales are however, found in jar test experiments where the residence time is infinite and therefore do not correspond to in situ conditions where differential settling can play role [78]. This is why a more through analysis of in situ data is required, based on long time series, which will be the topic of the following chapter.

4

THE ROLE OF ORGANIC MATTER ON SUSPENDED PARTICULATE MATTER DYNAMICS IN THE RHINE REGION OF FRESHWATER INFLUENCE

In this chapter we investigate the Suspended Particulate Matter (SPM) source and dynamics in terms of resuspension and advection in the mid field region of the Rhine Region Of Freshwater Influence (Rhine-ROFI). In this area of the Rhine-ROFI, the sediment transport mechanisms are governed by the Rhine freshwater plume originating from the Rhine-Meuse estuary and propagating towards the coast in northward direction. During the neap tides strong salinity stratification and low turbulence result in SPM accumulation at the bottom forming a fluff layer, if the weather is calm. At spring tides in contrast, a fast switch between stratified and well-mixed water column conditions caused by tidal mixing results in resuspension of SPM. The freshwater front transports algae and biological species and related organic matter from the estuary into the coastal area. These algae and organic matter debris can interact with sediment, contributing to SPM formation and accumulation.

The SPM near the bottom is analyzed in term of concentration, particle size and shape in correlation with frontal dynamics and weather conditions for two seasons of winter 2013 (12 February -0 7 March) and autumn 2014 (17 September - 06 October). Stormy weather conditions play an important role in resuspending fine sediment from the bed. Seasonal variations change the algae and phytoplankton species and biogenic organic matter availability which contribute to the observed changes in the particle size over time.

Particle Size Distribution (PSD) and mean particle diameter are correlated to water column stratification, current direction and bed stresses to differentiate between resuspended and advected particles.

An article based on this chapter is in preparation.

The interactions between natural organic matter and algae were studied under controlled laboratory experiments in Chapter 3. It was found that algae and organic matter interact with clay particles and natural sediment and that salt plays a crucial role promoting their flocculation. Consequently the transitions between fresh and saline water, that cause stratification in the Rhine-ROFI, play an important role in SPM formation and dynamics in the Dutch coastal area.

In the present chapter we are analyzing SPM particle dynamics in correlation with the hydrodynamics based on in situ data acquired over periods of several weeks. The in-situ observations are given in terms of Particle Size Distribution (PSD), shape and concentrations during the late winter of 2013 and autumn of 2014 using LISST 100X (Laser In-Situ Scattering and Transmissometry) in conjunction with LISST-HOLO (Submersible Digital Holographic Camera). This analysis aims to firstly, differentiate between the advected and resuspended particles by short time scale analysis, based on spring-neap tidal cycle. Secondly, the aim is to analyse the impact of organic matter and biological species on SPM dynamics based on availability of organic matter and biogenic species in winter and autumn.

The ultimate goal is to get a better understanding of SPM dynamics and fluff formation, whereby the role of organic matter is discussed, based on available literature and the in situ data analysis. At present, sediment transport models are primarily calibrated for the clay mineral fraction settling and transport, while the organic matter content in the river-estuary mouth and coastal area plays a crucial role in SPM dynamics.

4.1. BACKGROUND

FRESHWATER PLUME INFLUENCE

River plumes play an important role in terms of sediment transport and have an enormous influence on the Suspended Particulate Matter (SPM) particle properties and dynamics. Tidally dominated river plume fronts are occurring every tidal cycle and stratify the water column by generating freshwater lenses. The Rhine river plume transports phytoplanktonic species such as algae and related organic matter 100 km along the dutch coast [84, 87, 94, 95, 163]. These particles can be advected by the freshwater front along the coast [32–36].

Studies on phytoplankton and biogenic species have shown tidal fluctuations with tidal currents and spring-neap tidal cycles in the Dutch coastal area and southern North sea [89, 166]. These species enrich the water column with organic matter content that can interact with suspended sediment and the created flocs can be transported over long distances northward the Rhine-ROFI due to their low densities [167]. This suspended matter, algal species and sediment can be temporary trapped in the halocline, at the interface between fresh and saline water layers. The possibility of accumulation of particles at the interface of different density water layers was also experimentally confirmed [162, 168]. The trapped particles can aggregate at this layer especially during slack water [32, 35], and the decoupling of surface layer from the bottom layer of the water column

impacts the SPM properties within these layers [169]. Jago et al. found different concentrations and particle sizes in the surface and bottom layer of a thermally stratified water column [170]. The relation between salinity stratification and SPM particle properties are to our knowledge poorly studied. The presence of different salt types with different concentrations in both fresh and saline water layers is crucial in SPM formation by aggregation.

In the Rhine-ROFI region that covers the Dutch coastal area, the near bottom sediment transport is mainly determined by the freshwater front dynamics which impact the hydrodynamics and sediment dynamics close to the bed. The interaction between tidal asymmetry, gravitational circulation, and river freshwater discharge makes the hydrodynamics in this part of Rhine-ROFI quite complicated [17, 98, 99]. The freshwater front is determining SPM dynamics and sediment transport in the shallow coastal region of the Rhine-ROFI. Different 'cross-shore' sediment transport mechanisms depend on the neap-spring tidal difference in stratified conditions. These mechanisms can be defined as frontal pumping during spring tides, stratified tidal transport during neap tides and storm transport during the stormy weather conditions [17, 98].

SEDIMENTOLOGY

The particle size analysis of the central part of Dutch coastal area, shows a mixture of fine and coarse sand in the range 175-325 μm. The coarse fraction > 325 μm is dominant close to the shore between Hoek van Holland and IJmuiden (Figure 1.2). The finer fraction containing a clay and silt fraction (< 50 μm -160 μm) is seaward located. This fine grained material originates mainly from the rivers (Rhine, Meuse) [171]. Fluvial suspended particles from the Rhine are composed of mineral particles aggregated with bacterial exopolymeric substances and organic matters debris. Eisma [172] and later Lartiges et al. [42] confirmed that these aggregates are formed within the river and cannot be simply related to particles inherited from eroded soils. From the fluvial system to the coastal region, the composition of flocs changes under the influence of coastal microorganisms present in the water and the change in salinity. The tidal resuspension and settling are the cause for the northward transport of SPM by the Rhine river plume.
De Nijs et al. have found that high concentrations of (inorganic) clay mineral settled and deposited at Botlek harbour at the mouth of Rotterdam Waterway, at the tip of the salt intrusion wedge. The wedge is associated with the presence of the Estuarine Turbidity Maximum zone (ETM) of the Rhine-Meus delta [173]. The cross-shore transport mechanism caused by the Rhine-ROFI appears also to contribute to the presence of the turbidity maximum in the area [163]. The clay/silt sediment fraction is tidally resuspended and settles again in the ETM where it accumulates by advection into the area. Differentiating between resuspended and advected sediment particles can be done in different ways. Li et al. estimated horizontal SSC time series, and vertical SSC profiles and decoupled advection-induced SSC and resuspension-induced SSC using a box model [174]. Another study [175] differentiates between the eroded material by analyzing the particle size distribution and settling velocity and Stokes driven effective density. They found that cohesive sediments are generally eroded as aggregates and not as single particles. These eroded aggregates have higher effective densities and higher settling velocities,

compared to not eroded particles [175].

Fluff material at the top of sediment bed can resuspend and accumulate on a tidal and seasonal basis. This fluff layer is easily erodible by relatively low bed stresses and can develop by settling and deposition during the calm periods combined with biological activity at the bed [170, 176–178]. On seasonal basis, Fettweis and Baeye who studied the southern North Sea, have found that SPM floc size and settling velocity differ seasonally rather than by SPM volume concentration. This is mainly due to the seasonal microbial activity which is the main driver of the observed variation in the floc size and settling velocity [179].

4.2. SETUP AND METHODS

The STRAINS I and II projects conducted moorings at two different seasons in late winter on 12 February to 7 March of 2013 (STRAINS I) and in autumn, 17 September to 10 October, of 2014 (STRAINS II) to study the impact of salinity stratification on the sediment transport along the Dutch coastal area of Rhine-ROFI. Both measurement campaigns covered spring-neap tidal cycles and a stormy period was captured at each season during the neap tides. The moorings were deployed at 12m and 18m depth, corresponding to 2 km and 6.5 km from the shoreline 10 km from the Port of Rotterdam and seaward of the Sand Engine (Figure 1.2). In this study, the 12m mooring data is analysed. A detailed description of the deployments is given in previous studies [17, 98, 99, 180] and it is not repeated here. These previous studies focused on the hydrodynamics of the ROFI system and the correlation between the frontal dynamics and sediment fluxes, using a variety of instruments. Water velocity profiles were measured using ADCP, SSC profiles with OBS, bed elevations with ABS (Acoustic Backscatter System), water column salinity profiles by CTD. The wind speed and directions, the significant wave heights and river discharge were obtained by the Dutch weather organizations KNMI and Rijkswaterstaat at Hoek van Holland (close to the Rhine-mouth).

LISST 100X

LISST 100X (Laser In-Situ Scattering and Transmissometry) was deployed in both 2013 and 2014 moorings at 0.95 meters above the bed (mab) and 1.65 mab respectively. LISST 100X uses laser diffraction to determine the volume concentrations of particles in 32 logarithmic spaced effective spherical diameter classes (PSD) ranging for the 100X type from 2.7 to 460 μm [59, 60]. The mean particle diameter is calculated by eq. (4.1):

$$D_{mean} = \frac{\Sigma(V_k \times D_k)}{\Sigma V_k} \tag{4.1}$$

where V_k and D_k represent the measured volumes and given the size of each class k.

LISST HOLO

LISST-HOLO (Submersible Digital Holographic Camera) was also deployed at the 2014 mooring at 1.4 mab. LISST- HOLO is an in-situ digital holographic technology that uses solid-state diode laser at 658 nm and 4.4 μm pixel size digital camera (1600 × 1200 pixels). The raw data is converted into equivalent spherical diameters in the size range of 25 - 2500 μm, within 50 log spaced size classes.

The LISST-HOLO data is available for the first period of the measurement (neap tide calm weather). As the storm initiated, the LISST-HOLO stopped working due to high suspended sediment concentration. The LISST-HOLO data, however gives useful insight on the particles shape during the neap tide and initiation of the storm. Combining the shape information obtained from the LISST-HOLO pictures with the PSD obtained from the LISST 100X allows to identify the impact of the shape on the PSD measured by LISST 100X. Taking the PSD peak modality as an indication of the shape of the particles (see Chapter 2), we can make an hypothesis on the composition and subsequently the source of the SPM.

SALINITY DIFFERENCE ΔS

The interaction between the PSD and the water column salinity stratification is analyzed by comparing the PSD at salinity differences. The salinity difference ΔS is defined as the difference between the bottom and surface salinities in PSU (Practical Salinity Units). The ΔS is taken as a measure for the degree of stratification.

4.3. RESULTS AND DATA ANALYSIS

As the Rhine-river plume is a tidal dominated plume, its frontal propagation dynamics differ on spring-neap tidal cycles. This results in different salinity stratification during each tidal cycles. In addition, weather conditions such as wind and wave activities impact the propagation of the front and its dynamics (see section 2.5).
During neap tides when the weather is calm with low mixing forces, strong fronts stratify the water column for long periods of the day. In contrast during spring tides, the water column stratification holds for short periods due to fast switches between stratified and well mixed conditions. This difference in frontal dynamics impacts SPM source and transport. In this section, we describe the observations for each season (autumn, winter) separately. We start with autumn 2014, because the LISST-HOLO was available only for this season. The second spring tide data of autumn 2014 are discarded due to bio-fouling.

4.3.1. AUTUMN 2014, NEAP TIDE

CALM WEATHER CONDITIONS

The first recorded neap tide (days 260 - 267) starts with a period of calm weather conditions (days 260-264 weather data are shown in Appendix A). During these days, the salinity stratification is strong, caused by front arrivals at the surface that divide the water column into layers of fresh and saline water (Figure 4.1a). The SSC concentrations measured with OBS over the entire water column were generally low, however OBS can

not properly record the organic matter or the algae species which are semi-transparent and have low densities, as it is calibrated with clay mineral particles [17]. At the near bottom a higher concentration peak is detected with both OBS and LISST 100X at specific periods of time that appears with a time lag of 1.0 - 1.5 h after the front arrival, Figure 4.1b. This peak cannot be attributed to local resuspension, because the current induced bed stresses (Figure 4.1c) are too low, as was stated by Flores et al. [17]. The mean diameter calculated from the LISST 100X is between of 150 - 200 μm and it correlates with the cross-shore current velocity (Figure 4.1d).

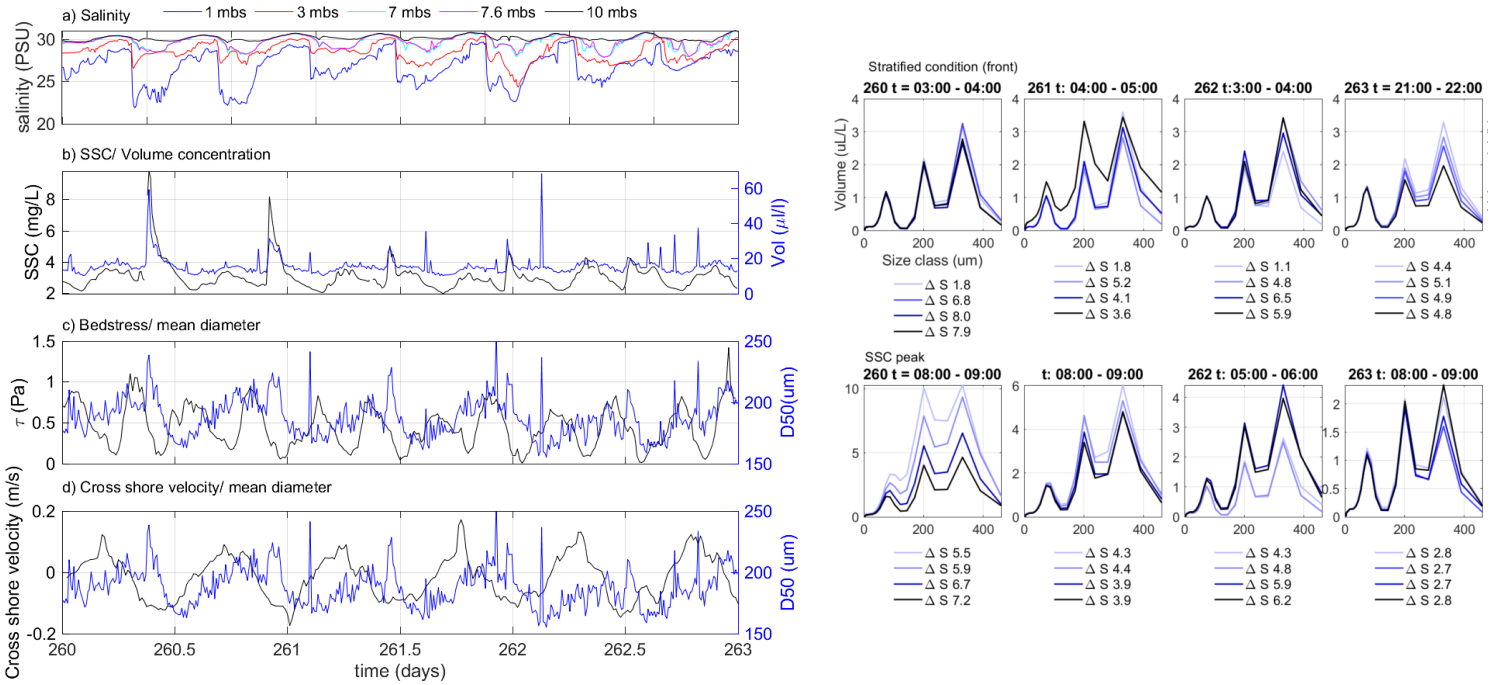

Figure 4.1: First recorded neap tide of autumn 2014 campaign: hydrodynamic conditions are obtained from [17], and the corresponding PSD obtained from the LISST 100X data. The ΔS (PSU) given in the legend is the difference between bottom and surface salinity and hence a degree for the stratification.

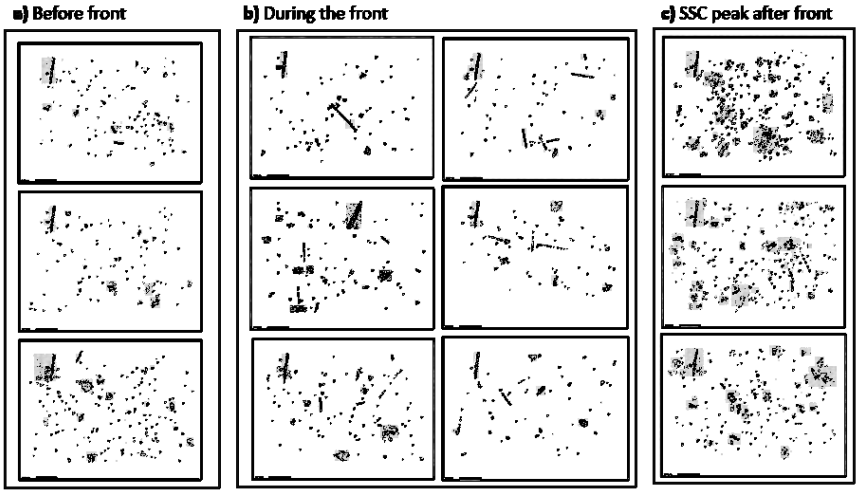

Figure 4.2: LISST-HOLO pictures during the calm weather period of the first recorded neap tide: a) before, b) during the frontal passage and c) during high SSC peaks occurring 1.5 hours after the frontal passage.

The observed PSD's are multimodal during these calm weather days of the neap tide. Figure 4.1 right panel shows the PSD during the frontal passage (upper row), and during the high SSC peak (lower row), for these days. These trimodal distributions are known to be caused by the presence of elongated particles (see Chapter 2). These particles are algae and other biological species and organic matter which not only can have elongated shapes but also a low density, enabling them to travel through the water column in the form of cell strings [65, 67, 181].

The presence of elongated biological species is also confirmed by the LISST-HOLO measurements. Before the front arrival (Figure 4.2a), the LISST-HOLO pictures show much less biological species and elongated particles before and during the front then 1.5 hours after. This occurred for three consecutive days of neap tide calm weather period. During the high SSC peak, however, the LISST-HOLO shows particles with different sizes and structures indicating different composition, such as open structures with low effective density, elongated particles and very dense almost spherical particles (Figure 4.2c). The density of the particles was estimated thanks to additional video microscopy experiments performed on board, as detailed in chapter 2. This high near bottom SSC peak is not significant in terms of quantitative sediment concentration, because it is still much lower in concentration than the SSC peaks found during the following periods of stormy weather or spring tide with high SSC [17].

FROM CALM WEATHER TO STORM

After these typical neap tide days, the weather conditions changed to storm (days 264 -266) with high wind speeds from the north and high wave heights (Appendix D). The water column turned to well mixed and the stratification broke down (Figure 4.3 a). The

near bed SSC increased up to 200 mg/L (Figure 4.3 b). The total bed stress (current and wave induced) increased due to wave action. The increase in the bed stress coincided with a decrease in the mean diameter (Figure 4.3c). The mean diameter started to decrease gradually at day 264, as the cross shore velocity increased in onshore direction, and decreased in offshore direction (Figure 4.3d).

The PSD measured during the front three hours before the storm initiates (Figure 4.3 right panel, upper row), is still sharply multimodal, while at the high SSC peak of the day (the lower row of this Figure), the measured PSD is less multimodal. This gradual transition from multimodal to monomodal is analyzed in more details with the last available LISST-HOLO measurements. In Figure 4.4a, the LISST-HOLO shows the particles measured during the front arrival before the storm and corresponding PSD obtained from the LISST 100X which is multimodal.

When the storm initiates at around 06:00 am (Figure 4.4b), the LISST-HOLO shows substantially higher concentration of particles of different size and shapes. This is also reflected in the PSD measured at this time, which is less multimodal but the volume concentration is still not very high and bed stresses are about > 2 Pa. As the storm proceeds (Figure 4.4c), and the bed stress increases gradually, the multimodality of the PSD decreases and the volume concentration increases, until the PSD turns into completely monomodal at bed stresses > 5 Pa, with high concentrations during the very well mixed conditions with low ΔS (Figure 4.4c-d). There are no LISST-HOLO measurements for this time period, because of the high SSC during the storm, that caused instrument saturation.

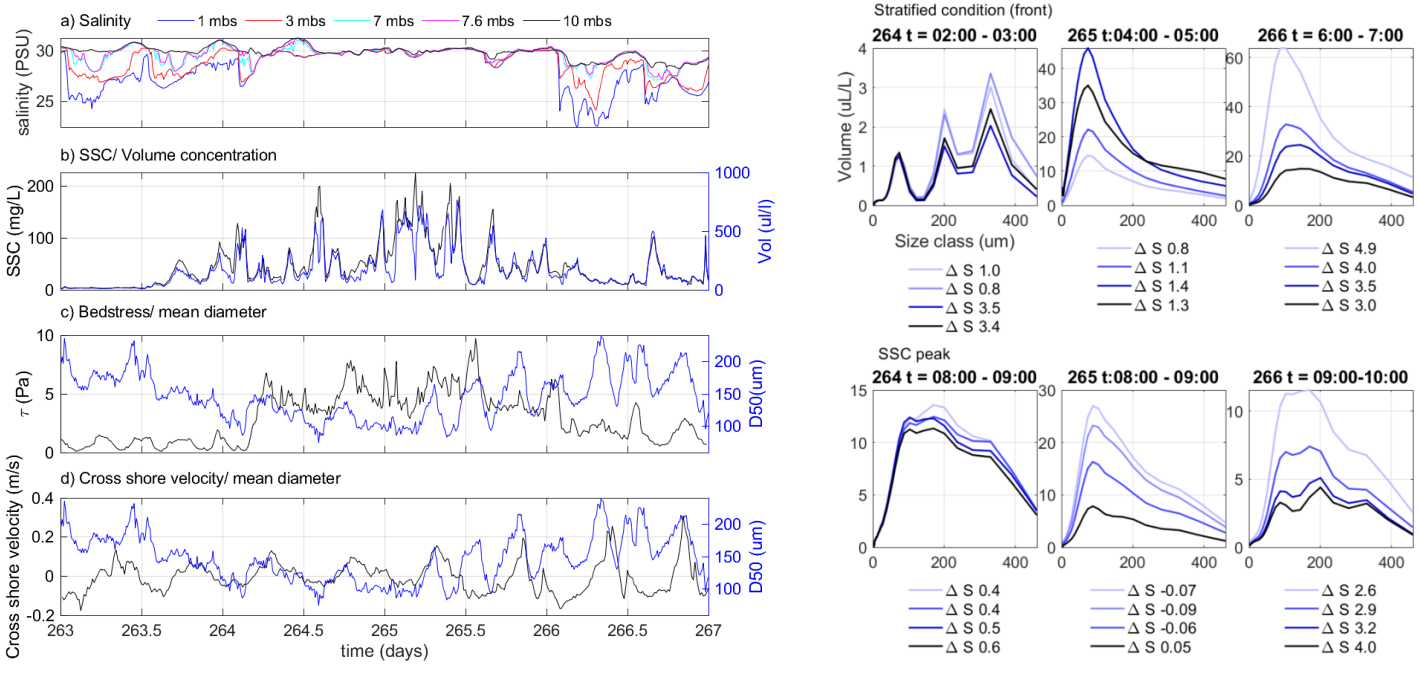

Figure 4.3: First recorded neap tide of autumn 2014: storm weather conditions and hydrodynamics obtained from [17] and corresponding PSD obtained from LISST 100X measurements.The ΔS given in the legend, represents the degree of stratification.

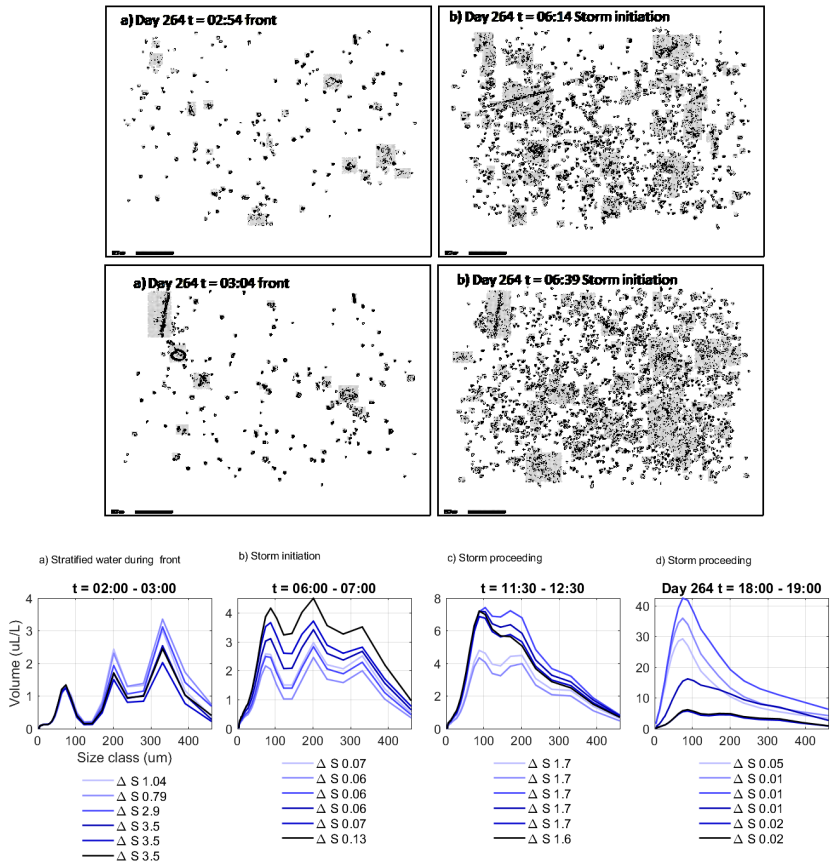

Figure 4.4: First storm day of autumn 2014 neap tide: Storm initiation and proceeding, comparison between the PSD obtained from LISST 100X and pictures obtained from LISST- HOLO

The second neap tide of the measurement period (days 274 - 280, data are shown in Appendix A and B), is comparable with the first one in terms of weather conditions and salinity stratification. The near bottom sediment concentrations are low during the fronts and relatively low bed shear stresses coincide with a high mean diameter indicating advection of large particles. From day 278 until the end of this period slightly higher wind and wave activities and a weaker stratification pattern was observed. These conditions resulted in higher bed stresses and higher SSC with lower mean diameter, indicating resuspension of finer, but denser particles.

The observed PSD's are mainly trimodal as they were during the first neap tide. However, there are sometimes bimodal PSD's observed especially during the sudden decrease in salinity at the front arrival. This might be caused by a near bottom cross-shore low tur-

bulent peak, as during the spring tide [17] (see section 4.1) which induces a resuspension of the fluff layer. Bimodal distributions turn to trimodal again as the water column stratifies again and different salinity layers are fully developed. As the well mixed periods of the water column are very short before the stratification period at the next front, the PSD is barely changing to monomodal. However monomodal distributions are observed at day 278, which is a windy day with a wind speed of almost 15 m/s and slightly higher significant wave heights that contribute to water column mixing (see Appendix A and B for the weather data and second neap tide data).

4.3.2. AUTUMN 2014, SPRING TIDE

During the spring tide of the autumn season (days 267 - 273) the weather conditions are normal with low to moderate wind speeds and low significant wave heights. The wind directions is downwelling favorable and forces the front coast-wards (Appendix A). This causes the front to contribute to the cross-shore transport of the sediments. The water column switches between stratified and well mixed conditions, with shorter periods of stratification by tidal forcing (Figure 4.5a).

Near bottom SSC is higher than at neap tides, with a high SSC peak that appears 0.5 h after the front arrival (Figure 4.5b). The mean diameter is correlated with the bed stress (Figure 4.5d) and high mean diameters coincide with high bed stresses at days 267 to 270. The mean diameter correlates with the cross shore velocity as well (Figure 4.5d). However for the rest of the period (days 270 - 272), the correlation between the mean diameter and bed stress is inverse. High mean diameter coincides with low bed shear stresses and vice versa (Figure 4.5e). The PSD's for these days fluctuate between multimodal, bimodal and monomodal (Figure 4.6). For this period the bed stresses are in phase with the cross shore velocities.

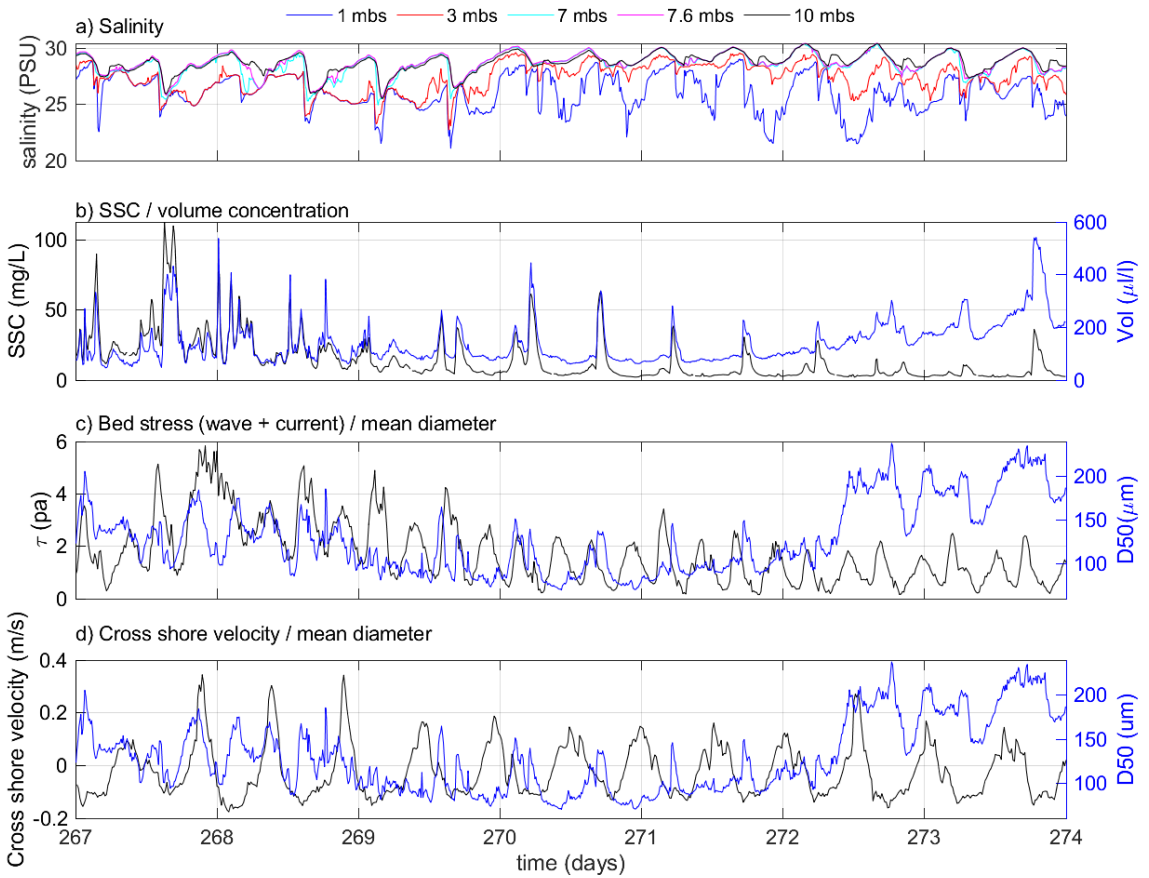

Figure 4.5: First recorded Spring tide of autumn 2014, Weather and hydrodynamic conditions obtained from [17] and the corresponding mean diameter calculated from the LISST 100X data

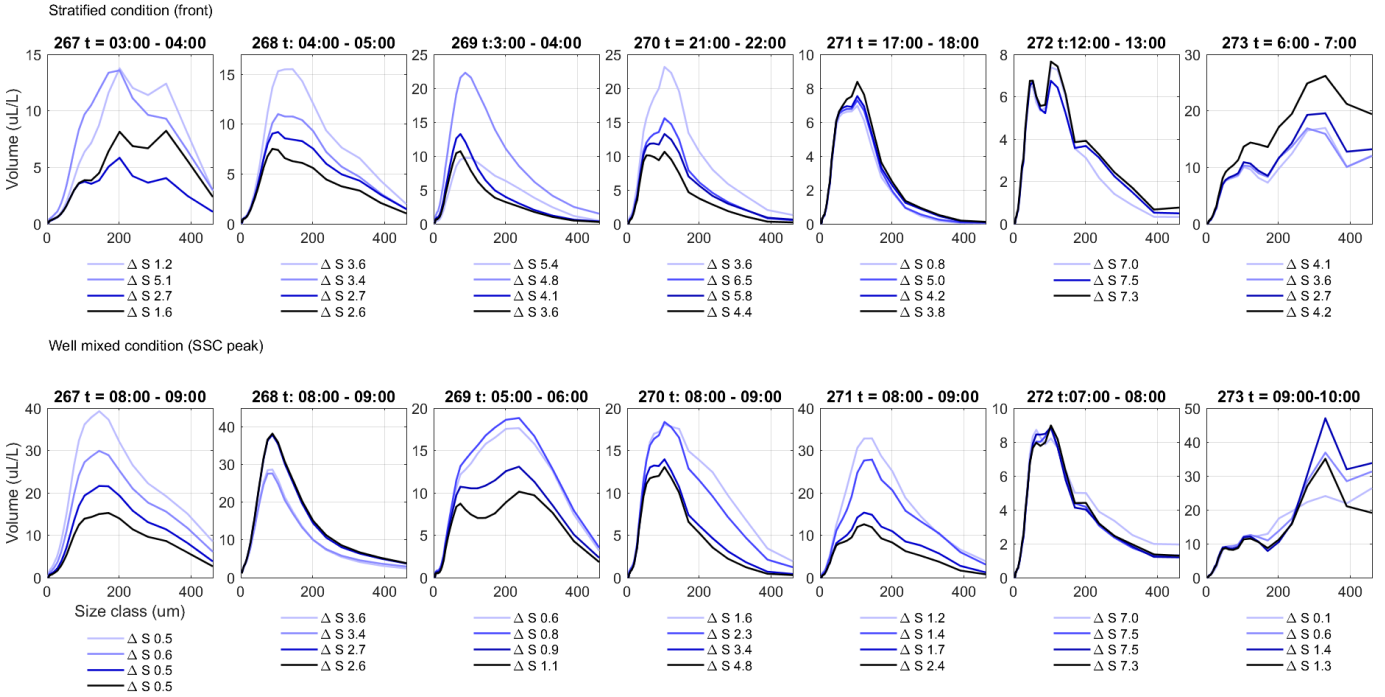

Figure 4.6: The PSD of first recorded Spring tide of autumn 2014, from LISST 100X. The ΔS given in the legend, represents the degree of stratification.

4.3.3. WINTER 2013, SPRING TIDES

The winter measurement campaign of 2013 covered almost two spring-neap tidal cycles in February and March (days 45-66). The weather conditions were normal during both spring tides (Appendix C). Wind speeds were generally moderate with some windy days in between, consistently from the northeast almost during the whole measurement period. These upwelling favorable winds from northeast force the freshwater front onshore contributing to the plume mixing and breakdown of stratification.

The front arrivals stratify the water column into different salinity layers but the water column switches to well mixed conditions by tidal forcing (Figure 4.7a). In addition the wind and wave contribute to mixing during the first days (43-46 and 57-60), whereas the stratification is stronger during the last four days (47 - 50, and 61-63) probably due to calmer weather conditions. At these days the SSC is high with a peak during the front arrival (Figures 4.7b).

The bed stress and the mean diameter are inversely correlated and fluctuate with the well mixed and stratified periods of the water column specially during the first windy days. These relatively high bed stresses and the fluctuations in mean diameter indicate resuspension of bed material (Figure 4.7c). The mean diameter is increasing during the last days (47-50 and 61-63) as the stratification becomes stronger and SSC and bed stresses are lower (Figure 4.7 c). The correlation between the mean diameter and cross shore velocity (Figure 4.7 d) is not clear.

The observed PSD's are generally monomodal with a mean diameter of 100 - 200 μm even during the stratified periods of front arrival (Figure 4.8). This indicates the presence of spherical particles with low anisotropy that are probably inorganic, rather than elongated 'algae' particles and organic matter rich SPM. In the first days when the mean diameter is fluctuating between high and low sizes, the PSD shows a slight multimodality especially during the SSC peak. This might be an indication of resuspension of fluff material from the bed. However the main appearance is momomodal with fine sand size that indicates fine particles resuspended from the bed, since the bed stresses are higher compared to the autumn season and algae particles are assumed to be absent during the winter. The second recorded spring tide shows almost the same patterns, the data are shown in Appendix D.

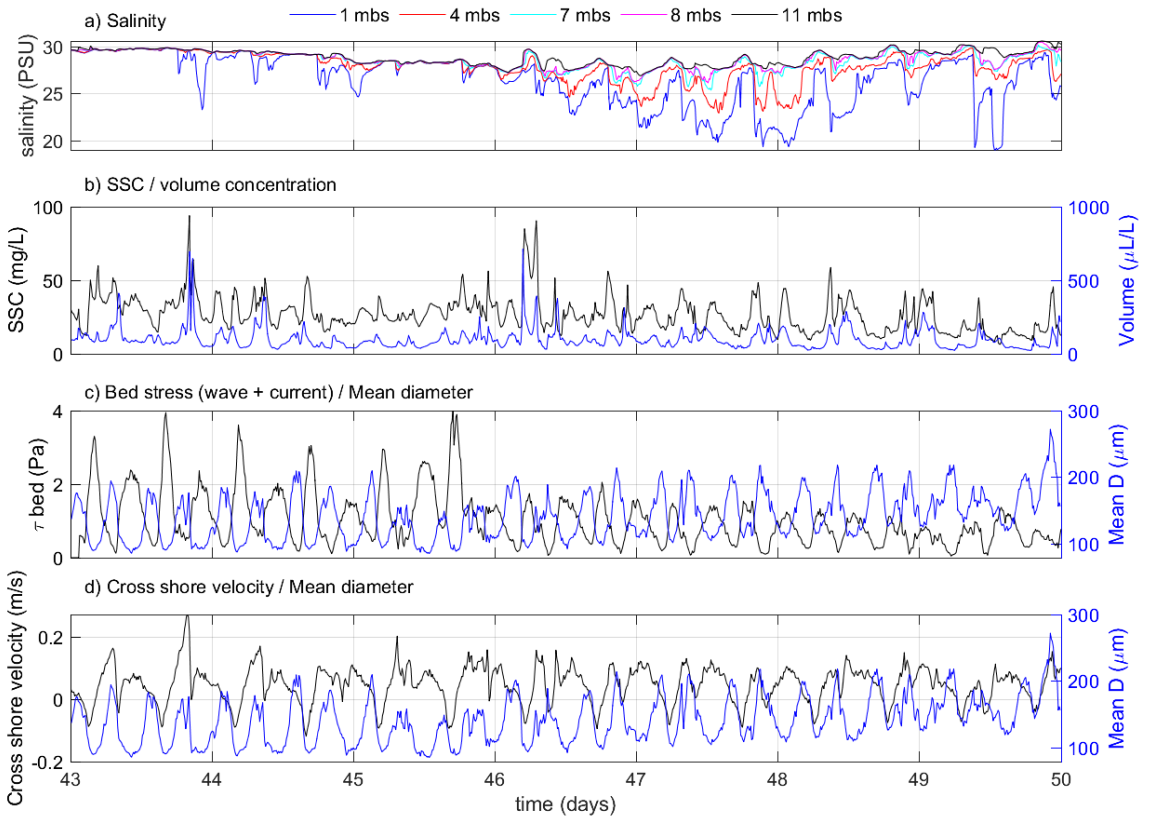

Figure 4.7: First recorded spring tide of winter 2013, Weather conditions and the hydrodynamics obtained from [98] and corresponding mean diameter calculated from LISST 100X data. The ΔS given in the legend, represents the degree of stratification.

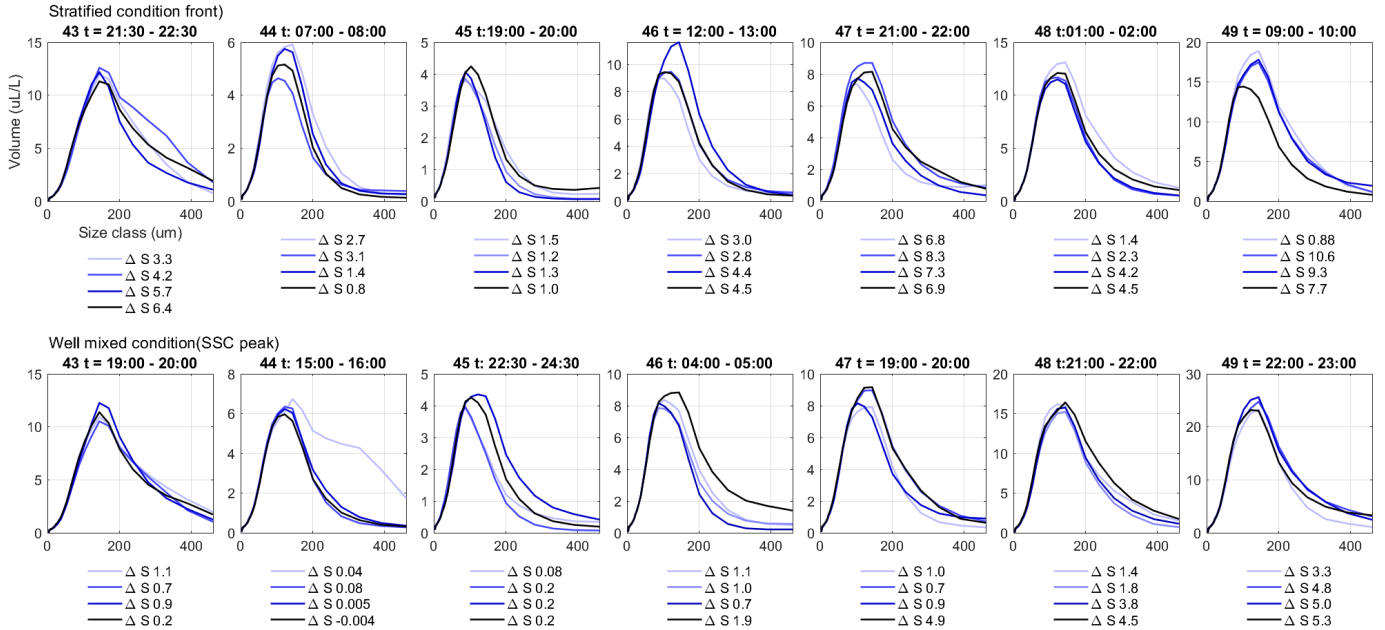

Figure 4.8: PSD of first recorded spring tide of winter 2013 obtained from LISST 100X data. The ΔS given in the legend, represents the degree of stratification.

4.3.4. WINTER 2013, NEAP TIDES

CALM WEATHER DAYS

The first recorded neap tide of the winter season (days 50 - 56) can be divided into calm and stormy periods in terms of weather conditions (Appendix C). The first two days (50 - 51) were characterized with typical neap tide conditions with moderate wind speed and wave heights. The freshwater fronts maintained long periods of strong stratification (Figure 4.9a). The SSC is low with a higher peak after the front arrivals as it was also observed during the neap tide calm weather days of the autumn season (Compare Figure 4.3b and Figure 4.9b). This peak is however small compared to the stormy weather with high SSC, but is representative for neap tides.

The mean diameter is high as the bed stress is low (Figure 4.9c) indicating advection of SPM, which is typical for neap tide conditions. The PSD's are different every day, for instance, at the first day directly after the spring tide monomodal distributions are observed during the front and during high SSC peaks (Figure 4.10), while multimodal distributions are observed at the second and the third days before the storm initiates. These multimodal distributions are typical for the neap tides during strong stratification with high ΔS, and indicate the presence of elongated particles. For the second neap tide only two days were recorded, these days show similar behavior in terms of weather conditions, bed stresses, SSC and corresponding PSD's (data are shown in Appendix D).

STORM DAYS

After these calm weather days, stormy weather conditions came into play at days 53-55 (Appendix C). The wind and wave activities elevated and the water column became well mixed (Figure 4.9a) with increased SSC (Figure 4.9b) due to increased bed stresses (Figure 4.9c). In agreement with the previous storm during the autumn season, these high bed stresses and high SSC coincide with low mean diameter that is also correlating with the cross shore velocity (Figure 4.9d). This indicates resuspension of bed fine sediments during this stormy period as the bed stress is higher during these days. The PSD's of these stormy days turned from multimodal to monomodal very fast (Figure 4.10). The PSD's show the resuspension of fine sand particles during the last day indicating, resuspension of fine sediment from bed.

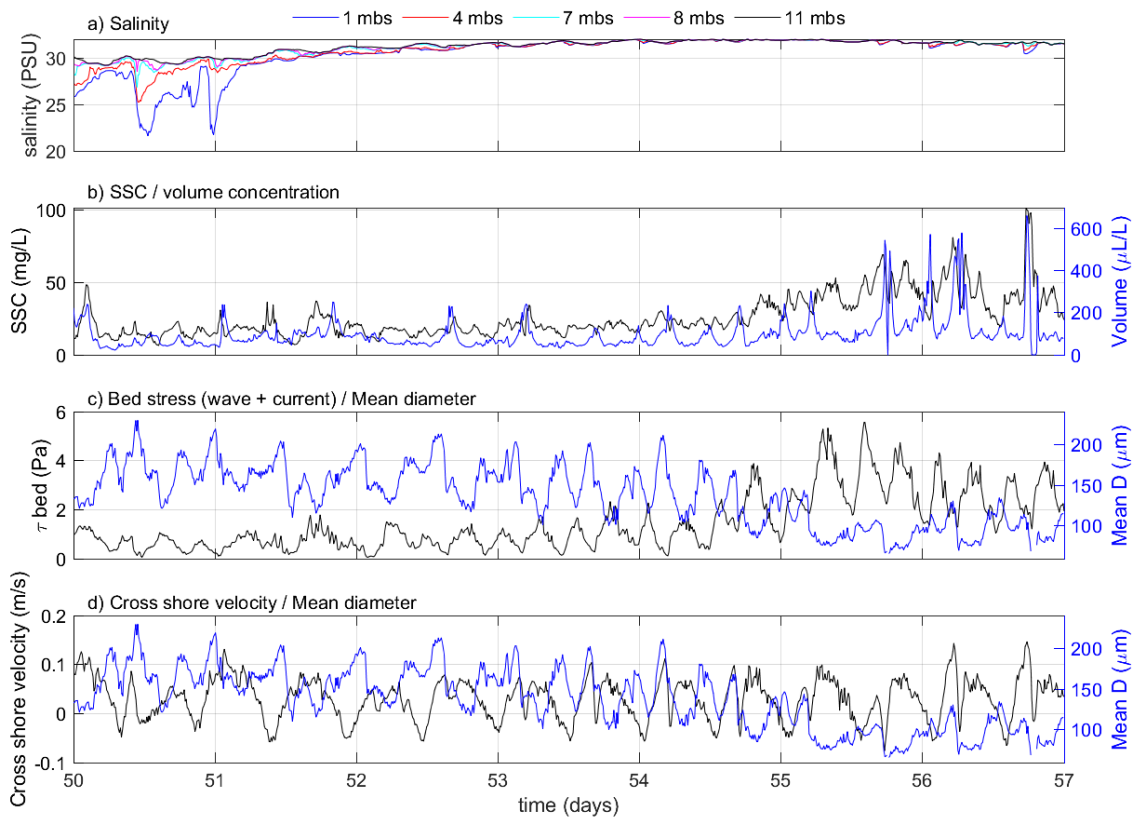

Figure 4.9: First recorded neap tide of winter 2013, weather and hydrodynamic conditions obtained from [98] and corresponding mean diameter calculated from LISST 100X. The ΔS given in the legend, represents the degree of stratification.

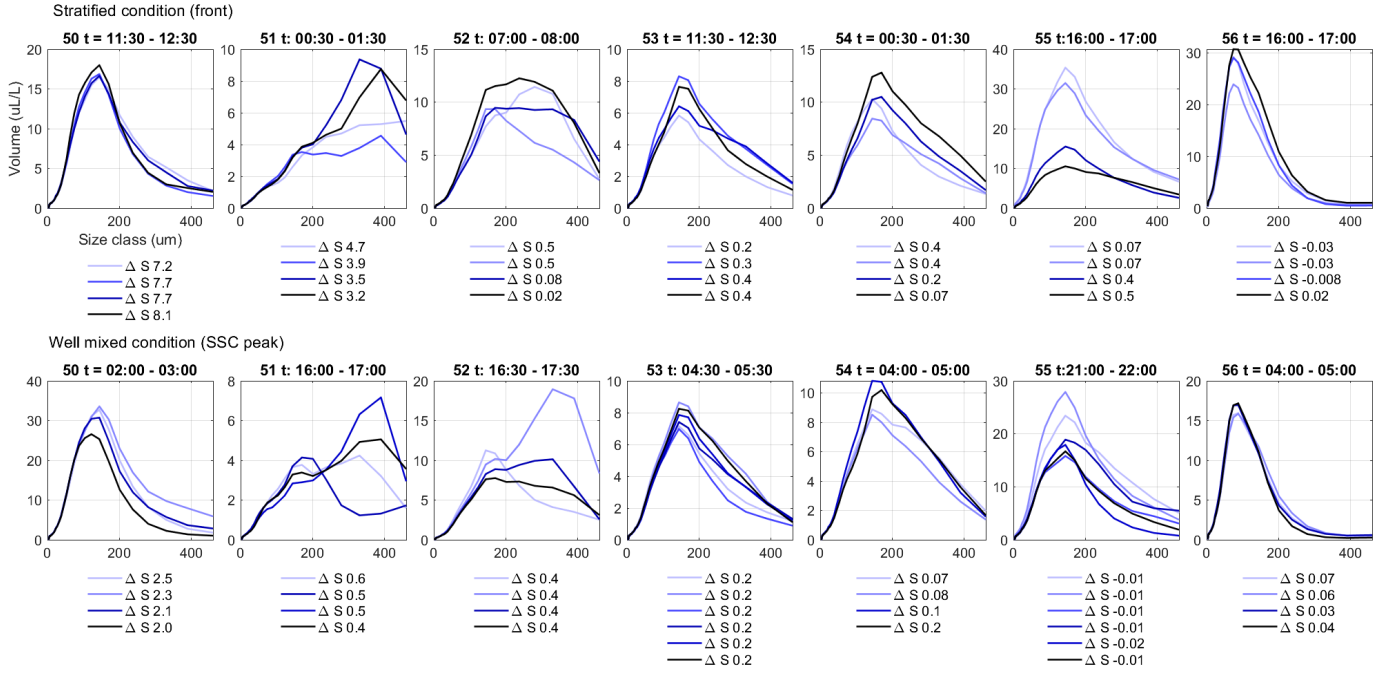

Figure 4.10: PSD of the first recorded neap tide of winter 2013, obtained from LISST 100X. The ΔS given in the legend, represents the degree of stratification.

4.4. DISCUSSION

SPM source in terms of advection and resuspension depends on the spring-neap tidal dynamics of the river plume and it is influenced by the weather and seasonal conditions. The Rhine freshwater fronts stratify the water column and transport biogenic species and organic matter along the coast [182–184]. Otsuki and Hanya [185] showed that most of dead algae cells can also remain as particulate organic matter [125, 185]. Besides this, organic matter availability is a seasonal variable depending on the algae blooms periods of the year [179, 186]. This dynamic behavior of organic matter with time and location (water column/ sediment bed) is reflected in the measured particle shape and densities of flocs. In most of the studies the biological activity is expressed in Chl-a concentration which is generally measured to be low during the winter months and high during the summer [78, 187].

4.4.1. SPM SOURCE AT NEAP TIDES

AUTUMN SEASON

At neap tides with calm weather conditions, the salinity stratification prevails for a long period of the day. The well mixed water column conditions are very short and the water column turns into stratified with the next front arrival and turbulence is dampened by this stratification [32–36]. The suspended sediment concentrations are generally low especially at the surface layer [17, 93], but algae, phytoplanktonic species and organic matter can not be detected properly with the OBS measurements and are generally not taken into account as SPM concentrations. The near bottom SSC is low as well during the neap tides, with a peak in SSC that appears 1.0 - 1.5 h after the front arrival during the calm weather days. This peak is still low in concentration compared to the spring tide and storm concentrations, but it is a recurring peak during the neap tides at calm weather conditions.

The composition of particles in this peak is analyzed by comparing the LISST-HOLO pictures with the PSD obtained from the LISST-100X. The observed PSD during this peak is multimodal, indicating that this SPM is composed of elongated particles. Comparison between the LISST-HOLO pictures before, during and after the front (Figure 4.2) showed clearly more elongated (fresh algae particles) during the fronts for three days of calm weather neap tides of autumn 2014 data. As the freshwater is nutrient rich, microorganism and planktonic species and related organic matter originating from the estuary can be transported with the river fronts [36, 44, 49, 88, 94], but unfortunately no measurements were performed in the freshwater lens to confirm this in our case.

The Multimodal PSD and LISST- HOLO pictures that show the presence of significantly more algae particles during the fronts, in addition to low bed stresses, confirm that the SSC peak can not be composed of resuspended local bed material. Taking this into account, front arrival and dynamics are determinant for the appearance of this near bottom SSC peak.

Front arrival at the surface of the water column, causes a return flow near the bed in opposite direction (onshore), see Figure 1.3. This flow can advect sediment from the

shoreline into the water column. This sediment interacts with the advected organic matter in the freshwater layer and forms this SPM cloud that appears finally as a high near bottom SSC peak at the mooring location 1-1.5 hour after the front arrival. During the calm weather conditions, the low density organic matter can be trapped in the freshwater layer due to salinity discontinuities and will experience a delayed settling. Back-of-the-envelope calculations indicate that this matter will reach the bottom 1.0 - 1.5 hour after the front arrival which is in agreement with the observed delay [32–36, 188]. Eventually this advected SPM cloud accumulates near the bed developing the fluff layer that can easily be resuspended [175, 177] during the storms or even by low mixing during the spring tides.

The settled material (composed in great part of organic matter) form a fluff layer at the bed. The presence of this fluff layer was detected during the first hours of the storm initiation. At the first hours of higher wind and wave activities, the increase in bed stress coincided with a decrease in mean diameter and the observed PSD turned gradually from multimodal into monomodal with increasing volume concentrations. This gradual change during the storm initiation confirms the presence of a fluff layer (formed of anisotropic flocculated particles and algae) that is depleted during the first hours of the storm.

The bed stress increased gradually as the storm proceeded, reaching the erosion threshold of sand and silt [180]. This is also reflected in the PSD modality and volume concentrations measured with the LISST 100X. At the second day of the storm, higher volume concentrations and monomodal distributions with fine sand sizes confirm the wave-induced resuspension of fine sediments from the bed. This fine sediment becomes available to interact with advected organic matter. It will then settle and accumulate again as the weather calms down, developing the fluff layer again after the storm. An other study in the far- field region confirmed the development of a fluff layer composed of settled Chl-a rich particles deposited after a storm [167].

WINTER SEASON

During winter, the biological activity is expected to be low [44], the observed PSD's are mainly monomodal for any degree of stratification. There are however some multimodal PSD's with high mean diameters observed during the neap tide of winter 2013. These multimodal distributions appear mainly during the strong stratified periods of freshwater front passage with low bed stress and at cross-shore water slack. The shape of these multimodal distribution is however different, there is no extra sharp peak present as it was for the PSD measured in the presence of elongated particles. These multimodal PSD's thus indicate different classes of particles present in the water column [71, 189]. The mean diameter however, is inversely correlated with the bed stress, a high mean diameter corresponding to a low bed stresses and vice versa. This indicates that the front advects organic material even during the winter.

The PSD's of the stormy days turned from multimodal to monomodal very fast and not gradually as was observed during the storm of autumn season. This fast change indi-

cates that the fluff layer is more depleted in winter than in autumn season. The SSC peak was about 100 mg/L with a mean diameter that decreased to below 100 μm in the winter indicating presence of sandy particles near bed which are not easily resuspended compared to the autumn season where concentrations were recorded up to 200 mg/L with gradually decreasing mean diameter from 200 to 150 - 100 μm during the storm, due to the presence of an easily resuspendable fluff layer.

4.4.2. SPM SOURCE DURING SPRING TIDES

AUTUMN SEASON

The particle size distribution for the spring tide of the autumn 2014, switches between a multimodal distribution and a monomodal distribution with fine sand size. This indicates that the SPM source during the spring tides can be advected algae and organic matter particles by the front as well as resuspended fine material from the bed.

During the spring tides, the freshwater front, in addition to advection, causes a near bottom turbulent peak during its arrivals due to higher velocities and tidal mixing forces. This higher turbulent peak can cause local resuspension of bed material. This resuspended sediment is advected in offshore direction. However this turbulent peak is caused only by thick fronts with cross shore propagation with high speeds (in order of 0.4 - 0.5ms^{-1}) [17]. This near bed turbulent peak results in resuspension of the fluff layer, because the bed stresses are lower than during stormy weather conditions and of shorter duration.

The fluctuations in the mean diameter are positively correlated with the cross shore velocity with higher mean diameter when the velocity is onshore directed. Higher mean diameter also coincided with low bed stresses and lower mean diameter coincided with high bed stresses. This typical contradiction between the mean diameter and the bed stress was found also by another study [190].

Due to lack of LISST-HOLO measurements for these periods, we can not visually confirm the presence of the algae and biological species in the water column. However, taking the neap tide pictures as a reference and other studies that confirmed the presence of planktonic species by multimodal distribution measured by the LISST 100X [67, 123, 191, 192], we can accept that these multimodal distributions are attributed to presence of elongated particles that are mainly biological species. This fluctuation in the PSD modality indicates that the measured particles are resuspended material that can be from the fluff layer (bi or multimodal), or fine sediments from the underlying bed (monomodal distributions). This resuspension might be caused by the frontal passage generating offshore near bottom sediment fluxes that are defined as near bottom turbulent peak by Flores et al. [17].

Accepting that the advected particles are mainly phytoplanktonic species and biogenic organic matter (as shown during the neap tide calm weather), this organic matter can interact with the resuspended bed sediment during the energetic mixing conditions. This interaction between advected organic matter with resuspended fine sediment from bed

contributes to SPM formation during the spring tides.

WINTER SEASON

In winter with low biological activity and high wind and wave activities, the fluff layer is depleted. Mainly monomodal PSD's with fine sand sizes are found in the near bottom layer. Despite the lack of LISST-HOLO measurements for this period, we can reasonably assume that these particles are mineral-based.
As monomodal distributions are combined with low concentrations, resuspension can be seen as the main source of SPM during the spring tides of this season. Higher SSC concentrations were found in winter compared to autumn, in agreement with other studies that have found higher sediment concentrations during the winter [164, 167, 177, 179].

4.4.3. FLUFF LAYER FORMATION AND EROSION

The presence of phytoplanktonic species and biogenic organic matter have large impact on the formation and particle properties of SPM, such as size, settling velocity and effective density on seasonal basis [126, 127, 130, 182, 193, 194]. In addition the presence of biological species and related organic matter in the near-bottom layer influence the erodibility of the fluff layer [195, 196]. This layer can be resuspended by low energetic mixing, bringing fine flocs and sediment into the water column to interact and flocculate again with newly advected organic matter and algae species with the freshwater front.

During the storm period of the autumn season, the fluff layer was resuspended during first hours of storm initiation (Figure 4.4), at bed stresses of about > 2 Pa. While the fine sand and silt were eroded after depletion of this layer at bed stresses of > 5-7 Pa. The fluff layer erosion threshold however depends on the compaction degree of this layer which in turn depends on the effective density of the particles and the portions of the clay, silt and sand within this layer and the layers beneath [96, 197, 198].

In addition seasonal changes in the weather conditions and availability of organic matter and biological species are deterministic for formation, compaction and erosion of this layer and its interaction with the underlying bed [199]. Sediment dynamic models algorithms modeling the bed, have to be calibrated with different size classes and different particle types to be able to predict the deposition and erosion rates of SPM and fine sediments [200]. Therefore understanding biologically mediated flocculation processes is important to predict the erosion threshold for this fluff layer on seasonal basis [37, 45, 47, 90]. In addition seasonal fluctuations in SPM concentrations and properties depending on the availability of organic matter play an important role in determining the source and transport of SPM [163, 164, 167, 179]. This aspect needs to be included in sediment transport models, as these models ignore the presence of phytoplanktonic species and organic matter and their substantial role in sediment dynamics. An average effect of the organic matter role is however empirically included (to certain extent) by calibration.

4.5. CONCLUSION

In this Chapter we identified the source of SPM during spring-neap tidal cycles at two seasons of winter and autumn in the mid-field region of Rhine-ROFI. During the neap tides with calm weather conditions, advection of organic matter and biological species by the Rhine front are the main source of SPM. This advected organic matter interacts with fine sediment in the water column and eventually accumulates at the bottom to form a fluff layer. This fluff layer is resuspended as first during stormy weather conditions after which the fine silt and sand are resuspended while the storm proceeds. Both SPM and fluff layer composition are seasonal dependent as they depending on the inorganic and organic matter present in the water column and/or advected by the Rhine freshwater front. The fluff layer is also resuspended by tidal currents notably at spring tide as a consequence both the arrival of freshwater front and tidal mixing forces.

Comparison of the autumn and winter seasons showed that multimodal Particle Size Distributions (PSD's) where observed mostly during the autumn season, indicting the presence of elongated particles in the water column (algae and organic debris). Algae and biogenic organic matter are indeed expected to be present during the autumn season. During winter, on the other hand, the observed PSD's where mainly monomodal indicating the presence of rather spherical particles that are expected to be mainly of inorganic origin.

The freshwater front is known to resuspend fine sediment from the coast and creating a return flow (seawards) near the bottom. The resuspended sediment interacts subsequently with the organic particles present in the water and form a SPM cloud that is observed 1.0 - 1.5 hour after the front arrival at the mooring location. Another hypothesis for the presence of the SPM cloud is linked to the organic matter trapped in the freshwater layer. Flocculation by differential settling can occur when this organic material slowly settles and aggregate with suspended inorganic particles present in the water column. The time for these flocs to reach the sea floor is alos of the order of 1.0 – 1.5 hour after the front arrival. This hypothesis could be tested by performing measurements as function of depth.

The gradual transition from multimodal PSD's into monomodal PSD's at the first hours of storm initiation in autumn confirms the presence of a fluff layer which is depleted first. Less multimodal PSD's appeared afterwards, when inorganic sediment is eroded. In the winter season, in contrast, the PSD's turned very fast into monomodal PSD's indicating a less thick fluff layer. The PSD's in winter were also less multimodal than in the autumn season at neap tide. During storm conditions, inorganic fine sediments are eroded after the depletion of the fluff layer and hence made available for flocculation in the water column. It was found that the fluff layer can resuspend at relatively low bed stresses (about 2 Pa). The released inorganic fines will aggregate with organic matter during the calm weather conditions and contribute to development of the a new fluff layer.

The mean particle diameter near bottom was found to be inversely correlated with the

bed stresses in both seasons: low bed stresses coincided with high mean diameter and vice versa. This correlation between the mean diameter and the bed stresses can be understood as follows: at low bed shear stresses the SPM found near bottom is composed of flocculated material of low density which is in general large in size as it contains large organic particles, whereas at high bed shear stresses the SPM is composed of (smaller) particles of higher density which contains more inorganic particles. Organic-rich particles are predominantly formed in the water column and advected whereas inorganic-rich flocs are mainly resuspended from the bed.

Large sediment transport models like Delft3D calculates the SPM concentration (SSC) based on inorganic particles dynamics solely and do especially not account for dissolved organic matter and its availability. Particulate organic matter is often included in the calibration, but its interaction with clay minerals is not well accounted for. From the work presented in this chapter, it can be concluded that in estuarine regions organic matter plays a crucial role in the creation of flocs and fluff and therefore organic matter needs to be accounted for in realistic sediment transport models. In the next chapter, a more general discussion is performed about sediment transport modelling, whereby results obtained from Delft3D modelling are taken as example.

4.6. APPENDICES

Appendix A: 1st Neap tide autumn 2014 weather data, Spring tide and second neap tide of autumn 2014

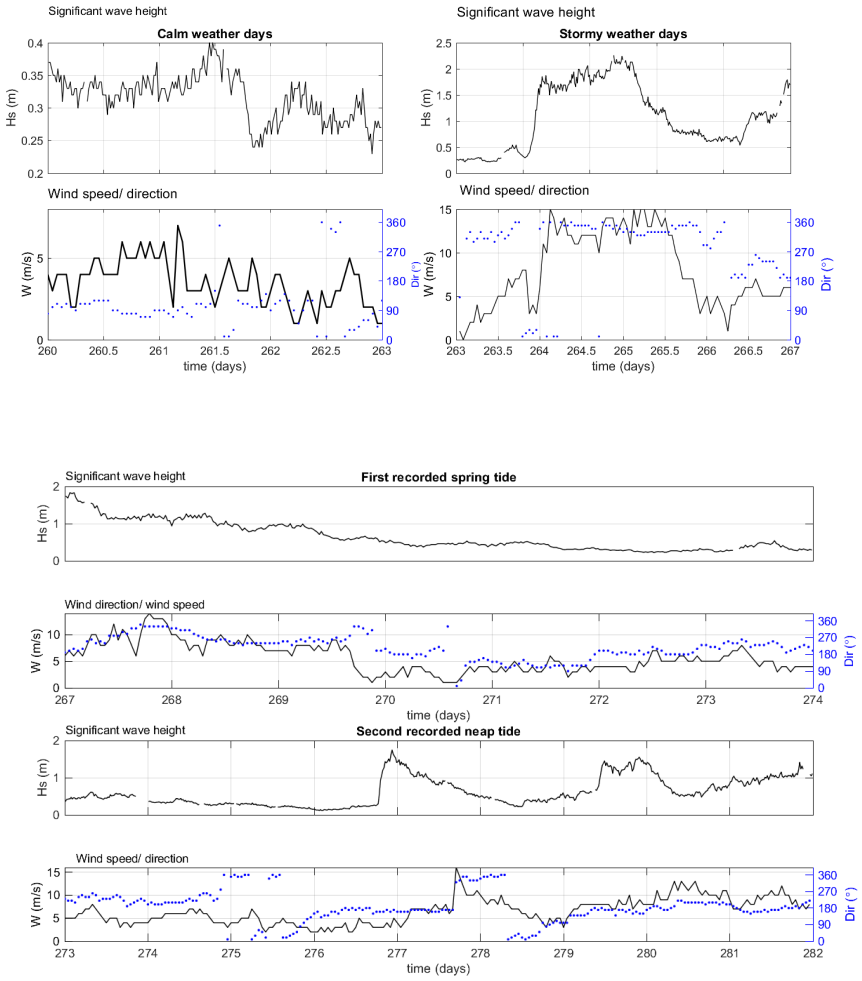

Figure 4.11: Wind and wave conditions obtained from Rijkswaterstaat for Hoek van Holland: upper panel: first recorded neap tide, middle panel: spring tide and lower panel: second recorded neap tide of autumn 2014

Appendix B1: hydrodynamics of second neap tide autumn 2014

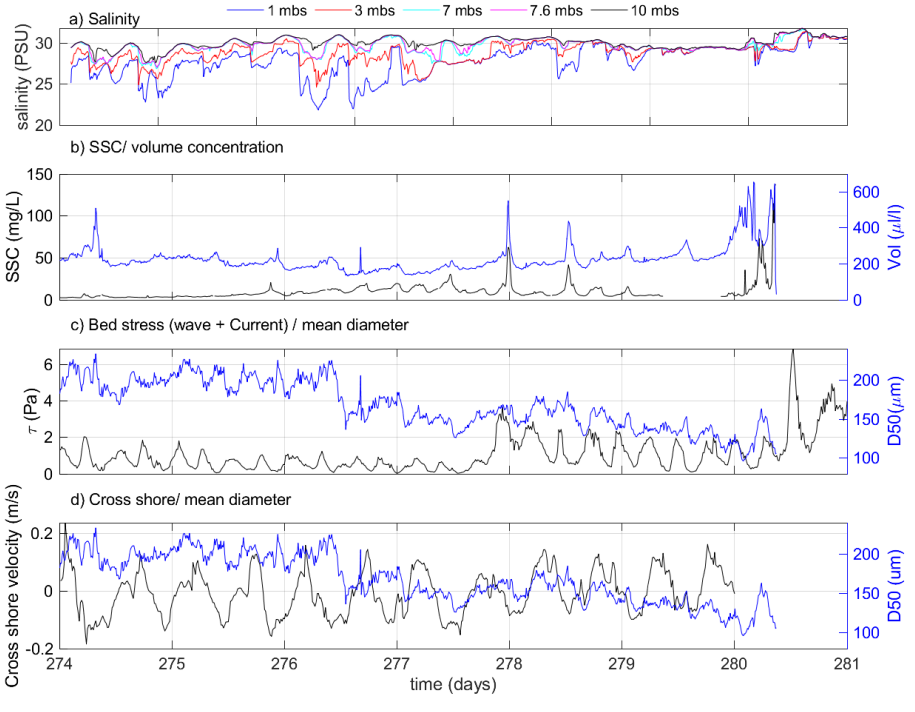

Figure 4.12: Second recorded neap tide of 2014, weather and hydrodynamic conditions obtained from [17].

Appendix B2: PSD of second neap tide autumn 2014

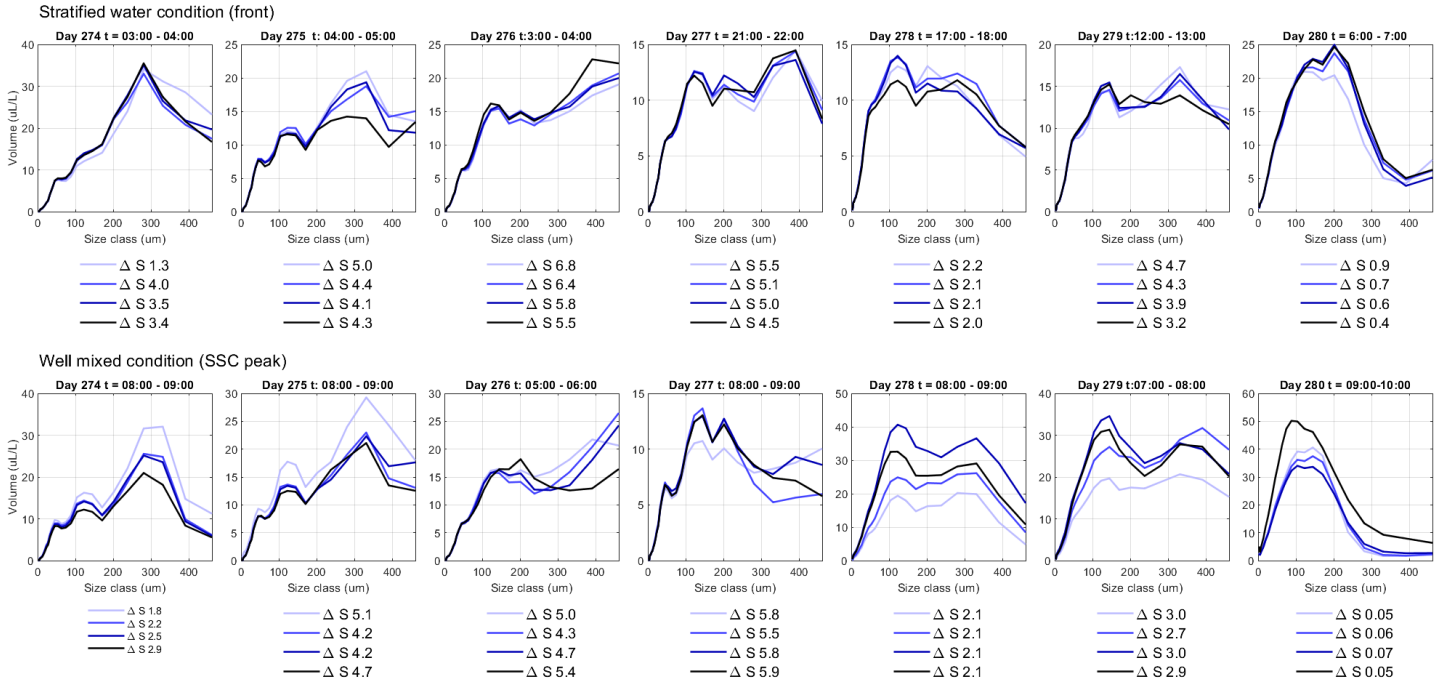

Figure 4.13: Second recorded neap tide of 2014, PSD obtained from LISST 100X. The ΔS given in the legend, represents the degree of stratification.

Appendix C: Winter 2013 weather data

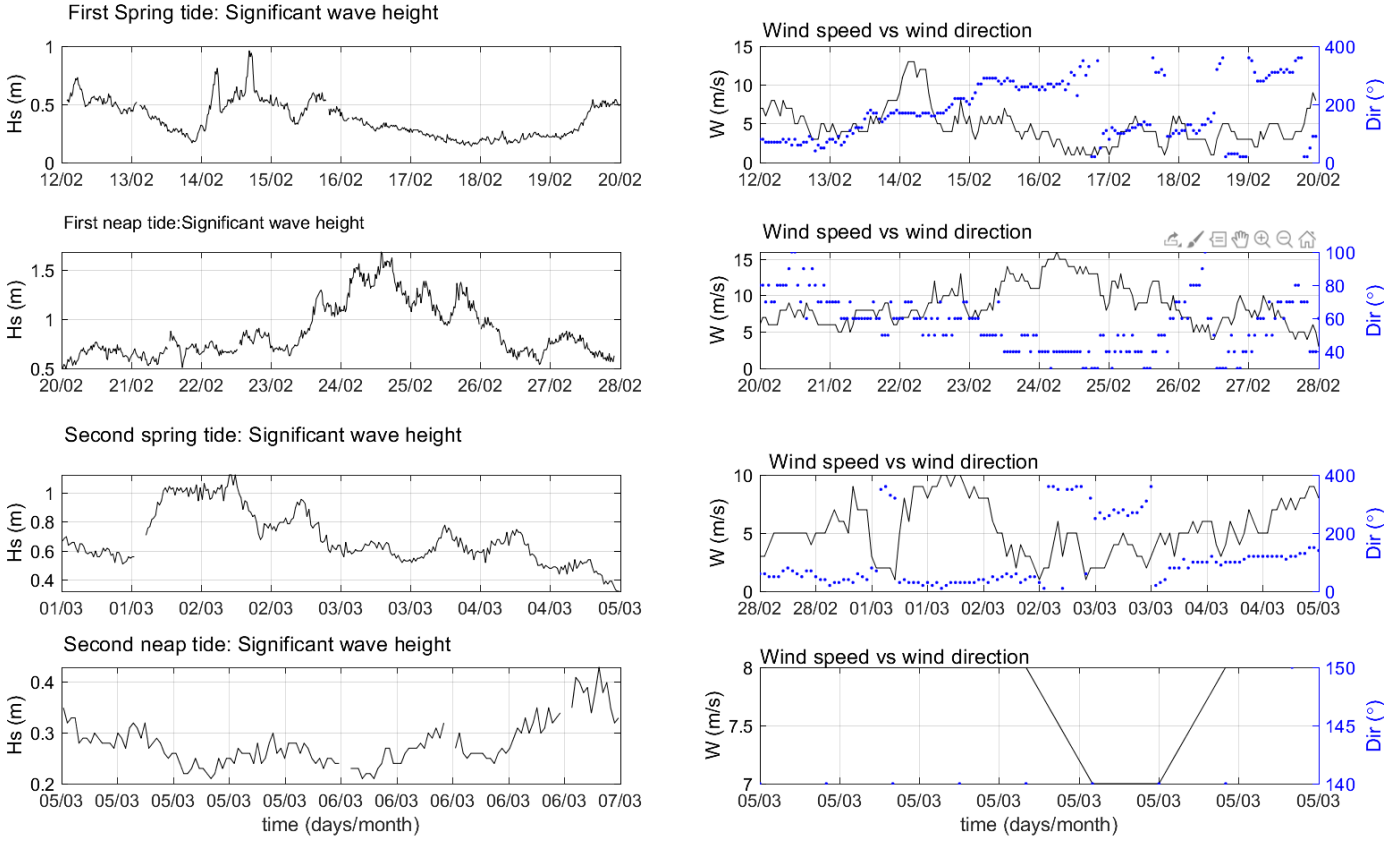

Figure 4.14: Wind and wave conditions during the winter 2013 measurement period.

Appendix D1: hydrodynamics of second spring and neap tides 2013

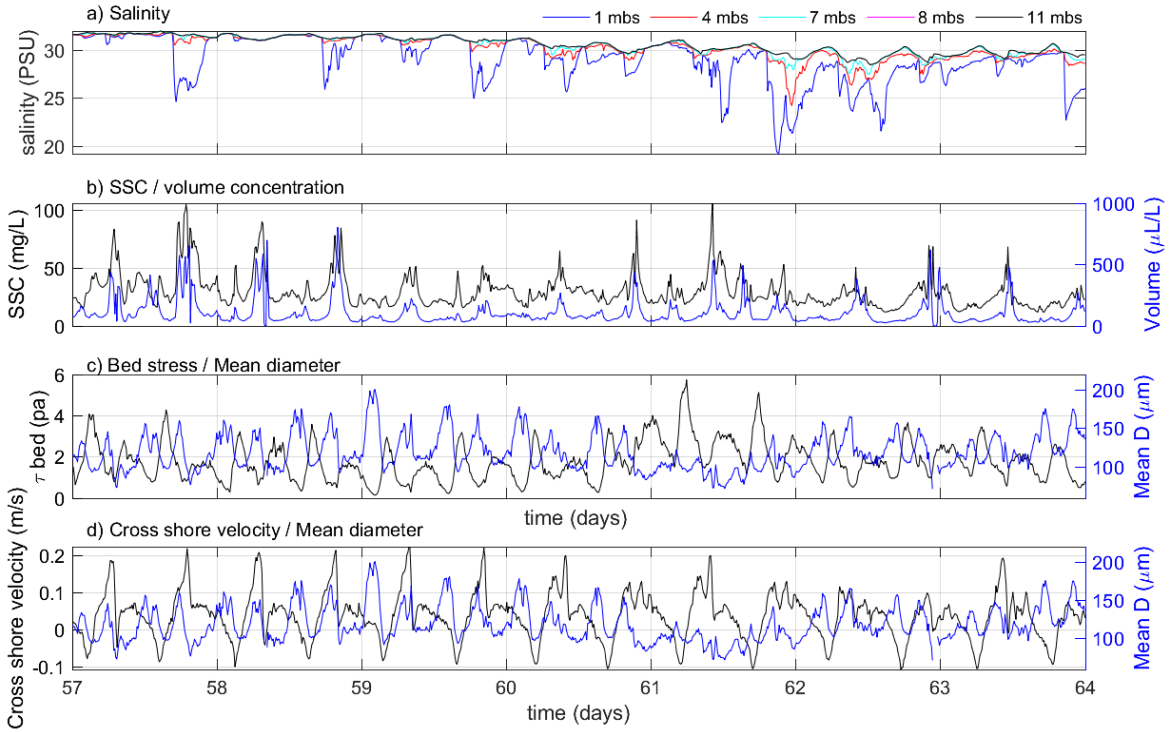

Figure 4.15: Second recorded spring tide of winter 2013, weather and hydrodynamic conditions obtained from [98].

Appendix D2: PSD of second spring tides 2013

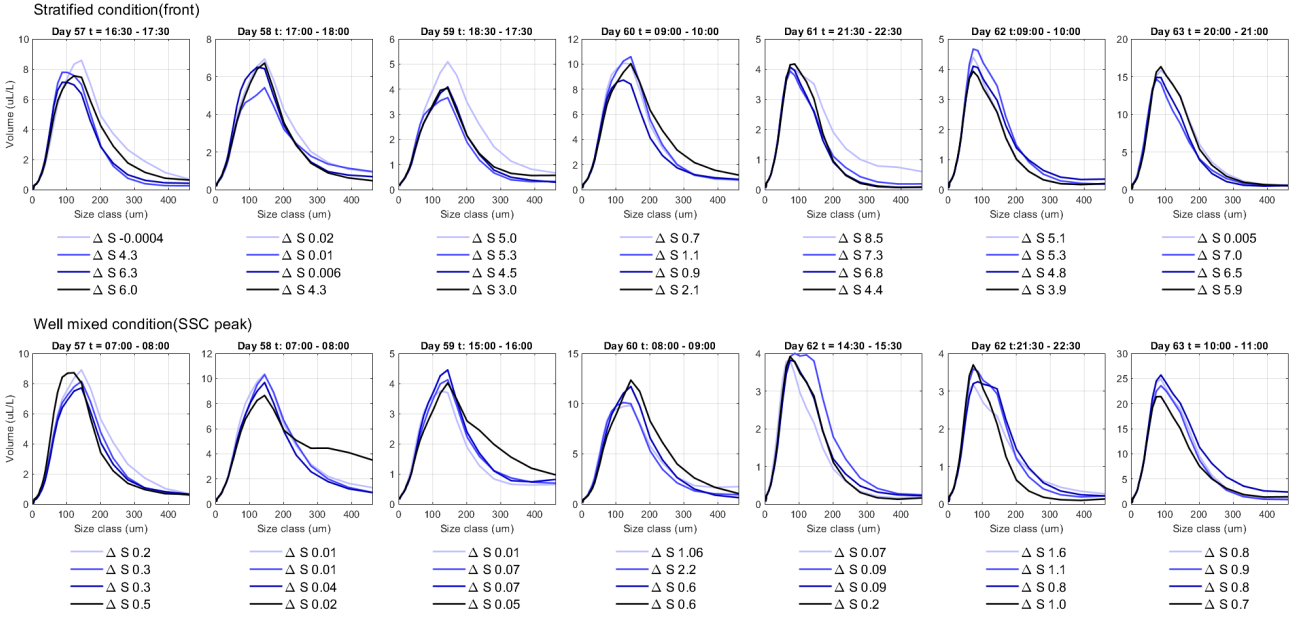

Figure 4.16: Second recorded spring tide of winter 2013, PSD obtained from LISST 100X. The ΔS given in the legend, represents the degree of stratification.

Appendix D3: Second spring and neap tides 2013

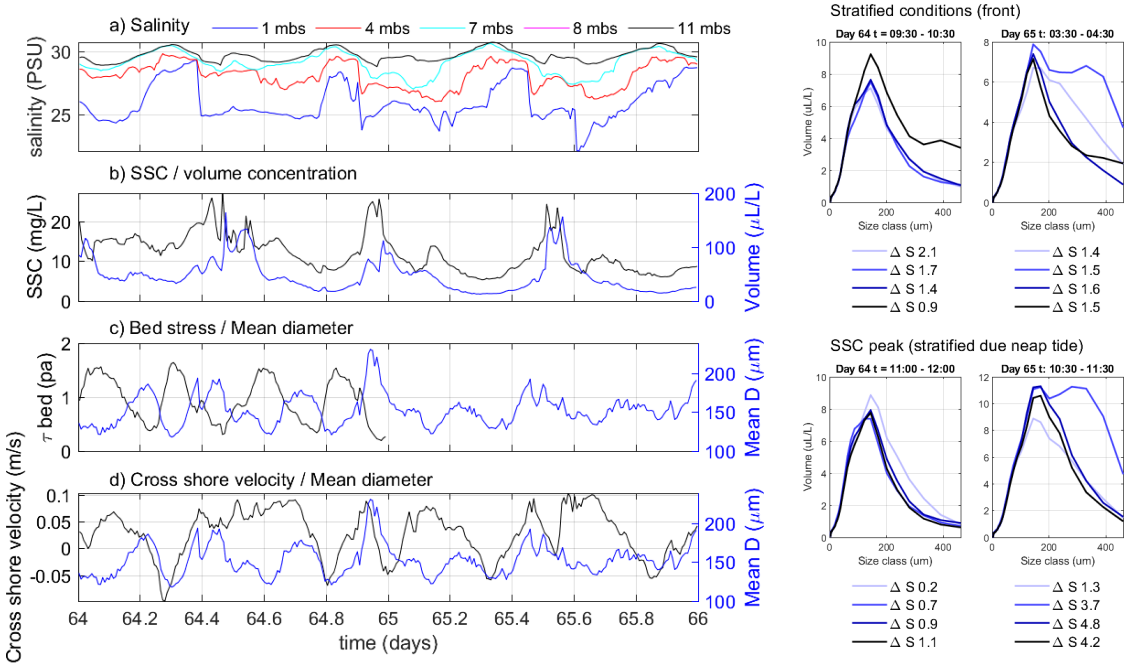

Figure 4.17: Second recorded spring tide of winter 2013, weather and hydrodynamic conditions obtained from [98] and corresponding PSD obtained from LISST 100X. The ΔS given in the legend, represents the degree of stratification.

Appendix E1: PSD of Flood and ebb tidal cycle 2013

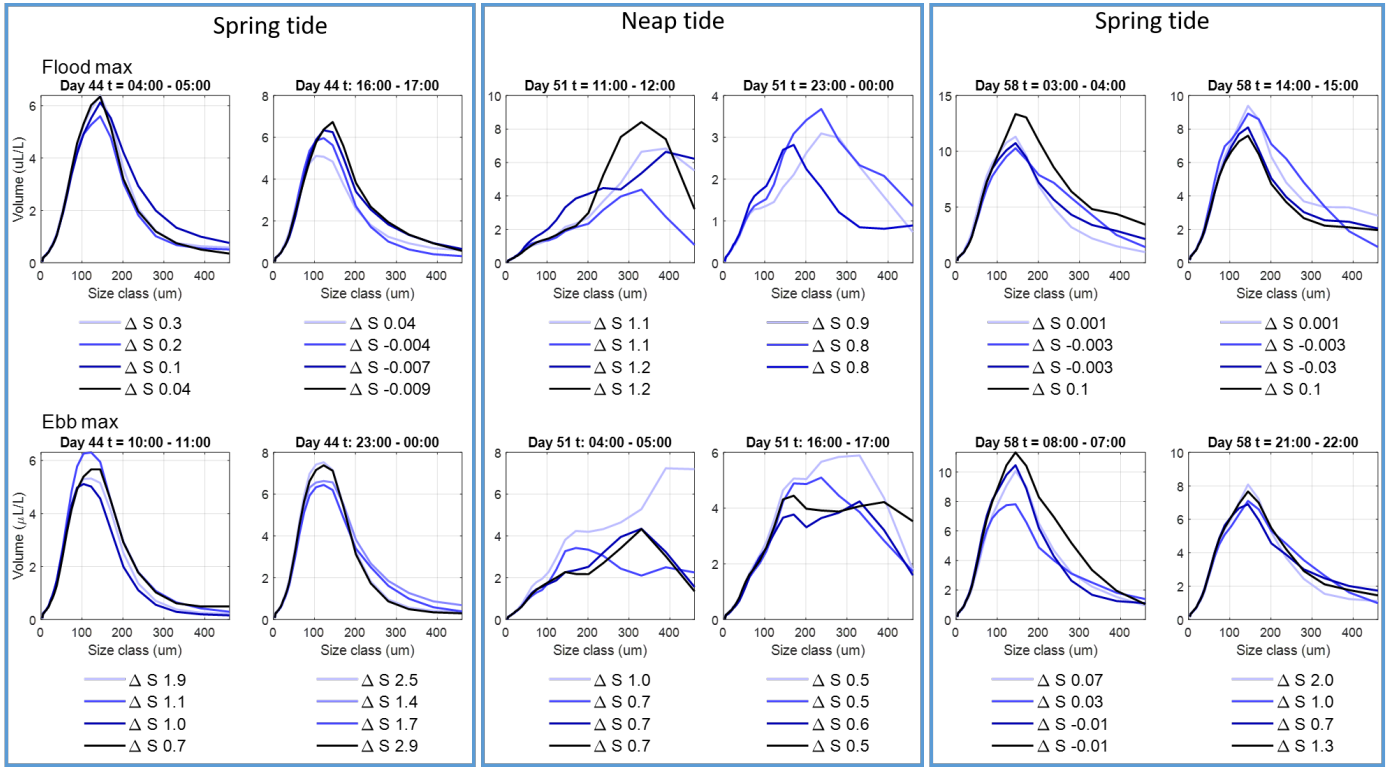

Figure 4.18: PSD at flood maxes and ebb maxes and corresponding HWS and LWS for one day per period (as an example) for winter of 2013. The ΔS given in the legend, represents the degree of stratification.

Appendix E2: PSD of Flood and ebb tidal cycle 2014

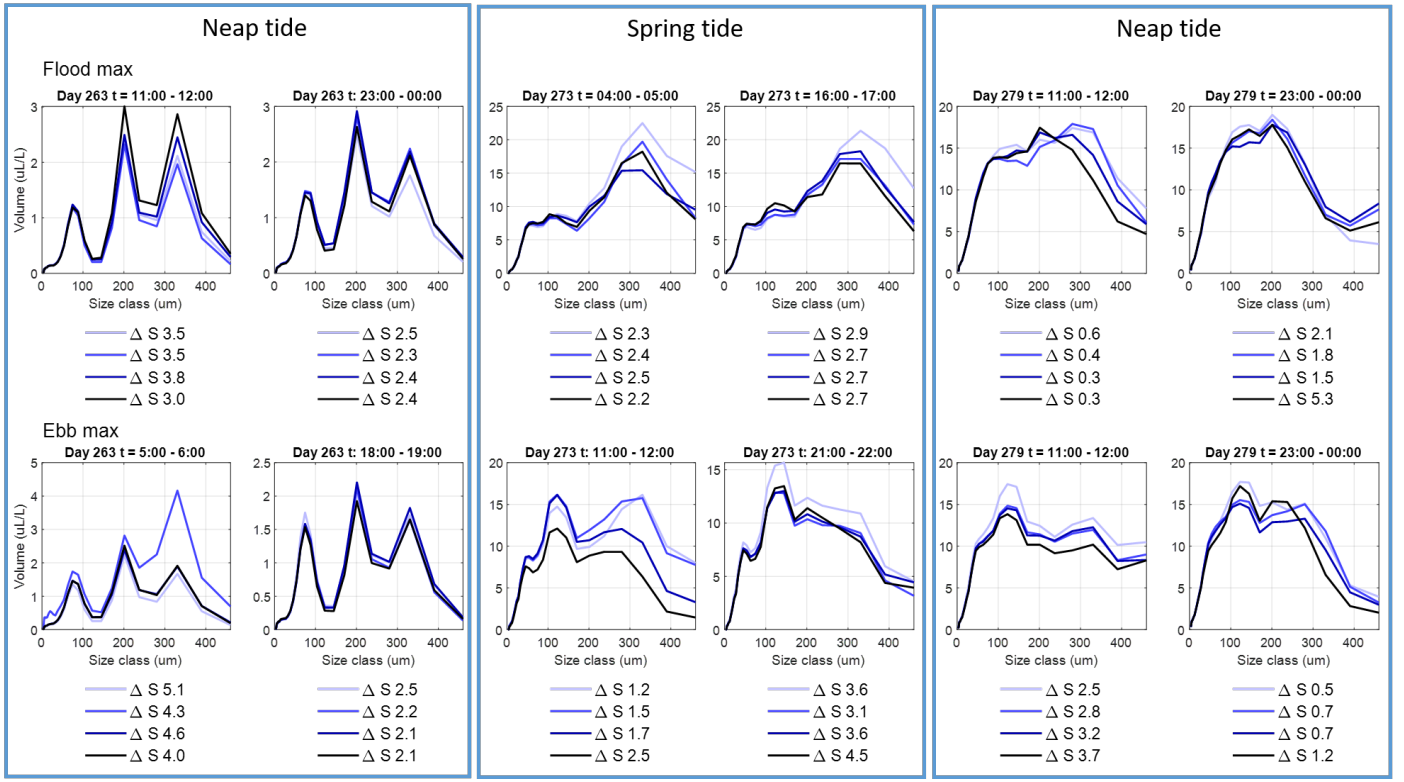

Figure 4.19: PSD at flood maxes and ebb maxes and corresponding HWS and LWS for one day per period (as an example) for winter of 2014. The ΔS given in the legend, represents the degree of stratification.

5

COMPARISON BETWEEN DATA AND MODEL NEW APPROACH AND CONCEPTUAL MODEL

Sediment transport models, such as Delft3D, typically use 2 or 3 classes of particles, each one being defined by its computed concentration (g/L) and a given settling velocity (mm/s), to predict fine grained sediment transport in coastal areas. In this chapter, the data set obtained from the LISST 100X presented in Chapter 4 will be used for comparison with Delft-3D (ZUNO-DD) numerical model output. A detailed analysis of the behavior of the classes is performed. The relation between size and settling velocity is analyzed in relation with the particles' shape, using the survey day data (see Chapter 2). The role of different environmental parameters on particle size distribution and settling velocity is summarized in a conceptual diagram at the end of the chapter.
The overall conclusion is that organic matter should be an input parameter for sediment transport models, as the presence of organic matter (living or dead) drastically changes the density of flocs and hence their settling behavior. From the analysis of the data, it was found that one class with a particular settling velocity can cover a wide range of particle sizes [70-160 µm]. The estimated densities for each size class cover a wide range. This density range indicates that most flocs observed during the survey (Chapter 2) have different organic matter content. From this, it can be concluded that sediment mass transport could be wrongly estimated in (coastal) regions where organic matter is abundant, if clayey particle mass concentration is estimated using a single density for a given floc size as is often done in the literature.

Sediment transport models are widely used to predict sediment dynamics, bathymetry, sediment erosion and deposition. Two of these models (ROMS and Delft3D) are generally without accounting explicitly for flocculation [201]. Another model, TELEMAC 3D, does account for flocculation. In that model, the settling velocity is a dynamic function of salinity and shear rate [145, 146, 202]. Recently Shen et al. [203] proposed a flocculation model based on Population Balance Equations (PBE's) for 3 size classes. This model that was implemented in TELEMAC and successfully used to simulate particle size evolution at the WZ Buoy station on the Belgian coast [141, 143, 203]. The model depends on 18 adjustable parameters most of which can only be fitted to the data [204].

PBE's containing a large number of classes, like the ones used by Mietta [28] cannot be used in sediment transport models as they are typically too CPU intensive to run. Moreover, as discussed in Chapter 3, PBE models apply to salt-induced flocculation and are not suited to describe organic-matter induced flocculation, due to different aggregation and breakup mechanisms. In Chapter 3 a two-class model is proposed that accounts for inorganic mass conservation during flocculation, and which relies on variables to be measured in situ. The model can be parameterized by performing lab experiments, as discussed in that chapter.

In Chapter 4 the mooring data, acquired during two monitoring surveys in winter 2013 (STRAIN I) and autumn 2014 (STRAIN II) was analysed. It was shown that the transitions between fresh and saline water, that cause stratification in the Rhine ROFI [17, 98, 99, 205], play an important role in SPM formation and dynamics in the Dutch coastal zone, but, importantly, this occurs in combination with the availability of organic matter.

Parts of this data are used in the present chapter and are compared with the Delft3D model data. We chose the first neap-spring tidal cycle of autumn 2014 for the comparison. This period was selected because it covered a period of calm and a period of stormy weather conditions. We focused on the comparison of the modelled sediment classes, their settling velocities and concentrations. In addition we investigated their correlation with hydrodynamics and salinity.

A brief description of Delft-3D and the ZUNO-DD module (Module for sediment dynamics) is given in Appendix F. Currently ZUNO-DD is running using 3 classes of sediment particles (defined as IM1, IM2 and IM3), each of them is defined by a single and constant settling velocity. Each class is defined based on its concentration (mg/L) and its associated (Stokes') settling velocity (Ws) as given in table 1.1. From the settling velocity, a corresponding range in possible diameters can be estimated, based on densities found for in situ particles (see Chapter 2). The three classes do not interact and their transport is governed by advection (in particular settling) and turbulent diffusion.

Flocculation kinetics have been studied in Chapter 3 and characteristic timescales for flocculation have been found. These timescales are very different from sediment transport timescales. The question therefore arises whether a flocculation model is required in large scale sediment transport modeling, or if it is sufficient to model the transport of

flocculated matter. In the latter case, using a dynamic settling velocity that would be a function of parameters such as salinity, organic matter content and shear stress would be sufficient to have meaningful large-scale sediment transport.

Three questions are addressed in this chapter:

1. Is the commonly used assumption of having three classes of sediment based on a constant settling velocity sufficient to capture the essence of sediment transport?

2. How does the interaction between particles (flocculation), change the size-settling velocity relation?

3. Do we need to implement a flocculation model into sediment transport models, or would the implementation of organic matter as an input parameter be sufficient to simulate the flocculated matter?

Before answering these questions, we will start by comparing numerical and in situ data. We will end by proposing a conceptual model that details the influence of environmental conditions on particle size distributions and settling velocities. The conceptual model can be used as a reference for further studies.

5.1. COMPARISON BETWEEN THE IN SITU AND THE MODEL DATA

The first neap-spring tidal cycle of the autumn 2014 measurement period was chosen for this study, because the neap tide covered a period of calm and a period of storm weather condition. The neap tide data for the calm and storm periods are plotted separately in Figures 5.1 and 5.2. As shown in Figure 5.1 and 5.2 a, the predicted salinity is in agreement with the measured one. The predicted SSC is relatively higher than the measured one, but it has a similar trend with a pronounced peak after the front arrival during the calm weather period (Figure 5.1 and 5.2b). This higher SSC is the result of a higher predicted bed stress (Figure 5.1 and 5.2 c), that is caused by the overestimation of the wave-induced bed stress by the model. During the storm days, the predicted SSC increases as the storm develops to a point where the predicted SSC is higher than the measured one. The predicted bed stress is at this point also higher in absolute values than the measured one but it agrees with the measured data in terms of trend and fluctuations during the storm days (Figure 5.1 and 5.2c). The predicted cross-shore velocity seems to be slightly out of phase, compared to the measured one. For the spring tide similar trends are observed, the SSC and the bed stress are slightly overestimated by the model (data not shown).

The characteristics of the three classes IM1, IM2 and IM3 are given in Table 1.1. Generally during normal (calm) weather conditions, the model results show that the IM1 and the IM3 classes have relatively similar concentrations at the surface and bottom layers (Figure 5.1 and 5.2 e and g), which means that they represent the fines that are evenly distributed through the water column. This implies based on density calculation, see table 5.1, that clay mineral of size $< 10\mu$m can populate the whole water column. The IM2

class, however shows higher concentration near the bottom, representing the fast settling silt particles that are not present in the surface layer (Figure 5.1 and 5.2f). This IM2 class can be composed of inorganic content of size of about 30 μm or of flocs as large as 300 μm, if their density is close to water. This class shows a significant increase in concentration during the storm days, due to bed resuspension (Figure 5.2 f). We recall that by definition, the 3 classes have no interactions and their concentrations change independently of each other, being a function of the hydrodynamics and gravity only. However, as the fluff layer resuspended by the storm contains sticky particles, it could well aggregate with the particles in suspension.

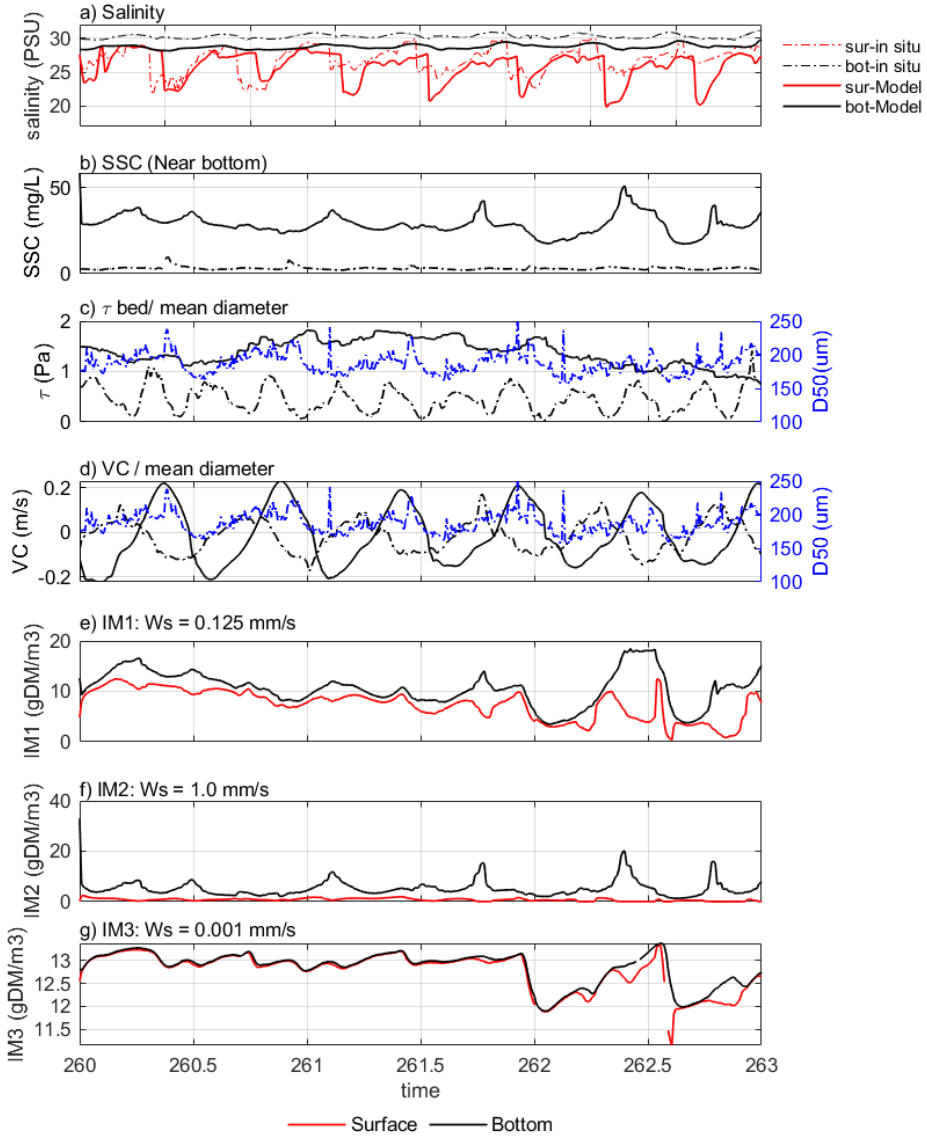

Figure 5.1: Comparison between the model and in situ data for the first neap tide of autumn 2014 during the calm weather period. The full lines correspond to the model results and the dashed lines represent the in situ data. The surface data are in red and the bottom are in black, the D50 diameter, in blue is estimated from LISST 100X data. a) Salinity (PSU), b) Near bottom SSC (mg/L), c) Bed stress versus mean diameter (D50), d) Cross-shore velocity versus mean diameter, e) IM1 class obtained from the numerical model, f) IM2 class and g) IM3 class, in gram Dry Material (DM) per cubic meter (equivalent to mg/l).

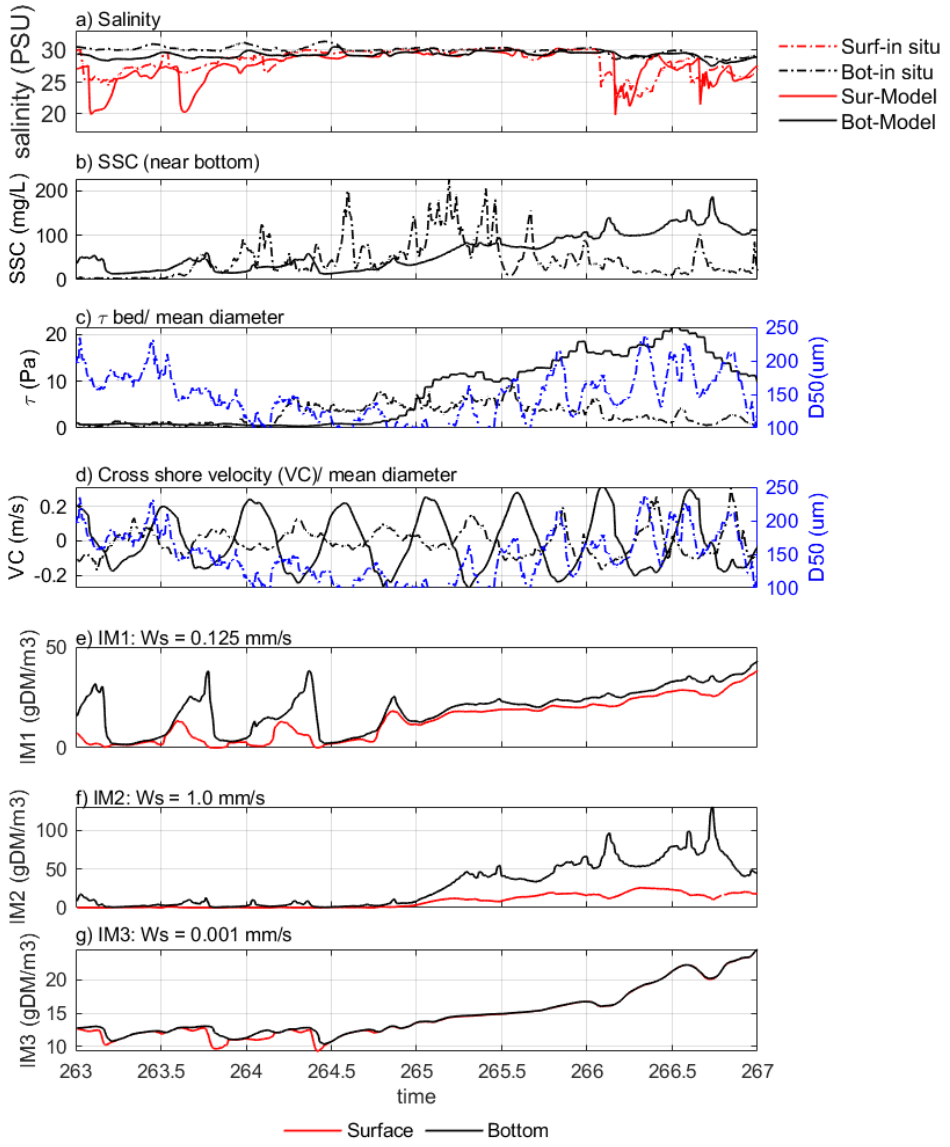

Figure 5.2: Comparison between the model and in situ data during the first neap tide of autumn 2014 for the storm period. The full lines correspond to the model results and the dashed lines represent the in situ data. The surface data are in red and the bottom are in black, the D50 diameter, in blue is estimated from LISST 100X data. a) Salinity (PSU), b) Near bottom SSC (mg/L), c) Bed stress versus mean diameter (D50), d) Cross-shore velocity versus mean diameter, e) IM1 class obtained from the numerical model, f) IM2 class and g) IM3 class, in gram Dry Material(DM) per cubic meter.

5.2. RELATION BETWEEN PARTICLE DIAMETER AND ITS SETTLING VELOCITY

In situ measurements and the laboratory experiments in the previous chapters have shed light on sediment-organic matter interactions. Particle classes have been defined based on particle's composition (clay, algae and/or EPS), see Chapter 2. It was found that composition and settling velocity are linked: low settling particles are mainly bare algae (Ws < 1 mm/s) that are present in the entire water column and the inorganic content in this class is negligibly low. Settling flocs cover a range of settling velocities between 1-10 mm/s.

The diameters that correspond to the particles classes from the ZUNO-DD models (IM1,IM2 and IM3) are evaluated by applying Stokes' law see table 5.1. The density range 1016-2600 kg/m^3 used to convert the settling velocities corresponds to the typical density range found in Chapter 2, obtained from the analysis of LabSFloc-2 camera data. The smallest diameter for each class corresponds to the highest density (2600 kg/m^3) which is the density of a pure clay particle. As organic matter has a lower density than clay, flocs containing organic material have a larger size for same settling velocity compared to a (pure) mineral sediment particle.

Table 5.1: Classes used in Delft-3D model; the equivalent diameter is calculated from Stokes' law using the density range $\rho = 1016 - 2600 kg/m^3$

Class	IM2	IM1	IM3
W_s(mm/s)	1	0.125	0.001
Diameter (μm)	33 - 338	11 - 119	1 - 10

The data obtained from LabsFLOC experiment (see Chapter 2) is plotted in terms of IM1 and IM2 classes. The plots represent the size range and effective density range corresponding to particles having a settling velocities of 0.125 mm/s (IM1) and 1 mm/s (IM2). This figure confirms that particles having very different sizes can have the same settling velocity, because their effective density is different. This result brings the relation between mass of clay content transported by flocs into question. It is usually assumed that the relation between floc density (and hence clay mass content per floc) and size is an inverse power law (density = $size^{-n}$, where n is a positive fitted exponent). However, from the measured data data it is found that density bandwidths should be attributed instead. This is particularly the case for the IM2 class.

This can be linked to the discussion initiated in Chapter 2 about the classification of flocs based on composition rather than on size (see Figure 2.3). For sediment transport models it is important to solve a mass balance for the clay minerals part, and hence to distinguish between flocs containing a lot of clay mineral content and the flocs predominantly composed of organic material. In Chapter 3, while analyzing laboratory data, a two class balance was proposed, whereby Class 1 is composed of mineral sediment and Class 2 of flocculated material. Clay mineral mass transfer between Class 1 and Class 2 will be the process leading to the largest change in settling velocity: a mineral particle

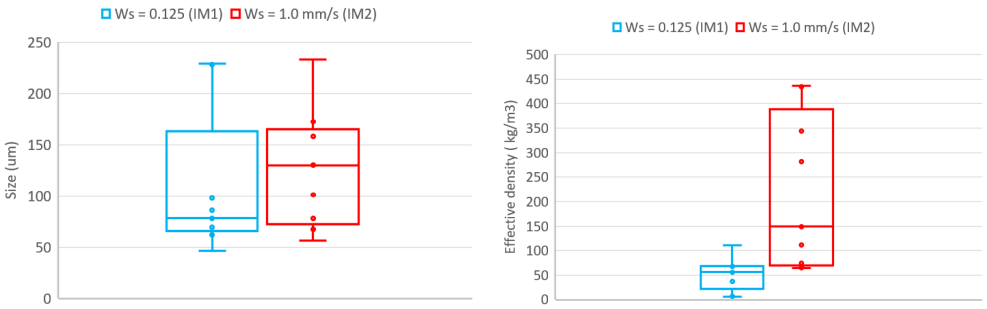

Figure 5.3: The size range (left) en the effective density range (right) that correspond to the settling velocity of the IM2 and IM3 particle classes obtained from the LabsFLOC measurements presented in figure 2.3

(density 2600 kg/m^3) from Class 1 that is bound to organic matter of low density (close to density of water) will have its settling velocity drastically changed when transferred to Class 2. The question that arises is where in the water column is this happening? To answer this question we will use the flocculation results described in Chapter 3. The laboratory experiments have shown the importance of salt ions in flocculating sediment to organic matter by electrostatically binding the negatively charged sediment particles to the negatively charged organic matter. Therefore flocculation is unlikely to occur in the freshwater part of the ROFI, in particular within the freshwater lens at the top of the water column originating from the river discharge. Moreover, this layer has been shown to contain very little suspended sediment particles [93] but is likely to contain significant supply of organic matter. Additional measurements should be able to confirm this.

When the organic matter is brought into contact with saline water, by settling or hydrodynamic advection/ diffusion flocculation can occur. The timescales for aggregation are very short in laboratory experiments. In situ it is expected that these timescales are sediment-concentration dependent. As confirmed by numerical modeling, sediment particles having a settling velocity of 0.001 and 0.125 mm/s and corresponding to clay particles (< 10 μm) fraction populate the whole water column. Clay particles of larger size (IM2, 1 mm/s) will mainly interact with organic matter close to the bottom. The sediment size is rather polydisperse at the bottom of the water column in the Port of Rotterdam (PoR), see Figure 5.4. This sample is representative for an in situ sample, containing small amounts of organic matter that could be degraded. When living algae is added to this sample in a flocculation experiment in the laboratory (see also Figure 3.12), it is observed that the spread in settling velocity is greatly reduced, reflecting the fact that even the silt particles (of settling velocity > 5 mm/s) are embedded in a flocculated matrix of lower density, which reduces their settling velocity (Figure 5.4). The samples are flocculated until steady state in less than 10 minutes, during the laboratory experiments. This might be not representative for in situ conditions (where a steady state might never be reached) but proves that the sticking efficiency of sediment to living algae is high.

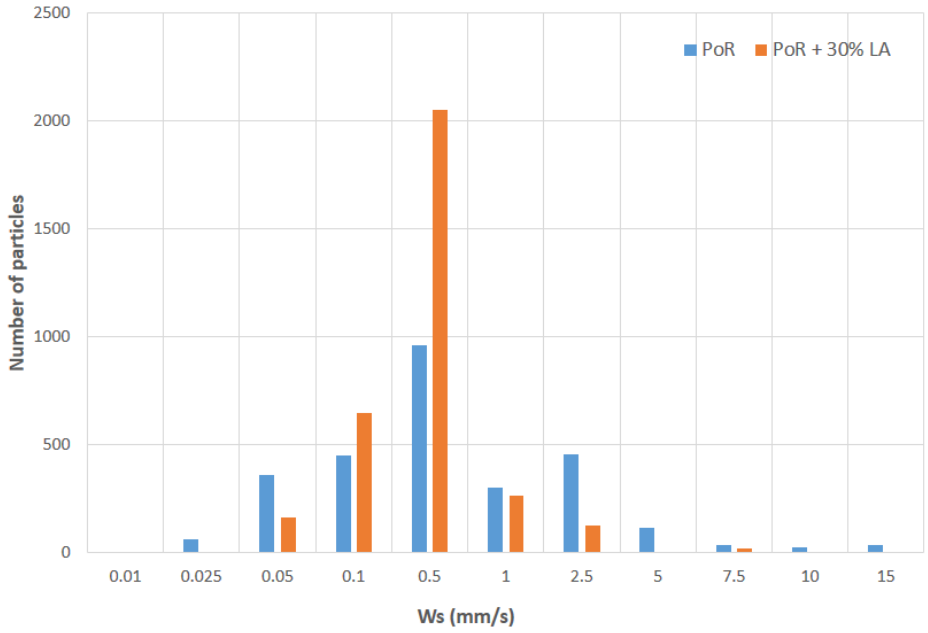

Figure 5.4: Settling velocity as function of number of particles measured by LabsFLOC for flocculated samples PoR and PoR with 30% LA corresponding to 5.10^6 cells/L. The sediment concentration is 0.2 g/L.

Due to differences in density between organic matter and sediment particles in in situ conditions, differential settling is playing an important role. Particle size measurements as function of depth correlated to SSC and Chlorophyl-a concentrations enable to show that in the Yangtze estuary differential settling between algae and clay is occurring [78]. Such measurements in the Rhine ROFI would confirm a similar mechanism in this coastal area. Because of flocculation the settling velocity of flocs would therefore become a function of depth.

5.3. PARTICLE STRUCTURE ANALYSIS, BASED ON IN SITU DATA

The LISST-HOLO and underwater camera have shown that the composition of the particles can be derived to some extend from the aspect ratio and the particle size distribution. From analyzing the in situ data in Chapter 4, we have seen that the mean diameter and particle shape (linked to its composition), depend on the water column stratification conditions and corresponding bed shear stress.

In this section we analyze this relation in more details, focusing on day 269 which is a spring tide day in autumn. The hydrodynamics of this day and in particular bed shear stresses, are covering both stratified and well mixed water column conditions. Figure 5.5a (upper panel), shows the SSC (mg/L) by OBS at near bottom and the volume con-

centration measured by LISST 100X (see Chapter 4 for details). In Figure 5.5 b ΔS and τ_{bed} are displayed. Some interesting time periods ("Spots") are highlighted in gray rectangles and labeled S1-S6. In Figure 5.5 (lower panel), the PSD corresponding to the times of these spots are plotted.

For S1 (Figure 5.5 b1) and S5 (Figure 5.5 b5), the PSD starts bimodal and becomes nearly monomodal. This is due to the fact that τ_{bed} increased over the same period. The shift from multimodal to monomodal indicates that particles are resuspended, which can be seen from the sharp increase in SSC. For S1, the period starts at a relatively high ΔS (at a value of 3). This ΔS increases in the next half hour up to 5.4 at around 3:00 AM. For S5 ΔS fluctuates over time.

For S2, the PSD (Figure 5.5 b2) starts relatively monomodal at the time where ΔS is low (0.7) and the water column is well mixed. The τ_{bed} remains low over the S2 period, implying that the particles are settling rather than eroding from the bed. As a consequence, the PSD is becoming more and more bimodal over time. This is due to the fact that only slow settling particles remain in suspension. These particles are anisotropic flocs containing a large amount of organic matter. The same happens for the time period S4 (Figure 5.5 b4 and s6 Figure 5.5 b6), whereby the shear stress is low over the whole period, and the PSD remains bimodal over the whole period.

During S2 period, the degree of stratification increases. The relationship between PSD modality and salinity stratification ΔS is different for S3 (Figure 5.5 b3). During that period, ΔS increases, but τ_{bed} as well. The increase in τ_{bed} leads to the fact that more particles are resuspended from the bed over time (see also the small increase in SSC during that period). Consequently the PSD becomes monomodal over time.

In conclusion, the near-bottom PSD behavior is primairly a function of shear stress and not salinity, which is to be expected as particles at that position never experience freshwater salinity. Low shear stresses are associated with bimodal PSD's and high shear stresses with monomoal ones. The fact that a PSD is monomodal is only implying that there is a majority of non-elongated flocs in suspension. In winter, the PSD's measured by LISST 100X were always monomodal as the bed stresses were high.

In Figure 5.6, the in situ data (day 269) is compared with the data obtained from the model. The mean diameter is calculated using the LISST 100X data. The gray rectangles correspond to the same periods S1-S6 as in Figure 5.5. The evolution of the mean floc size observed in situ is correlated with the IM1 and IM2 classes for S1, S2, and S3. When D50 is increasing the concentrations of IM1 and IM2 classes increases and vice-versa. For S4 and S5 a different trend is observed, the D50 obtained from the LISST data is observed to decrease, while the concentration of all three classes increases. This is primarily due to the mismatch between the modeled shear stress and the measured one. The model predicts an increase in shear during the period before S4, hence more particles get suspended in the water column. The estimated stress displays a decrease in the period prior S4 that leads to a decrease in D50 and SSC. It confirms that the sediment

concentration in suspension in the numerical model is a function of shear stress. Therefore high shear stresses are correlated with a high suspended sediment concentration and vice-versa.

It is expected that when the shear stresses are high, a large amount of sediment particles is in suspension. In that case, it seems reasonable to assume that current transport models are doing well in predicting sediment transport. When particles in suspension are primarily clayey particles, flocculation does not play an important role. Flocculated material and organic matter present in the water column can aggregate with clay and silt sized clayey material, but overall this effect will be that a bulk of pure clayey particles is transported from one part to another.

When the shear rates are moderate or low, on the other hand, it is found that a large amount of organic matter remains in suspension. This organic material can be coated with clayey particles. In that case, the question arises whether the predicted transported amounts of clayey particles are in line with the actual ones. This will be discussed in the subsection after the next, where existing sediment transport models including flocculation are analyzed. In the next subsection, we will study how the flocculation model presented in Chapter 3 can be adapted to account for the presence of organic matter.

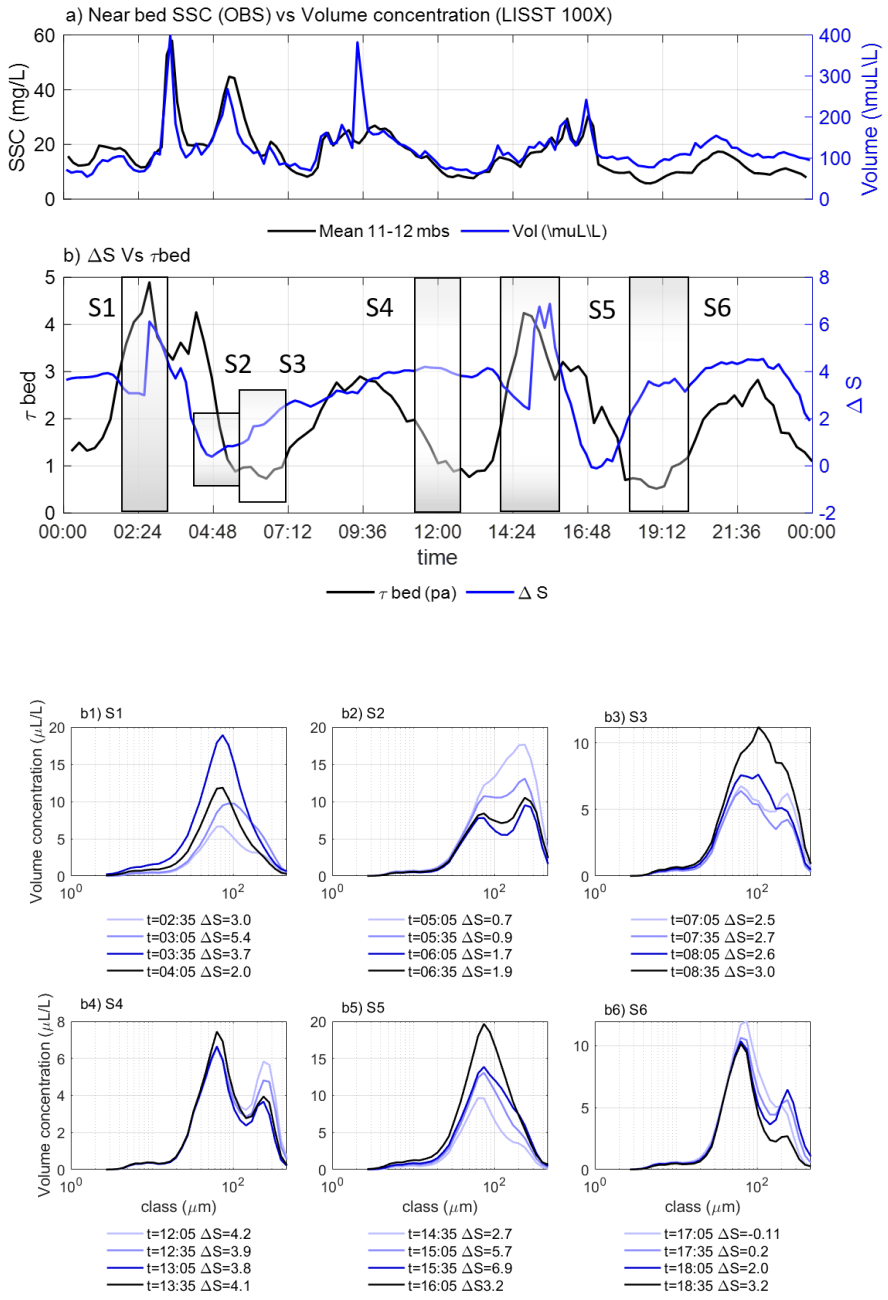

Figure 5.5: Data analysis of day 269 (a spring tide day of the autumn season 2014), (a) SSC of the surface (1 mbs) dashed blue line and near bottom, full black line. (b) ΔS versus bed stress. The lower panel shows the PSD's that correspond to the rectangles chosen in the upper panel graph, representing the relevant times in terms of hydrodynamics.

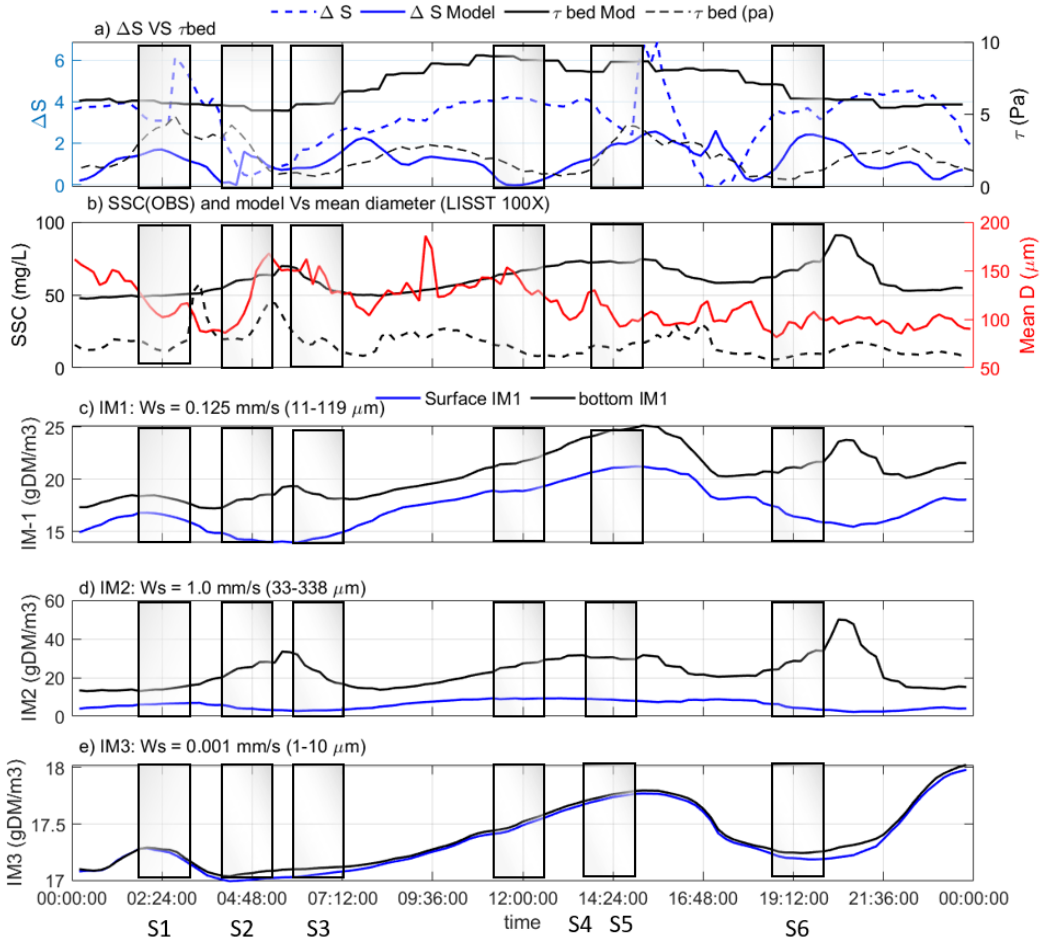

Figure 5.6: Comparison between in situ and model data for day 269. The full lines correspond to the model data and the dashed line to in situ data. a) τ_{bed} vs ΔS, b) SSC (mg/L) and the mean diameter (μm) obtained from LISST measurements, c) the IM1 class, d) IM2 class and d) the IM3 class. In these last three graphs the blue line represents surface concentration, and the bottom concentration is given in black. The rectangles in this Figure correspond to the times of rectangles in Figure 5.5.

5.4. TOWARDS A NEW APPROACH IN MODELING FLOCCULATION

As was done in Chapter 3, two classes of particles are considered, Class 1 corresponding to sediment particles (whereby, the salt-induced flocs can be included as discussed before). A Class 2, corresponding to flocs created by the aggregation of organic matter and sediment particles. A recent study has shown that Chl-a concentration (CC) and in particular the CC/SSC ratio can be used to study the dynamics of Class 2, when Class 2 is predominantly formed by aggregation with living algae [78]. Recalling from Chapter 3, the sediment particles mass transfer between Class 1 and Class 2 is expressed as:

$$\frac{dm_2}{dt} = -\frac{dm_1}{dt} \tag{5.1}$$

The transfer from Class 1 to Class 2 is described by:

$$\frac{dm_2}{dt} = b_{floc}(t) \times m_2 \tag{5.2}$$

where b_{floc} is the birth rate of Class 2 which is proportional to the concentration of organic matter present in the water column: i.e. C_{OM}:

$$b_{floc}(t) \approx C_{OM}(t)) \tag{5.3}$$

When $C_{OM} = 0$, $b_{floc} = 0$ there will be no flocculation, and thus no mass transfer between classes. Laboratory experiments [206] have demonstrated a faster than linear dependence of the flocculation rate D50/dt on flocculant dose, and therefore the proper dependence of b_2 on C_{OM} remains to be investigated. In contrast to laboratory experiments, as studied in Chapter 3, the sediment mass balance is conditioned to inflow and outflow of mass through the boundaries of the system. A numerical approach is given in [204]. For near-bed transport the suspension/erosion flux is of great importance. This flux is expressed as [26, 200]:

$$F_{z=0} = S_1 - E_1 \tag{5.4}$$

where $F_{z=0}$ represents the flux (mass transport in space and time). S_1 represents the mass settling flux and E_1 represents the erosion flux. The settling flux of Class 1 particles can be expressed as:

$$S_1 = w_{s,1} \times m_{1(z=0)} \tag{5.5}$$

where $w_{s,1}$ represents Stokes' settling velocity. The associated sediment density can be taken constant over time and size of Class 1 particles is then the mean particle size of the suspended sediment fraction. If required, Class 1 can be divided into sub classes as explained in [26]. Equations similar to eq.(5.4) and (5.5), can be set-up for Class 2 particles and this class could also be divided in sub classes [26].

In a first step it is assumed that Class 1 and Class 2 are represented by the mean settling velocity value of particles within these classes. It has been shown in Chapter 4 that at the onset of a storm (or during well mixed periods of spring tides) first the fluff top layer of the bed is eroded, this fluff layer contains in majority Class 2 particles. Subsequently

mainly Class 1 particles are resuspended. Expression for erosion (rate or coefficient) E_1 used in literature are [200]:

$$E_1 = C_1(\frac{\tau}{\tau_{c,1}} - 1)^m m_{1(z=0)} \tag{5.6}$$

whereby the empirical exponent m is found to be close to 1 for fine sediment bed. The parameter C_1 depends on the bottom contact forces between particles. A similar equation can be set-up for Class 2 particles. The precise formulation of such an erosion is an ongoing topic of research. It is expected that quite a substantial amount of flocculation is occurring in the fluff layer when sediment is deposited and it comes into contact with the previously deposited flocs or biofilm that might grow on the bed. It remains to be investigated whether this type of flocculation is dominant compared to water column flocculation.

5.5. DISCUSSION

Other authors proposed different flocculation models to be implemented in large-scale sediment transport models. Some of these models are based on a simplified PBE model, whereby three classes are defined based on the multimodal PSD's obtained from LISST data. These classes are therefore size-dependent and labeled fines, macro-flocs and mega-flocs [102, 186, 203]. As discussed in Chapter 2, the trimodality observed in measured PSD is mostly caused by the anisotropy of organic-rich particles [67]. A disadvantage of even a simplified PBE is the number of unknown parameters to use which amounts to 18 parameters for a 3-class PBE [203, 206]. Simplifying the PBE to the extreme, as is done by for example Winterwerp [145, 146, 207], who proposed a single representative class related to D50 size cannot be seen as a flocculation model in the sense that a proper mass balance between classes is missing. Moreover, this type of model does not account for the bimodal distribution (un-flocculated fines/ flocs) that is measured in-situ.

Other authors use Lattice Boltzmann simulation to model flocculation during differential settling and turbulence-induced flocculation [208, 209]. A drawback of the approach used by these authors is that they use DLVO forces and monodisperse primary particles in their simulations. Moreover, this type of simulation cannot be implemented in large-scale sediment transport for being too CPU intensive.

A pragmatic approach, used in particular in the large-scale sediment transport model TELEMAC-3 and also coded in Delft-3D is to use a variable settling velocity for a given size-class, which enables to avoid the problem of mass conversation. Different settling velocities have been proposed [113]. The changes in settling velocity should however be coupled with a clear understanding about the timescales associated to these changes, which is still an open research question.

5.6. CONCLUSION

In this chapter in situ data was compared with the output from the ZUNO-DD (Delft3D) numerical model. The salinity predicted by the model is in broad agreement with the measured one as was also found by Rijnsburger et al. [210]. The predicted SSC is relatively higher than the measured one, this is mainly due to higher predicted bed stresses that are caused by overestimation of the wave-induced bed stress. In general the trend of the modeled SSC is in agreement with the measured one.

The sediment classes IM1 and IM3 used in the numerical model represent particles having settling velocities of 0.001 and 0.125 mm/s, and are shown to have relatively similar concentration at the surface and bottom layers. The IM2 settling class have a settling velocity of 1 mm/s and have a concentration that increase near the bottom during the storm period due to resuspension. This class does not occur in the surface layer. After comparison with the measured in situ data, it was found that particles having settling velocities corresponding to IM1 and IM3 classes cover a wide range in terms of size. There is however, no interaction between the classes and their concentration changes independently from each other, they are distinguished by their settling velocities that are obtained from Stokes by using the clay, silt and sand sizes.

At this stage, there is no good link between particle size and settling velocity in coastal regions where the amount of organic matter is high. The organic matter content is highly variable depending on the seasons with the highest concentrations during the spring season as the primary production is highest in this season [136]. From analyzing the data collected during the survey day (in autumn season, during neap tide), it was found that most flocs in the water column have high organic matter content. The presence of this organic matter in the flocs leads to a wide range of effective densities, sizes and settling velocities. At present the link between sediment content of a floc and floc size is done using an inverse power-law function, which does not account for the observed large spread in floc density. Consequently, sediment mass transport could be overestimated in (coastal) regions where organic matter is abundant, if the mass concentration is estimated from this relation.

Organic matter should therefore be an important input parameter for sediment transport models. It has been found that one way to estimate organic matter content is to use Chl-a measurements (which is a proxy for algae content) and the ratio between Chl-a and SSC (CC/SSC), which is a promising parameter for further studies [78].

The flocculation model proposed in this thesis is based on a mass balance between two classes of particles that are defined on floc composition base rather than its size. The transfer between classes, and the processes leading to that, are schematically given in the conceptual model presented in Figure 5.7 at the end of this chapter. This conceptual model can be used as a reference to implement organic matter as a parameter into sediment transport models. It is expected (but not yet verified) that most of the exchange between classes occur at the bed. To study this, new laboratory experiments should be set-up whereby the interaction between the bed and water column can be studied in de-

tail. The results of this thesis are based on time series during autumn and winter, seasons that do not have a high primary production. It would be interesting to compare this data with a spring and/or summer season of high primary production.

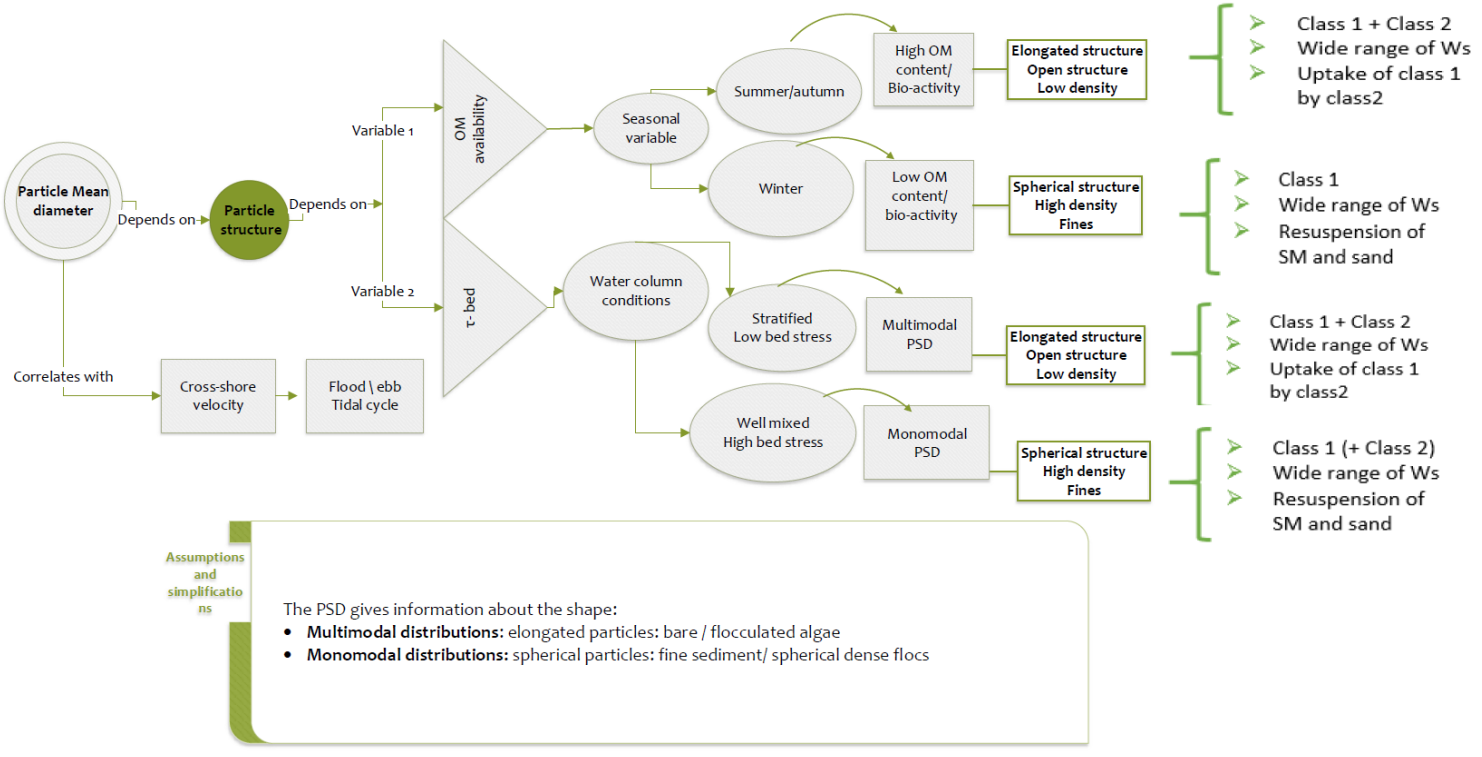

Figure 5.7: Conceptual representation of the parameters influential on particle diameter and structure. Sediment Mineral (SM), Organic Matter (OM) and Class 1 and 2 dominance are demonstrated in relation with the water column structure.

5.7. APPENDIX

Appendix F

DESCRIPTION OF ZUNO-DD MODEL

Zuno-DD is part of large Delft3D program developed by Deltares. Delft3D It is a fully integrated software suitable for a multi-disciplinary approach and 3D computations for coastal, river and estuarine areas. It calculates non-steady flow and transport phenomena resulting from tidal and meteorological forcing on a rectilinear or a curvilinear grid. The numerical system solves the unsteady shallow water equations in two or three dimensions using finite difference methods. The system of the equations consists of the horizontal equation of motion, the continuity equation and the transport equation for conservative constituents.

ZUNO-DD GRID

The ZUNO-DD module has three grids covering the North sea, especially the southern part of Dutch coastal area. The coarse grid is 61 × 133 cells, the intermediate grid is 64 × 244 cells and the fine grid is 109 × 213 cells. The intermediate and the fine grids describe the SPM fluxes from the Maasvlakte area towards the south and vice versa (Figure 8).

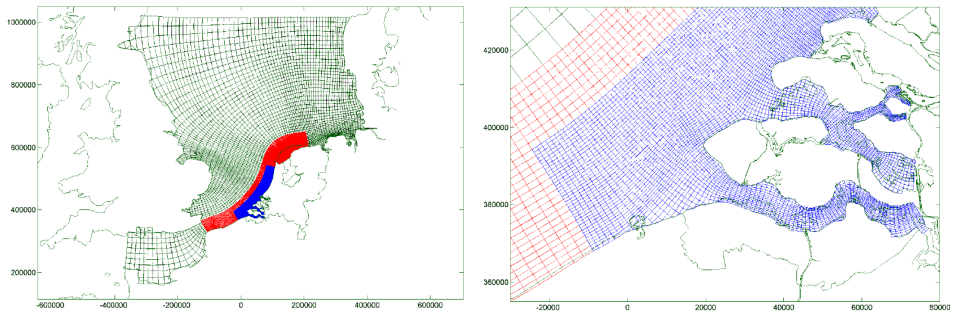

Figure 8: Right panel: The ZUNO-DD grids, Left panel: A zoom in the intermediate and fine ZUNO-DD grid.

By applying domain decomposition, the computational grid resolution can be optimized for the areas of interest, while keeping the overall grid size limited. In this way, the hydrodynamics are adequately represented in the model and therefore suitable for modelling sediment transport in the region. This hydrodynamic conditions are used for the SPM transport computations. By analyzing the difference in SPM flux over the cross-shore transects, a quantification of the change in the residual alongshore SPM flux is obtained [211].
S. Rijnsburger developed a 4^{th} domain version with a very fine grid around the Sand Engine (Zandmotor) near the Rhine and Meuse mouth [7].

6

Conclusions and Recommendations

6.1. GENERAL FINDINGS AND SUMMARY

Flocculation models that are used at present in sediment transport models are based on Population Balance Equations [24, 25, 107, 212]. This type of model is only valid for salt-induced flocculation whereby primary particles are all alike [26]. Therefore as discussed in the thesis, it is doubtful that this type of model would be suited to capture the key processes in the case of organic matter induced flocculation, i.e flocculation of clay minerals with organic matter. This type of flocculation represents the dominant flocculation type in estuaries and coast, where organic matter is known to be abundant [21, 169, 190].

The aim of this PhD research was to propose a flocculation model that properly predicts the SPM formation by flocculation in space and time in a Region Of Freshwater Influence (ROFI) like the Rhine-Meus delta which was the study site of this thesis. One requirement was that the model ought to be easy to implement in a numerical sediment transport model.

To confirm the abundance of organic matter in the composition of flocs, a first research question was addressed in chapter 2:

1. What are the type of particles that are found in situ (in the Rhine ROFI)? what are their properties (size, effective density, shape/ composition and settling velocity)?

It was confirmed that most particles found in situ of size > 10 μm are composed of sediment aggregated by organic matter in different amount. These flocs are hence formed by organic matter induced flocculation. Three major classes of particles were identified:

Class 1 corresponds to inorganic particle, having an effective density close to 1600 kg/m^3. These particles have a rather compact (spherical) form and appear with dark color (high density) on the video images.

Class 2 particles correspond to flocculated sediment particles with organic matter having an effective density in the range 16-160 kg/m^3. These particles may display a non-spherical structure and have overall a lighter color than Class 1 particles in the images, indicating a lower density. Some flocs have a high anisotropy that is caused by the presence of elongated algae strings which are recognizable in the flocs' structure. In other cases the algae strains are in some state of coiling and the flocs are hence rounder in shape. These particles exhibit a wide spread in settling velocity of the order of 1-10 mm/s.

Class 3 particles correspond to the bare algae, or algae bound to very little amount of sediment and have a very low effective density of about 16 kg/m^3. This implies that they have a low settling velocity. These bare algae particles have the highest anisotropy among all recorded particles and can have an aspect ratio of about 8.

As any model calibration relies on in situ monitoring, the quality of in situ monitoring is addressed by the second research question:

2. How do particle shape and composition affect light scattering measurements? How reliable is the obtained in situ data?

It was shown that the elongated particles cause an additional peak in the particle size distribution when measured by laser diffraction techniques (LISST 100X equipment). Moreover the detected light signal is affected by particles having sizes beyond the LISST 100X measurement range and by water column stratification (schlieren effect) [62–64]. This makes the interpretation of the laser diffraction measurements not straightforward and additional data is required to correct for the biased signal. This can be done using video camera images, which enable to record particles of size > 10 μm. Particles below 10 μm can only be assessed by LISST. It is expected that since these particles are not strongly anisotropic and have homogeneous density, they are correctly estimated by LISST.

Numerical fine sediment transport models give sediment concentration as function of space and time by class of particles. These models are not directly function of particle size or shape. The classes are sediment fractions to which, a given (constant) settling velocity is associated. The reason that numerical models depend indirectly on particle size is due to the fact that models are used to estimate settling velocity from in situ data. From particle size and concentration, a mean density of particles is estimated, and applying Stokes' law a mean settling velocity is deduced [26]. As discussed above, in situ particles are of different size, shape and composition. This is why it is very difficult to associate a settling velocity to a particle of a given size. Therefore it is shown in chapter 2, that a given particle size is rather associated with a range of settling velocities.
A flocculation model expresses the transfer of mass between one class of particles an another. Traditional flocculation models make use of Population Balance Equations (PBE) to express this mass transfer. This type of models rely on the ability of a floc to aggregate and break-up, whereby aggregation and break-up parameters are function of shear, sticking probability and break-up distribution function. A recent model, based on the mass transfer between 3 classes (microflocs, macroflocs and megaflocs) has as many as 18 parameters [26], which cannot be assessed from in situ measurements. PBE models are suitable to study systems composed of monodisperse particles, i.e salt induced flocculation [25, 206, 213, 214]. In the case of organic matter induced flocculation, as is the case in estuarine systems, these models do not capture some of the essential physical processes [204]:

- The size of a floc is not an unique function of the number of primary mineral clay particles that is made of, since for a same size, a floc could be formed by aggregation of different amounts of organic matter and mineral sediment.

- Particles can break-up due to shear, but polymeric flocs are elastic and usually tend to coil under shear without breaking. Their shape and size thus can change over time from elongated to spherical without loss of mass.

- The collision frequency in PBE models is a function of the diameter of the colliding particles. Organic matter can have very anisotropic shape, and extracellular polymeric substances (EPS) that are a major driver for flocculation consist of elongated, flexible polymeric chains (such as Polysaccharides, proteins and DNA). Their radius of gyration is a function of shear and water properties (such as salinity). The expression for the collision frequency in unknown.

For these reasons, a new type of model was introduced in this thesis to describe flocculation of suspended matter in situ. This model, based on logistic growth theory which is a theory that is used for example to estimate the auto-catalysis rate [80] or growth rate of bacteria [81].
The model has the advantage to be analytical, and therefore easy to implement in a sediment transport model. The amount of classes of particles can be arbitrary chosen. The sediment transport model Delft3D is often used in combination with 3 sediment fractions with settling velocities of the order of ≤ 0.01 mm/s, 0.1 mm/s and ≥ 1 mm/s. These fractions enable to correctly predict the Suspended Particulate Matter (SPM) in space and time for a large number of situations in coastal areas [18–21, 215].

In this thesis it was chosen to work with two sediment classes, based on floc composition rather than settling velocity: Class 1 (clay mineral), with a constant settling velocity and Class 2 (flocculated particles class), with a time dependent settling velocity. It is shown that the mass transfer between these two classes can be studied by laboratory experiments from which characteristic timescales for flocculation can be obtained (Chapter 3). This enabled to answer the third research question:

3. What are the flocculation timescales and how are these associated with different flocculation mechanisms?

To understand how these particles are formed and which timescales describe their formation, laboratory experiments were conducted to create flocs under different conditions. The growth of the particle size in time was analysed by the analytical logistic growth model. The flocculation timescales t_b and t_d that describe the 'birth' and 'decay' of particles respectively, where identified by parameterizing the flocculation model with experimental data. It was found that the salt induced flocculation is fundamentally different from the organic matter induced one.
The D50 in the salt induced case at constant shear, reaches a steady state over time. This steady state does not exceed the Kolmogrov microscale, as was already found by other authors [28] and hence no reduction in floc size (associated to the decay time t_d) was found. The birth time t_b was found to represent the characteristic flocculation time scale. Typical timescales for birth, in lab experiments, were t_b = 200-1000s for salt-induced flocculation.
The flocculation in presence of EPS and salt is faster than salt-induced flocculation and it was found that t_b < 500s. In contrast to salt-induced flocculation, it was found that the D50 first experienced an increase ('birth') and then a decrease ('decay') as function of time (for a given shear).
The decay occurred at times > 500s. This decay was associated to the coiling or breakage

of flocs under shear. From the experimental results, the mineral class (Class 1) which consists of pure clay mineral particles could be associated with a D50 of < 7 μm for the used clay samples and the Class 2 (flocs) were presented by the D50 size.
Class 1 particles flocculate in less than 500s generating flocs that grow over time during this period, reflected by the increase in D50 over time. For longer times (t > 500s), the D50 is decreasing, but class 1 is not populated, implying that if the flocs break, they break into smaller flocs and not into clay mineral particles. It was indeed shown that flocs created by organic matter have a size at steady state that exceed the Kolmogrov microscale, after a shear up/ shear down cycle, and remain elastic [29]. The relative fractions of Class 1 and Class 2 particles can be assessed from in situ measurements, by combining LISST and OBS measurements to obtain the volume concentrations of these classes. Their mass concentrations are obtained though sampling.
By using the two classes defined above it is therefore possible to test and calibrate the flocculation model proposed in this thesis using in situ data, which is an advantage over existing models that require to adjust parameters that cannot be quantified. It was also shown that ions (and in particular divalent cations) promote aggregation of organic matter, which confirms the role of fresh/salt water transition in flocculation process.
To get better understanding of the temporal and spatial distribution of suspended particles in the Rhine-ROFI a large data set was analysed (Chapter 4). This data set consists of Particles Size Distribution (PSD) measured by LISST 100X and LISST-HOLO in winter 2013 and autumn 2014, during two monitoring campaigns named STRAIN 1 and STRAIN II [17, 99]. These data shed light on the longer term SPM dynamics in Rhine-ROFI. With this data the following research questions are addressed:

4. How do the SPM concentration and size correlate with water column hydrodynamic conditions (when are they advected, and when resuspended)?

5. How do the seasonal changes in hydrodynamics and organic matter availability determine the composition and shape of the SPM particles and fluff layer development and depletion?

From the data analysis it was found that the SPM was organic matter rich during the autumn season. Both flocs (clay mineral with organic matter) and algae strains (without or with very little sediment attached) were found. Due to the lack of Chl-a measurements (a proxy for algae concentration), a chl-a to clay ratio could not be calculated as was done in [78]. SPM particles were found to be mainly advected during strong stratified periods at neap tides with calm weather conditions. The particles are originating from the Rhine front or from the shoreline due to the return flow near the bottom caused by the front arrival at the surface. Due to the lack of depth profile measurements through the water column, these hypothesis cannot be proved.
Particles settle and accumulate at the bottom at low shear, developing a fluff layer during the neap tides. This fluff layer resuspends during spring tides and settle again limiting its consolidation. Storm weather also causes this layer to resuspend, but in this case the fluff layer depletion is reached, after which the silt and sand fraction layer underneath is resuspended as well. It was found that the resuspension threshold of the fluff layer at the beginning of the storm was about 2 Pa.
Mainly clay mineral particles (silt and sand) are found during the winter season, and no

fluff layer erosion was observed during the winter storm. This is expected as the biological activity is low during the winter period and therefore the fluff layer, if present, would be very thin. These observations are in line with previous studies in different estuaries [170, 176–178].

The last research question that was defined in the introduction chapter is related to the general aim of the thesis:

6. What are the main features of a flocculation model that could be implemented in sediment transport models?

A first underlying question to answer is: how well do current sediment transport models whereby no flocculation is implemented perform? This question is answered in chapter 5. In this chapter the is-situ data is compared with the data obtained from the numerical sediment transport model Delft3D. The suspended sediment concentration (SSC) at the measurement location was calculated with the so called ZUNO-DD model [82, 83]. It was found that the model overestimates the SSC. This is attributed to the fact that the calculated SSC is a function of bed shear stress which is overestimated by the model.
In the model, particle classes are defined according to settling velocity, whereas the in situ measurements to which these classes could be compared are based on size. It was therefore not possible to comment further on the numerical results at this stage, since for a given particle size a range of settling velocities is observed.
The only flocculation that could be observed from the video imaging was an occasional floc-floc aggregation. The present video data was insufficient to allow for a statistically representative study of this type of aggregation. Flocculation occurring at the microscopic scale cannot be monitored in situ. It is however the most interesting type of flocculation from a sediment transport modeling point of view. The two classes defined in the present thesis have distinct settling velocities: the settling velocity of Class 1 particles can easily be estimated, since the density of sediment mineral is known, and it is constant. The settling velocity of Class 2 particles, on the other hand, is depending on several variables: the organic matter/ sediment mineral ratio of the floc and the state of coiling (which is a function of shear and floc history). Floc-Floc aggregation (called also macro-flocculation) will probably not affect the output of sediment transport models, because when a floc aggregates with another floc, their settling velocities is not affected much, especially when the organic matter content of the flocs is high since the density of organic matter is close to water.
The aggregation of a sediment particle by organic matter (called also microflocculation) is the type of flocculation creating the largest changes in the system. When a clay particle of 20 μm is captured by organic material it will become part of a floc with a size that is much larger than 20 μm, and its settling velocity will be changing from $<$ 1 mm/s to a value of the order of 1-10 mm/s. Micro-flocculation is therefore of key importance in areas where unflocculated sediment comes into contact with organic matter. This happens for instance during dredging works, or during storm events, when the fluff layer is depleted.
The micro-flocculation happens very fast(at very small time scales) in laboratory conditions. However, the experiments performed in the laboratory are performed in ideal

mixing conditions and do not account for the diffusion and advection of particles that occur in natural environment.
A flocculation model to be included in a numerical sediment transport model, based on two classes as proposed in this thesis, should be function of several parameters:

- Organic matter content: both living and dead organic matter play a role in the flocculation process (Chapter 3)'

- Salinity: a change in salinity can enhance the flocculation rate (Chapter 2 and 3).

- Shear: it influenced both the collision probability and the coiling / break-up of flocs (Chapter 2 and 3)

Salinity and shear are currently available in numerical models. Ecological models are available, which describe primary production, respiration and mortality of phytoplankton. Biochemical models also exist that could be used to estimate Particulate Organic Matter (POM) and Dissolved Organic Matter (DOM) to be used as input parameters [89]. These models could serve as input for a flocculation model.

6.2. OUTLOOK AND RECOMMENDATIONS

In order to pursue the work initiated in this thesis, several research lines and recommendations are proposed. From the in situ monitoring perspective, it is advised for future monitoring campaigns to:

- Monitor SPM as function of depth. It will be extremely interesting to observe the differences in SPM between the freshwater lens layer of the water column and the saline environment underneath. This study will allow to verify whether a majority of particles trapped above the pycnocline settle through it until reaching the sea floor or if a majority is advected with the freshwater front till the coast, where it is transported back seawards by bottom return currents.

- Combine several monitoring techniques: besides LISST and OBS, it is recommended to use an underwater camera. Current camera's combined with LED illumination allows to use video imaging as a regular monitoring tool. In addition combining optical and acoustic measurement techniques is of great benefit to study mud/sand mixtures as shown by Pearson et al. [216].

- Link the suspended sediment studies to ecological studies, whereby at each location, the type and concentration of organic matter is recorded. In recent studies, Chlorophyll-a (Chl-a) is routinely monitored as a proxy for algae concentrations [39, 78]. Furthermore other fractions of organic matter such as TEP, POC, PON measurements can provide more insight on the role of organic matter content and biomass in formation and dynamics of SPM in coastal and marine environment,

as presented by [136]. Ecological studies will also enable to link flocculation to the seasonal variability of organic life.

- Sampling: take samples to be used in the laboratory for further characterization and flocculation studies, as micro-flocculation cannot be monitored in situ. Particles' settling velocities can be monitored onboard, as was done in this study.

From a modeling perspective, in order to extend the flocculation model proposed in this thesis, the following steps are suggested:

- The flocculation study should be extended to larger tanks, to study the effect of differential settling and sediment concentration gradients on the flocculation kinetics. This study can be linked to the numerical modeling following the steps proposed in [204].

- Large flocculation tanks can also serve to study the erosion of fluff layers. This study is of prime importance for sediment transport models, as the bed acts as source/sink for sediment particles [26, 204].

- Additional laboratory experiments should be performed to parameterize the settling velocity of flocs (Class 2 particles) as function of organic matter content and shear history. New video imaging techniques are currently developed to link the gray-scale of floc images to density. In the future, underwater imaging could record this gray-scale and each floc' settling velocity could be derived from it. From video imaging mean settling velocities could therefore be deduced on a statistical basis. This would greatly benefit sediment transport models.

ACKNOWLEDGEMENTS

My PhD journey was a instructive and enjoyable at the same time. It opened a new world of coastal science for me and I could bring new knowledge to this field from a geochemistry point of view. I have met wonderful people, that helped me though this journey and I made new friends.

Therefore I would like to specially thank my promotor Prof. Dr. Julie D. Pietrzak for her supervision and contribution during my PhD project. I have learned a lot about the coastal hydrodynamics, river plumes and the Region Of Freshwater Influence (ROFI) which was a new discipline for me.

I would like to thank my co-promotor Dr. Claire Chassagne for her supervision, contribution and huge effort during my PhD project and improving my writing. Claire, it was pleasurable to work with you. I appreciate your open minded way of working and discussion during my PhD and before. I also value your patience for my slow and moderate writings skills.

I would like to specially thank Prof Andrew J. Manning for his valuable contribution to the data and experimental results, enabling the use of LabSFLOC camera system and providing a very crucial data for this thesis. Andy, I would like to thank you for the nice time we spend together in the Deltares laboratory working on the experiments.

I would like to thank Dr. ir. Thijs van Kessel for providing Delft3D data for comparison with the measured field data and for his contribution and advices during my PhD. Thijs, special thanks for providing feedback on the Dutch summary of this thesis, it was very useful. I would like to thank the committee members for reading this thesis and providing valuable comments and for previous discussions during different meetings and conferences.

This PhD project was a grant application of The Netherlands Scientific Organization (Nederlandse Wetenschappelijke Organisatie, NWO) project: New Delta, Flocs and fluff in Delta: towards dynamic particle properties in a SPM model for the Rhine - Scheldt ROFI. The mooring and frame data are supported by the Netherlands Technology Foundation STW program project: sustainable engineering of coastal systems in Regions Of Freshwater Influence (project 12682), ERC-advanced grant 291206 Nearshore Monitoring and Modeling (NEMO), and Rijkswaterstaat. Richard Cooke and Christopher Balfour are thanked for their valuable contribution during the measurement campaign. Additionally, the authors are grateful for support provided by NOC to deploy the three bottom frames.

Special thanks to the Navicula boat crew for enabling the one-day field survey. I would like also to thank Deltares for facilitating the use of their Physical laboratories (FL) and their devices.

I would like to thank Prof. Alejandro Souza and Alexander Horner-Divine and other PhD candidates in the group for providing the mooring and frame data and their contribution to the data collection. Special thanks to Alejandro Souza for providing insight in the LISST-data and its interpretation. Prof. Souza was funded by NERC through NOC National Capability funding.

Many thanks for my colleges and friends Zhirui Deng en Sabine Rijnsburger for helping processing the LISST data and for the nice time we spent together in the lab or at TU-Delft. Deng, we had a nice time in lab working together on the algae experiments and travelling by public transport to buy and bring the living algae from Yerseke. Sabine, I would specially thank you for your help with Matlab on processing the data and for the nice time we had together at TU-Delft. I also would like thank the colleagues in my office, Maria, Gonzalo, Merel, Erik and Yorick for the nice time in the office and their help with Matlab and Latex.

Nevertheless, it is impossible to thank everybody with whom I enjoyed working with and made me feel at home during my work. Therefore I would like to thank everybody I didn't mentioned by name who helped me during my PhD and contributed to enabling my success.

Zeinab Safar
June 2022

LIST OF PUBLICATIONS

1. **C. Chassange and Z. Safar**, *Modelling flocculation: towards an integration in large-scale transport modles*, Marine Geology **430**, 106361 (2020).

2. **A. Shakeel, Z. Safar. M. Ibanez, L. van Passen and C. Chassagne**, *Flocculation of clay suspension by anionic and cationic polyelectrolytes: A systematic analysis*, Minerals **10**, 999 (2020).

3. **C. Chassagne, Z. Safar, Z. Deng, Q. He and A. Manning** , *Chapter: Flocculation in Estuaries: Modeling Laboratory and In-situ studies*, Book: IntechOpen (2021).

4. **A.T. Lima, Z. Safar. J.P. Loch**, *Evaporation as the transport mechanism in arid regions*, Chemosphere**47**, (2014).

CURRICULUM VITÆ

Zeinab SAFAR

EDUCATION

2015–2022	PhD Candidate Delft university of Technology (TU Delft) Faculty of Civil Engineering and Geosciences, Hydraulic Engineering Dept. *Thesis*: Suspended Particulate Matter formation and accumulation in the Delta *Promotors:* Prof. Dr. J.D. Pietrzak and Dr. C. Chassagne
2009–2011	Master of science study program Geochemistry, Department of Earth Sciences Utrecht University
2005–2008	Higher General secondary education (HBO) analytical chemistry Hoge School Utrecht
2001–2005	Laboratory primary education ROC Leiden

JOB EXPERIENCE

2021–2022	researcher KWR BV. Institute for water research
2014–2015	research assistant Delft University of Technology Faculty of Civil Engineering and Geosciences, Hydraulic Engineering Dept. *Project:* Link between Zeta potential and viscosity consolidation and flocculation
2007–2008	Lab analyst TNO voeding Analysis of Mercury concentration in milk and food (1 year) Method development for characterization of organic acids concentration with Ion Chromatography (6 months)
2006–2007	Lab Analyst Akzo Nobel BV. Organic solvent characterization with Gas Chromatography (GC) polymer characterization with High Pressure liquid chromatography (HPLC),(1 year)

DESCRIPTION OF MASTER THESIS

The master thesis was an investigation of the upward migration of heavy metals in soils by evaporation. In this study the migration behavior of six heavy metals: Cd, Cr, Cu, Pb, Ni and Zn were investigated, the samples were collected from Saudi Arabian soils (representative for arid climate), because the arid weather condition soils were important in the study. In the semi- arid and arid regions the evaporation rates exceed the precipitation rates, what can cause an upward movement of the heavy metals dissolved in pore water in case of contaminated soils. After a dry period with high evaporation rates, these toxic metals will migrate upward with evaporating pore water and will precipitate on the soil texture and transform in to complexes with soil alkali metals, eventually they can reach the top soil and the surface with evaporating pore water and cause health issues for people contacting these soils. Furthermore they can come into the air with the dust particles depending on the bond formation with the clay or sand particles. These dust particles can be inhaled by human and cause other health problems.

REFERENCES

[1] S. Lee, R. Dunn, R. Young, R. Connolly, P. Dale, R. Dehayr, C. Lemckert, S. McKinnon, B. Powell, P. Teasdale, *et al.*, "Impact of urbanization on coastal wetland structure and function," *Austral Ecology*, vol. 31, no. 2, pp. 149–163, 2006.

[2] J. P. Syvitski, "Supply and flux of sediment along hydrological pathways: research for the 21st century," *Global and Planetary Change*, vol. 39, no. 1-2, pp. 1–11, 2003.

[3] J. P. Syvitski, C. J. Vörösmarty, A. J. Kettner, and P. Green, "Impact of humans on the flux of terrestrial sediment to the global coastal ocean," *science*, vol. 308, no. 5720, pp. 376–380, 2005.

[4] S. Smith, W. Renwick, R. Buddemeier, and C. Crossland, "Budgets of soil erosion and deposition for sediments and sedimentary organic carbon across the conterminous united states," *Global Biogeochemical Cycles*, vol. 15, no. 3, pp. 697–707, 2001.

[5] A. Kirichek, A. Shakeel, and C. Chassagne, "Using in situ density and strength measurements for sediment maintenance in ports and waterways," *Journal of Soils and Sediments*, pp. 1–7, 2020.

[6] B. M. Hickey, R. M. Kudela, J. Nash, K. W. Bruland, W. T. Peterson, P. MacCready, E. J. Lessard, D. A. Jay, N. S. Banas, A. M. Baptista, *et al.*, "River influences on shelf ecosystems: introduction and synthesis," *Journal of Geophysical Research: Oceans*, vol. 115, no. C2, 2010.

[7] S. Rijnsburger, "On the dynamics of tidal plume fronts in the rhine region of freshwater influence," 2021.

[8] J. van Wiegeren, "Modelling the wind-driven motion in the rhine rofi."

[9] J. de Boer, J. Pietrzak, and C. Winterwerp, "Sst observations of upwelling induced by tidal straining in the rhine rofi," *Continental Shelf Research*, vol. 29, pp. 263–277, 2009.

[10] A. Souza and J. Simpson, "Controls on stratification in the rhine rofi system," *Journal of Marine Systems*, vol. 12, pp. 311–323, 1997.

[11] J. De Kok, C. De Valk, J. Van Kester, E. De Goede, and R. Uittenbogaard, "Salinity and temperature stratification in the rhine plume," *Estuarine, Coastal and Shelf Science*, vol. 53, pp. 467–475, 2001.

[12] J. De Kok, "Baroclinic eddy formation in a rhine plume model," *Journal of Marine Systems*, vol. 12, pp. 35–52, 1997.

[13] G. J. D. Boer, *On the interaction between tides and stratification in the Rhine Region of Freshwater Influence.* 2008.

[14] J. Simpson and A. Souza, "Semidiurnal switching of stratification in the region of freshwater influence of the rhine," *Journal of Geophysical Research: Oceans*, vol. 100, no. C4, pp. 7037–7044, 1995.

[15] G. J. De Boer, J. D. Pietrzak, and J. C. Winterwerp, "On the vertical structure of the Rhine region of freshwater influence," *Ocean Dynamics*, vol. 56, no. 3-4, pp. 198–216, 2006.

[16] J. Simpson, "Physical processes in the rofi regime," *Journal of Marine Systems*, vol. 12, pp. 3–15, 1997.

[17] R. Flores, S. Rijnsburger, A. Horner-Devine, and A. Souza, "The impact of strom and stratification on sediment trasport in the rhine region of fresh water influence," *Journal of Geophysical Reseach: Oceans*, vol. 122, 2017.

[18] G. R. Lesser, J. v. Roelvink, J. Van Kester, and G. Stelling, "Development and validation of a three-dimensional morphological model," *Coastal engineering*, vol. 51, no. 8-9, pp. 883–915, 2004.

[19] C. L. Normant, "Three-dimensional modelling of cohesive sediment transport in the loire estuary," *Hydrological processes*, vol. 14, no. 13, pp. 2231–2243, 2000.

[20] A. Manning and K. Dyer, "A comparison of floc properties observed during neap and spring tidal conditions," in *Proceedings in Marine Science*, vol. 5, pp. 233–250, Elsevier, 2002.

[21] A. J. Manning, S. J. Bass, and K. R. Dyer, "Floc properties in the turbidity maximum of a mesotidal estuary during neap and spring tidal conditions," *Marine Geology*, vol. 235, no. 1-4, pp. 193–211, 2006.

[22] A. Manning, R. Whitehouse, and R. Uncles, "Suspended particulate matter: the measurements of flocs," *ECSA practical handbooks on survey and analysis methods: Estuarine and coastal hydrography and sedimentology*, pp. 211–260, 2017.

[23] G. Many, F. Bourrin, X. D. de Madron, I. Pairaud, A. Gangloff, D. Doxaran, A. Ody, R. Verney, C. Menniti, D. Le Berre, *et al.*, "Particle assemblage characterization in the rhone river rofi," *Journal of Marine Systems*, vol. 157, pp. 39–51, 2016.

[24] M. Fettweis, "Uncertainty of excess density and settling velocity of mud flocs derived from in situ measurements," *Estuarine, Coastal and Shelf Science*, vol. 78, no. 2, pp. 426–436, 2008.

[25] W. B. Russel, W. Russel, D. A. Saville, and W. R. Schowalter, *Colloidal dispersions*. Cambridge university press, 1991.

[26] C. Chassagne and Z. Safar, "Modelling flocculation: towards an integration in large-scale sediment transport models," *Marine Geology*, vol. 430, p. 106361, 2020.

[27] M. Elimelech, J. Gregory, and X. Jia, *Particle deposition and aggregation: measurement, modelling and simulation*. Butterworth-Heinemann, 2013.

[28] F. Mietta, C. Chassagne, R. Verney, and J. C. Winterwerp, "On the behavior of mud floc size distribution: Model calibration and model behavior," *Ocean Dynamics*, vol. 61, no. 2-3, pp. 257–271, 2011.

[29] A. Shakeel, Z. Safar, M. Ibanez, L. van Paassen, and C. Chassagne, "Flocculation of clay suspensions by anionic and cationic polyelectrolytes: A systematic analysis," *Minerals*, vol. 10, no. 11, p. 999, 2020.

[30] B. E. Logan, U. Passow, A. L. Alldredge, H. P. Grossartt, and M. Simont, "Rapid formation and sedimentation of large aggregates is predictable from coagulation rates (half-lives) of transparent exopolymer particles (TEP)," *Deep-Sea Research Part II*, vol. 42, no. 1, pp. 203–214, 1995.

[31] A. L. Alldredge, U. Passow, and B. E. Logan, "The abundance and significance of a class of large, transparent organic particles in the ocean," *Deep-Sea Research Part I*, vol. 40, no. 6, pp. 1131–1140, 1993.

[32] J. Naudin, G. Cauwet, M.-J. Chretiennot-Dinet, B. Deniaux, J.-L. Devenon, and H. Pauc, "River discharge and wind influence upon particulate transfer at the land-ocean interaction: case study of the rhone river plume," *Estuarine, coastal and shelf science*, vol. 45, pp. 303–316, 1997.

[33] J. Ren and J. Wu, "Sediment trapping by haloclines of a river plume in the pearl river estuary," *Continental Shelf Research*, vol. 82, pp. 1–8, 2014.

[34] H. Y. Yao, N. Leonardi, J. F. Li, and S. Fagherazzi, "Sediment transport in a surface-advected estuarine plume," *Continental Shelf Research*, vol. 116, pp. 122–135, 2016.

[35] J. Lee, J. T. Liu, C. C. Hung, S. Lin, and X. Du, "River plume induced variability of suspended particle characteristics," *Marine Geology*, vol. 380, pp. 219–230, 2016.

[36] J. Tao, P. S. Hill, E. S. Boss, and T. G. Milligan, "Variability of suspended particle properties using optical measurements within the columbia river estuary," *Journal of Geophysical Research: Oceans*, vol. 123, no. 9, pp. 6296–6311, 2018.

[37] P. Chen, J. C. S. Yu, and M. Fettweis, "Modeling Storm-Influenced Suspended Particulate Matter Flocculation Using a Tide-Wave-Combined Biomineral Model," *Water Environment Research*, vol. 90, no. 3, 2018.

[38] K. R. Dyer and T. J. Moffat, "Fluxes of suspended matter in the East Anglian plume Southern North Sea," *Continental Shelf Research*, vol. 18, no. 11, pp. 1311–1331, 1998.

[39] M. Fettweis and J. L. B., "Spatial and seasonal variation of biomineral suspended particulate matter properties in high- turbid nearshore and low- turbid offshore zones," *water*, vol. 9, no. 694, 2017.

[40] I. G. Droppo, G. G. Leppard, D. T. Flannigan, and S. N. Liss, "The freshwater floc: A functional relationship of water and organic and inorganic floc constituents affecting suspended sediment properties," vol. 99, no. 1-4, pp. 43–53, 1997.

[41] J. A. Wheatland, A. J. Bushby, and K. L. Spencer, "Quantifying the Structure and Composition of Flocculated Suspended Particulate Matter Using Focused Ion Beam Nanotomography," *Environmental Science and Technology*, vol. 51, no. 16, pp. 8917–8925, 2017.

[42] B. S. Lartiges, S. Deneux-Mustin, G. Villemin, C. Mustin, O. Barres, M. Chamerois, B. Gerard, and M. Babut, "Composition, structure and size distribution of suspended particulates from the Rhine River," *Water Research*, vol. 35, no. 3, pp. 808–816, 2001.

[43] M. Ibanez Sanz, *Flocculation and Consolidation of cohesive sediment under the influence of coagulant and flocculant.* Dissertation.

[44] D. Eisma, J. Kalf, and M. Veenhuis, "The formation of small particles and aggregates in the Rhine estuary," *Netherlands Journal of Sea Research*, vol. 14, no. 2, pp. 172–191, 1980.

[45] M. Brocchini, M. Postacchini, C. Lorenzoni, A. Russo, S. Corvaro, A. Mancinelli, L. Soldini, A. Russo, J. Calantoni, A. H. Reed, E. F. Braithwaite, A. Sheremet, T. Staples, and J. Smith, "Comparison between the wintertime and summertime dynamics of the Misa River estuary," *Marine Geology*, vol. 385, pp. 27–40, 2017.

[46] J. Morelle, M. Schapira, and P. Claquin, "Dynamics of phytoplankton productivity and exopolysaccharides (EPS and TEP) pools in the Seine Estuary (France, Normandy) over tidal cycles and over two contrasting seasons," *Marine Environmental Research*, vol. 131, 2017.

[47] L. E. Frostick and I. Nicholas, "Seasonal Shifts of Sediment Within Estuary Mediated by Algal Growth an," pp. 569–576, 1979.

[48] B. J. Lee, J. Hur, and E. A. Toorman, "Seasonal Variation in Flocculation Potential of River Water: Roles of the Organic Matter Pool," *Water (Switzerland)*, vol. 9, no. 5, pp. 1–14, 2017.

[49] H. J. van der Woerd, A. Blauw, L. Peperzak, R. Pasterkamp, and S. Peters, "Analysis of the spatial evolution of the 2003 algal bloom in the Voordelta (North Sea)," *Journal of Sea Research*, vol. 65, no. 2, pp. 195–204, 2011.

[50] C. Paper and C. Van, "Variability of suspended particulate matter composition at Egmond , The Netherlands," no. January, 2012.

[51] D. C. Fugate and C. T. Friedrichs, "Controls on suspended aggregate size in partially mixed estuaries," *Estuarine, Coastal and Shelf Science*, vol. 58, no. 2, pp. 389–404, 2003.

[52] H. Burchard and H. Baumert, "The Formation of Estuarine Turbidity Maxima Due to Density Effects in the Salt Wedge. A Hydrodynamic Process Study," *Journal of Physical Oceanography*, vol. 28, no. 2, pp. 309–321, 2002.

[53] S. Papenmeier, K. Schrottke, and A. Bartholomä, "Over time and space changing characteristics of estuarine suspended particles in the German Weser and Elbe estuaries," *Journal of Sea Research*, vol. 85, pp. 104–115, 2014.

[54] S. Bass, A. Manning, and K. Dyer, "Preliminary findings of a study of the upper reaches of the tamar estuary, uk, throughout a complete tidal cycle: Part i: Linking hydrodynamic and sediment cycles," 2007.

[55] R. Verney, R. Lafite, J. Brun-Cottan, and P. Le Hir, "Behaviour of a floc population during tidal cycle: Laboratory experiments and numerical modelling," *Continental Shelf Research*, vol. 31, pp. s64–s83, 2011.

[56] C. Sahin, H. A. Ari Guner, M. Ozturk, and A. Sheremet, "Floc size variability under strong turbulence: Observations and artificial neural network modeling," *Applied Ocean Research*, vol. 68, pp. 130–141, 2017.

[57] P. Jarvis, B. Jefferson, and S. A. Parsons, "Breakage, regrowth, and fractal nature of natural organic matter flocs," *Environmental Science and Technology*, vol. 39, no. 7, pp. 2307–2314, 2005.

[58] P. Jarvis, B. Jefferson, J. Gregory, and S. A. Parsons, "A review of floc strength and breakage," *Water Research*, vol. 39, no. 14, pp. 3121–3137, 2005.

[59] Y. Argrawal and P. Traykovski, "Particles in the bottom boundary layer: Concentration and size dynamics through events," *Journal of Geophysical research*, vol. 106, pp. 9533–9542, 2001.

[60] P. Traykovski, J. Latter, and J. D. Irish, "A laboratory evaluation of the laser in situ scattering and transmissometery instrument using natural sediments," vol. 159, pp. 355–367, 07 1999.

[61] E. Boss, C. R. Sherwood, P. Hill, and T. Milligan, "Advantages and limitations to the use of optical measurements to study sediment properties," *Applied Sciences*, vol. 8, no. 12, p. 2692, 2018.

[62] E. Steele, W. Nimmo-Smith, D. E.J., and A. Souza, "Indentification of contamination by schlieren of optical measurements of suspended sediments," *Limonology and Oceanography: Methods*.

[63] O. A. Mikkelsen, T. G. Milligan, P. S. Hill, R. J. Chant, C. F. Jago, S. E. Jones, V. Krivtsov, and G. Mitchelson-Jacob, "The influence of schlieren on in situ optical measurements used for particle characterization," *Limnology and Oceanography: Methods*, vol. 6, no. 3, pp. 133–143, 2008.

[64] R. Styles, "Laboratory evaluation of the lisst in a stratified fluid," *Marine Geology*, vol. 227, pp. 151–162, 2006.

[65] E. J. Davies, W. A. M. Nimmo-Smith, Y. C. Agrawal, and A. J. Souza, "LISST-100 response to large particles," *Marine Geology*, vol. 307-310, pp. 117–122, 2012.

[66] E. J. Davies, A. M. Nimmo-Smith, Y. C. Agrawal, and A. J. Souza, "Scattering signatures of suspended particles: an integrated system for combining digital holography and laser diffraction," vol. 19, no. 25, pp. 2187–2197, 2011.

[67] L. Karp-Boss, L. Azevedo, and E. Boss, "LISST-100 measurements of phytoplankton size distribution: Evaluation of the effects of cell shape," *Limnology and Oceanography: Methods*, vol. 5, no. 11, pp. 396–406, 2007.

[68] C. Schwarz, T. Cox, T. Van Engeland, D. Van Oevelen, J. Van Belzen, J. Van de Koppel, K. Soetaert, T. J. Bouma, P. Meire, and S. Temmerman, "Field estimates of floc dynamics and settling velocities in a tidal creek with significant along-channel gradients in velocity and spm," *Estuarine, Coastal and Shelf Science*, vol. 197, pp. 221–235, 2017.

[69] G. M. Cartwright, "Application of acoustics and optics for the characterization of suspended particulate matter within an estuarine observing system," 2013.

[70] G. Graham, E. Davies, W. Nimmo-Smith, D. Bowers, and K. Braithwaite, "Interpreting lisst-100x measurements of particles with complex shape using digital in-line holography," *Journal of Geophysical Research: Oceans*, vol. 117, no. C5, 2012.

[71] X. Shen, E. A. Toorman, M. Fettweis, B. J. Lee, and Q. He, "Simulating multimodal floc size distributions of suspended cohesive sediments with lognormal subordinates: Comparison with mixing jar and settling column experiments," *Coastal Engineering*, vol. 148, no. August 2018, pp. 36–48, 2019.

[72] Y. Zhao, "Settling behaviour of polymer flocculated water-treatment sludge i: analyses of settling curves," *Separation and Purification Technology*, vol. 35, no. 1, pp. 71–80, 2004.

[73] G. Chen, I. Chang, W. Hung, and D. Lee, "Regimes for zone settling of waste activated sludges," *Water Research*, vol. 30, no. 8, pp. 1844–1850, 1996.

[74] C. Fargues and C. Turchiuli, "Structural characterization of flocs in relation to their settling performances," *Chemical Engineering Research and Design*, vol. 81, no. 9, pp. 1171–1178, 2003.

[75] F. Maggi, "Biological flocculation of suspended particles in nutrient-rich aqueous ecosystems," *Journal of Hydrology*, vol. 376, no. 1-2, pp. 116–125, 2009.

[76] W. Van Leussen and J. Cornelisse, "The determination of the sizes and settling velocities of estuarine flocs by an underwater video system," *Netherlands Journal of Sea Research*, vol. 31, no. 3, pp. 231–241, 1993.

[77] C. Mietta, F.and Chassagne, A. J. Manning, and J. C. Winterwerp, "Influence of shear rate, organic matter content, pH and salinity on mud flocculation," *Ocean Dynamics*, vol. 59, no. 5, pp. 751–763, 2009.

[78] D. Zhirui, H. Qing, S. Zeinab, and C. Claire, "The role of algae in fine sediment flocculation: In-situ and laboratory measurements,"

[79] T. R. Malthus, *An Essay on the Principle of Population.*. 1872.

[80] Y.-P. Tsai, "Simulation of biofilm formation at different assimilable organic carbon concentrations under lower flow velocity condition," *Journal of Basic Microbiology: An International Journal on Biochemistry, Physiology, Genetics, Morphology, and Ecology of Microorganisms*, vol. 45, no. 6, pp. 475–485, 2005.

[81] X. Chen, C. Zhang, Z. Zhou, Z. Gong, J. Zhou, J. Tao, D. Paterson, and Q. Feng, "Stabilizing effects of bacterial biofilms: Eps penetration and redistribution of bed stability down the sediment profile," *Journal of Geophysical Research: Biogeosciences*, vol. 122, no. 12, pp. 3113–3125, 2017.

[82] K. Blaas, M, G. Cronin, Y. Friocourt, S. Gracia, Triana, G. Gaytan Aguilar, and K. G., "Model setup, data assimilation and skill assessment: Model support of spm in the dutch coastal zone.."

[83] G. Keetels, T. van Kessel, A. van Rooijen, Y. Friocourt, T. van der Kaaij, and H. Los, "Winning suppletiezand noordzee 2013-2017."

[84] E. D. De Ruyter Van Steveninck, W. Admiraal, L. Breebaart, G. M. J. Tubbing, and B. Van Zanten, "Plankton in the River Rhine: Structural and functional changes observed during downstream transport," *Journal of Plankton Research*, vol. 14, no. 10, pp. 1351–1368, 1992.

[85] F. Roozen, "Transparency of floodplain lakes, a study of plankton and suspended matter along the lower rhine," 2005.

[86] W. van Leussen, "The variability of settling velocities of suspended fine-grained sediments in ems estuary," *Journal of Sea Research*, vol. 41, pp. 109–118, 1999.

[87] D. van de Meent, "Particulate organic matter in the river rhine delta," 1982.

[88] J. Rijstenbil, "Phytoplankton composition of stagnant and tidal ecosystems in relation to salinity, nutrients, light and turbulence," *Netherlands Journal of sea research*, vol. 21, no. 2, pp. 113–123, 1987.

[89] A. Blauw, "Monitoring and prediction of phytoplankton dynamics in the north sea."

[90] T. Prins, X. Desmit, and J. Baretta-Bekker, "Phytoplankton composition in dutch coastal waters responds to changes in rivirine nutrient loads," *Journal of sea research*, vol. 73, pp. 49–62, 2012.

[91] K. N. I. Razaz, M. Kawanisi, "Tide-driven controls on maximum near-bed floc size in a tidal estuary," *Journal of hydro-environmental Research*, vol. 9, pp. 465–471, 2015.

[92] C. Schwarz, T. Cox, T. van Engeland, D. van Oevelen, J. van Blezen, J. van de Koppel, K. Soetaert, T. Bouma, P. Meire, and S. Temmerman, "Field estimates of floc dynamics and settling velocities in a tidal creek with significant along-channel gradients in velocity and spm," *Estuarine, Coastal and Shelf Science*, vol. 197, pp. 221–235, 2017.

[93] J. Pietrzak, G. de Boer, and M. Eleveld, "Mechanisms controlling the intra-annual mesoscale variability of SST and SPM in the southern North Sea," *Continental Shelf Research*, vol. 31, no. 6, pp. 594–610, 2011.

[94] O. Schofield, M. Moline, B. Cahill, T. Frazer, A. Kahl, M. Oliver, J. Reinfelder, S. Glenn, and R. Chant, "Phytoplankton productivity in a turbid buoyant coastal plume," *Continental Shelf Research*, vol. 63, no. 3, 2013.

[95] J. Cross, W. A. M. Nimmo-Smith, P. J. Hosegood, and R. Torres, "The role of advection in the distribution of plankton populations at a moored 1-D coastal observatory," *Progress in Oceanography*, vol. 137, pp. 342–359, 2015.

[96] O. E. Ganaoui, E. Schaaff, P. Boyer, M. Amielh, F. Anselmet, and C. Grenz, "Erosion of the upper layer of cohesive sediments: characterization of some properties," *Journal of Hydraulic Engineering*, vol. 133, no. 9, pp. 1087–1091, 2007.

[97] M. Stive, M. d. Schipper, A. Luijendijk, S. Aarninkhof, C. v. Gelder-Maas, J. v. T. d. Vries, S. d. Vries, M. Henriquez, S. Marx, and R. Ranasinghe, "A new alternative to saving our beaches from sea-level rise: The sand engine," *Journal of Coastal Research*, vol. 29, pp. 1001–1008, 2013.

[98] A. Horner-Divine, J. Pietrzak, A. Souza, M. McKoen, S. Meirelles, M. Henriquez, R. Flores, and S. Rijnsburger, "Cross-shore transport of nearshore sediment by river plume frontal pumping," *Geophysical Reseach Letters*, vol. 44, 2017.

[99] S. Rijnsburger, R. P. Flores, J. D. Pietrzak, A. R. Horner-Devine, and A. J. Souza, "The Influence of Tide and Wind on the Propagation of Fronts in a Shallow River Plume," *Journal of Geophysical Research: Oceans*, vol. 123, no. 8, pp. 5426–5442, 2018.

[100] R. Sternberg, I. Berhane, and A. Ogston, "Measurement of size and settling velocity of suspended aggregates on the northern california continental shelf," *Marine geology*, vol. 154, no. 1-4, pp. 43–53, 1999.

[101] S. Smith and C. Friedrichs, "Image processing methods for in situ estimation of cohesive sediment floc size, settling velocity, and density," *Limnology and Oceanography: Methods*, vol. 13, no. 5, pp. 250–264, 2015.

[102] X. Shen and J. P. Y. Maa, "A camera and image processing system for floc size distributions of suspended particles," *Marine Geology*, vol. 376, pp. 132–146, 2016.

[103] T. Benson and J. R. French, "Insipid: A new low-cost instrument for in situ particle size measurements in estuarine and coastal waters," *Journal of Sea Research*, vol. 58, no. 3, pp. 167–188, 2007.

[104] *LISST HOLO Manual 2014*.

[105] S. M. Choi, H. K. Seo, J. Yand Ha, and G. hong Lee, "Estimating effective density of cohesive sediment using shape factors from holographic images," *Estuarine, Coastal and Shelf Science*, vol. 215, no. October, pp. 144–151, 2018.

[106] M. A.J., "Video measurement of flocculated sediment in lakes and estuary in the usa," *2nd Joint Federal Interagency Conference on sedimentation and Hydrologic Modeling*.

[107] A. Manning, R. Whitehouse, and R. Uncles, "Suspended particulate matter: The measurements of flocs."

[108] A. Manning, P. Friends, N. Prows, and C. Amos, "Preliminary findings from a study of medway estuary (uk) natural mud floc properties using a laboratory mini-flume and the labsfloc system," *Continental Shelf Research*, pp. 211–260, 2007.

[109] T. Benson and A. Manning, "Digifloc: The development of semi-automatic software to determine the size and settling velocity of flocs," 2016.

[110] A. Manning and K. Dyer, "The use of optics for the in situ determination of flocculated mud characteristics," *Journal of optics A: Pure and Applied optics*, vol. 4, no. 4, p. S71, 2002.

[111] A. Manning and D. Schollhamer, "Factors controlling floc settling velocity along a longitudinal estuarine transect," *Marine Geology*, vol. 345, pp. 266–280, 2013.

[112] M. Fettweis and M. Baeye, "Seasonal variation in concentration, size, and settling velocity of muddy marine flocs in benthic boundary layer," *Journal of geophysical research: Oceans*, vol. 120, pp. 5648–5667, 2015.

[113] A. Khelifa and P. Hills, "Models for effective density and settling velocity of flocs," *Journal of Hydraulic Research*, vol. 44, pp. 390–401, 2006.

[114] F. Maggi, "Variable fractal dimension: A major control for floc structure and flocculation kinematics of suspended cohesive sediment," *Journal of geophysical research: oceans*, vol. 112, 2007.

[115] L. Karp-Boss, L. Azevedo, and E. Boss, "Lisst-100 measurements of phytoplankton size distribution: Evaluation of the effects of cell shape," *Limnology and Oceanography: Methods*, vol. 5, no. 11, pp. 396–406, 2007.

[116] G. Many, X. Durrieu de Madron, R. Verney, F. Bourrin, P. Renosh, F. Jourdin, and A. Gangloff, "Geometry, fractal dimension and settling velocity of flocs during flooding conditions in the Rhône ROFI," *Estuarine, Coastal and Shelf Science*, vol. 219, pp. 1–13, apr 2019.

[117] P. Jarvis and A. Jefferson, B. Parsons, "How the natural organic matter to coagulant ratio impacts on floc structural properties," *Environmental sciennce and Technology*, vol. 39, pp. 8919–8924, 2005.

[118] K. Spencer, I. Manning, A.J. Droppo, G. Leppard, and T. Benson, "Dynamic interactions between cohesive sediment tracers and natural mud," *Journal of soils sediment*, vol. 10, pp. 1401–1414, 2010.

[119] A. Alldredge and C. Gotschalk, "Direct observation of the mass flocculation of diatom blooms: Characteristics, settling velocities and formation of diatom aggregates," *Deep Sea Research*, vol. 36 (2), pp. 159–171, 1989.

[120] H. G. Dam and D. Drapeau, "Coagulation efficiency, organic matter glues and dynamics of particles during a phytoplakton bloom in a mesocosm study," *Deep-sea Research*, vol. 42, pp. 111–123, 1995.

[121] U. Passow, A. Alldredge, and B. Logan, "The role of particulate carbohydrates exudate's in the flocculation of diatom blooms," *Deep Sea Research*, vol. 41 (2), pp. 335–357, 1994.

[122] J. Pavoni, M. Tenney, and W. Echelberger, "Bacterial exocellular polymers and biological flocculation," *Journal WPCF*, vol. 41, pp. 414 – 431, 1972.

[123] V. Smetacek, "Role of the sinking diatom life-history cycles: ecological, evolutionary and geological significance," *Marine biology*, vol. 84, pp. 239–251.

[124] T. Malone, "Algal size [influence on response to environment, physiological processes].," *Studies in ecology (USA). v. 7.*, 1980.

[125] E. Foree and P. McCarty, "Anaerobic decomposition of algae," *Environmental science and technology*, vol. 4 (10), pp. 842–849.

[126] G. Vaezi, R. Sanders, and J. H. Masliyah, "Flocculation kinetics and aggregate structure of kaolinite mixtures in laminar tube flow," *Journal of Colloid and Interface Science*, vol. 355, no. 1, pp. 96–105, 2011.

[127] S. Al Ani, K. R. Dyer, and D. A. Huntley, "Measurement of the influence of salinity on floc density and strength," *Geo-Marine Letters*, vol. 11, no. 3-4, pp. 154–158, 1991.

[128] R. Ram, "Flocculation Controls in a Hypertidal Estuary," *TU Delft, Netherlands*, 2014.

[129] A. J. Mehta, A. Manning, and Y. P. Khare, "A note on the Krone deposition equation and significance of floc aggregation," *Marine Geology*, vol. 354, pp. 34–39, 2014.

[130] R. Gibbs, "Estuarine flocs: Their size, settling velocity and density," *Journal of geophysical research*, vol. 90, pp. 3249–3251, 1985.

[131] A. Manning, P. Friend, N. Prowse, and C. Amos, "Estuarine mud flocculation properties determined using an annular mini-flume and the labsfloc system," *Continental Shelf Research*, vol. 27, no. 8, pp. 1080–1095, 2007.

[132] O. Mikkelsen, T. Hill, P.S.and Milligan, and R. Chant, "In situ particles size distribution and volume concentrations from lisst-100 laser particle sizer and digital floc camera," *Continental Shelf Research*, vol. 25, pp. 1959–1978, 2005.

[133] G. W. Graham, E. J. Davies, W. A. Nimmo-Smith, D. G. Bowers, and K. M. Braithwaite, "Interpreting LISST-100X measurements of particles with complex shape using digital in-line holography," *Journal of Geophysical Research: Oceans*, vol. 117, no. 5, pp. 1–20, 2012.

[134] W. A. Nimmo-smith, G. W. Graham, and W. A. M. N. Smith, "The application of holography to the analysis of size and settling velocity of suspended cohesive sediments OCEANOGRAPHY : METHODS velocity of suspended cohesive sediments," *Limnology And Oceanography-Methods*, vol. 8, no. October, pp. 1–15, 2016.

[135] Y. C. Agrawal, A. Whitmire, O. A. Mikkelsen, and H. C. Pottsmith, "Light scattering by random shaped particles and consequences on measuring suspended sediments by laser diffraction," *Journal of Geophysical Research: Oceans*, vol. 113, no. 4, pp. 1–11, 2008.

[136] M. Fettweis, M. Schartau, X. Desmit, B. J. Lee, N. Terseleer, D. Van der Zande, and R. Riethmüller, "Organic matter composition of biomineral flocs and its influence on suspended particulate matter dynamics along a nearshore to offshore transect," *Earth and Space Science Open Archive*, p. 47, 2021.

[137] J. Cross, W. A. M. Nimmo-smith, R. Torres, and P. J. Hosegood, "Biological controls on resuspension and the relationship between particle size and the Kolmogorov length scale in a shallow coastal sea," *Marine Geology*, vol. 343, pp. 29–38, 2013.

[138] H. Lai, H. Fang, L. Huang, G. He, and D. Reible, "A review on sediment bioflocculation: Dynamics, influencing factors and modeling," *Science of the Total Environment*, vol. 642, pp. 1184–1200, 2018.

[139] R. Passow, U.and Shipe, A. Murray, M. Pak, D.K.and Brezezinski, and A. Alldredge, "The origin of transparent exopolymer particles (tep) and their role in sedimentation of particulate matter," *Continental Shelf Research*, vol. 21, pp. 327–346, 2001.

[140] U. Passow, "Transparent exopolymer particles (tep) in aquatic environment," *Progress in Oceanography*, vol. 55, pp. 287–333, 2002.

[141] B. J. Lee, E. Toorman, F. J. Molz, and J. Wang, "A two-class population balance equation yielding bimodal flocculation of marine or estuarine sediments," *Water Research*, vol. 45, no. 5, pp. 2131–2145, 2011.

[142] G. A. Jackson, "A model of the formation of marine algal flocs by physical coagulation processes," *Deep Sea Research Part A, Oceanographic Research Papers*, vol. 37, no. 8, pp. 1197–1211, 1990.

[143] A. J. Cuthbertson, F. Samsami, and P. Dong, "Model studies for flocculation of sand-clay mixtures," *Coastal Engineering*, vol. 132, pp. 13–32, feb 2018.

[144] J. Zhang, X. Shen, Q. Zhang, J. P. Maa, and G. Qiao, "Bimodal particle size distributions of fine-grained cohesive sediments in a settling column with oscillating grids," *Continental Shelf Research*, vol. 174, no. October 2017, pp. 85–94, 2019.

[145] J. C. Winterwerp, "A simple model for turbulence induced flocculation of cohesive sediment," *Journal of hydraulic research*, vol. 36, no. 3, pp. 309–326, 1998.

[146] J. C. Winterwerp, "On the flocculation and settling velocity of estuarine mud," *Continental Shelf Research*, vol. 22, no. 9, pp. 1339–1360, 2002.

[147] C. Selomulya, G. Bushell, R. Amal, and T. D. Waite, "Understanding the role of restructuring in flocculation: the application of a population balance model," *Chemical Engineering Science*, vol. 58, no. 2, pp. 327–338, 2003.

[148] R. I. Jeldres, P. D. Fawell, and B. J. Florio, "Population balance modelling to describe the particle aggregation process: A review," *Powder Technology*, vol. 326, pp. 190–207, 2018.

[149] R. I. Jeldres, F. Concha, and P. G. Toledo, "Population balance modelling of particle flocculation with attention to aggregate restructuring and permeability," *Advances in colloid and interface science*, vol. 224, pp. 62–71, 2015.

[150] F. Maggi, "Flocculation dynamics of cohesive sediment," no. september, p. 154, 2005.

[151] H. J. Shin, M. Son, and G. H. Lee, "Stochastic flocculation model for cohesive sediment suspended in water," *Water (Switzerland)*, vol. 7, no. 5, pp. 2527–2541, 2015.

[152] R. D. Boer, *Modeling Population Dynaics: a Graphical approach*.

[153] W. Jin, S. W. McCue, and M. J. Simpson, "Extended logistic growth model for heterogeneous populations," *Journal of Theoretical Biology*, vol. 445, pp. 51–61, 2018.

[154] A. Lambert *et al.*, "The branching process with logistic growth," *The Annals of Applied Probability*, vol. 15, no. 2, pp. 1506–1535, 2005.

[155] B. Zhang, H. Su, X. Gu, X. Huang, and H. Wang, "Effect of structure and charge of polysaccharide flocculants on their flocculation performance for bentonite suspensions," *Colloids and Surfaces A: Physicochemical and Engineering Aspects*, vol. 436, pp. 443–449, 2013.

[156] F. Mietta, C. Chassagne, R. Verney, and J. C. Winterwerp, "On the behavior of mud floc size distribution: model calibration and model behavior," 2011.

[157] J. C. Winterwerp, "The fractal structure of cohesive sediment aggregates," *Estuarine, Coastal and Shelf Science*, vol. 39, pp. 451–460, 1994.

[158] A. L. Alldredge and P. McGillivary, "The attachment probabilities of marine snow and their implications for particle coagulation in the ocean," *Deep Sea Research Part A, Oceanographic Research Papers*, vol. 38, no. 4, pp. 431–443, 1991.

[159] H. P. Vu, L. N. Nguyen, G. Lesage, and L. D. Nghiem, "Synergistic effect of dual flocculation between inorganic salts and chitosan on harvesting microalgae chlorella vulgaris," *Environmental Technology & Innovation*, vol. 17, p. 100622, 2020.

[160] F. Roselet, D. Vandamme, M. Roselet, K. Muylaert, and P. C. Abreu, "Effects of ph, salinity, biomass concentration, and algal organic matter on flocculant efficiency of synthetic versus natural polymers for harvesting microalgae biomass," *BioEnergy Research*, vol. 10, no. 2, pp. 427–437, 2017.

[161] K. H. Skinnebach, M. Fruergaard, and T. J. Andersen, "Biological effects on flocculation of fine-grained suspended sediment in natural seawater," *Estuarine, Coastal and Shelf Science*, vol. 228, p. 106395, 2019.

[162] B. R. Sutherland, K. J. Barrett, and M. K. Gingras, "Clay settling in fresh and salt water," *Environmental Fluid Mechanics*, vol. 15, no. 1, pp. 1–15, 2015.

[163] C. M. van der Hout, T. Gerkema, J. J. Nauw, and H. Ridderinkhof, "Observations of a narrow zone of high suspended particulate matter (SPM) concentrations along the Dutch coast," *Continental Shelf Research*, vol. 95, pp. 27–38, 2015.

[164] M. Fettweis and B. J. Lee, "Spatial and Seasonal Variation of Biomineral Suspended Particulate Matter Properties in High-Turbid Nearshore and Low-Turbid Offshore Zones," *Water (Switzerland)*, vol. 9, no. 9, 2017.

[165] D. Palomino, D. Hunkeler, and S. Stoll, "Salt concentration influence on the efficiency of two cationic polymeric flocculants," *Colloid and Polymer Science*, vol. 290, no. 13, pp. 1301–1308, 2012.

[166] M. Fettweis, B. Nechad, and D. Van den Eynde, "An estimate of the suspended particulate matter (spm) transport in the southern north sea using seawifs images, in situ measurements and numerical model results," *Continental Shelf Research*, vol. 27, no. 10-11, pp. 1568–1583, 2007.

[167] C. M. van der Hout, R. Witbaard, M. J. Bergman, G. C. Duineveld, M. J. Rozemeijer, and T. Gerkema, "The dynamics of suspended particulate matter (SPM) and chlorophyll-a from intratidal to annual time scales in a coastal turbidity maximum," *Journal of Sea Research*, vol. 127, no. April 2016, pp. 105–118, 2017.

[168] K. Kindler, A. Khalili, and R. Stocker, "Diffusion-limited retention of porous particles at density interfaces," *Proceedings of the National Academy of Sciences*, vol. 107, no. 51, pp. 22163–22168, 2010.

[169] S. M. Figueroa, G.-h. Lee, and H.-J. Shin, "The effect of periodic stratification on floc size distribution and its tidal and vertical variability: Geum Estuary, South Korea," *Marine Geology*, vol. 412, pp. 187–198, jun 2019.

[170] C. F. Jago, S. E. Jones, R. J. Latter, R. R. McCandliss, M. R. Hearn, and M. J. Howarth, "Resuspension of benthic fluff by tidal currents in deep stratified waters, northern North sea," *Journal of Sea Research*, vol. 48, no. 4, pp. 259–269, 2002.

[171] D. Eisma, "Composition, origin and distribution of dutch coastal sands between hoek van holland and the island of vlieland," *Netherlands Journal of Sea Research*, vol. 4, no. 2, pp. 123–267, 1968.

[172] D. Eisma, "Flocculation and de-flocculation of suspended matter in estuaries," *Netherlands Journal of Sea Research*, vol. 20, no. 2, pp. 183–199, 1986.

[173] M. de Nijs, J. Winterwerp, and J. Pietrzak, "On harbour siltation in the fresh-salt water mixing region," *Continental Shelf Research*, vol. 29, pp. 175–193, 2009.

[174] Y. Li, J. Jia, Q. Zhu, P. Cheng, S. Gao, and Y. P. Wang, "Differentiating the effects of advection and resuspension on suspended sediment concentrations in a turbid estuary," *Marine Geology*, vol. 403, no. June, pp. 179–190, 2018.

[175] P. Forsberg, K. Skinnebach, M. Becker, V. Ernstsen, A. Kroon, and T. Andersen, "The influence of aggregation on cohesive sediment erosion and settling," *Continental Shelf Research*, vol. 171, pp. 52–62, dec 2018.

[176] C. F. Jago and S. E. Jones, "Observation and modelling of the dynamics of benthic fluff resuspended from a sandy bed in the southern North Sea," *Continental Shelf Research*, vol. 18, no. 11, pp. 1255–1282, 1998.

[177] R. McCandliss, S. Jones, M. Hearn, R. Latter, and C. Jago, "Dynamics of suspended particles in coastal waters (southern north sea) during a spring bloom," *Journal of Sea Research*, vol. 47, pp. 285–302, 2002.

[178] S. E. Jones, C. F. Jago, a. J. Bale, D. Chapman, R. J. M. Howland, and J. Jackson, "Aggregation and resuspension of suspended particulate matter at a stratified site in the southern North Sea: physical and biological controls," *Continental Shelf Research*, vol. 18, pp. 1283–1309, 1998.

[179] M. Fettweis and M. Baeye, "Seasonal variation in concentration, size, and settling velocity of muddy marine flocs in the benthic boundary layer," *Journal of Geophysical Research: Oceans*, vol. 120, no. 8, pp. 5648–5667, 2015.

[180] R. P. Flores, S. Rijnsburger, S. Meirelles, A. R. Horner-Devine, A. J. Souza, J. D. Pietrzak, M. Henriquez, and A. Reniers, "Wave Generation of Gravity-Driven Sediment Flows on a Predominantly Sandy Seabed," *Geophysical Research Letters*, vol. 45, no. 15, pp. 7634–7645, 2018.

[181] S. Andrews, D. Nover, and S. G. Schladow, "Using laser diffraction data to obtain accurate particle size distributions: the role of particle composition," *Limnology and Oceanography: Methods*, vol. 8, no. 10, pp. 507–526, 2010.

[182] J. Joordens, A. Souza, and A. Visser, "The influence of tidal straining and wind on suspended matter and plankton distribution in the rhine outflow region," *Continental Shelf Research*, vol. 21, pp. 301–325, 2001.

[183] l. Pepperzak, F. Colijin, R. Koeman, W. Gieskes, and C. Joordens, "Phytoplankton sinking rates in the rhine region of freshwater influence," *Journal of Plankton Research*, vol. 25, pp. 365–383, 2003.

[184] R. Witbaard, G. C. A. Duineveld, M. J. N. Bergman, H. Ij, L. Groot, and M. J. C. Rozemeijer, "The growth and dynamics of Ensis directus in the near-shore Dutch coastal zone of the North Sea," *Journal of Sea Research*, vol. 95, pp. 95–105, 2015.

[185] A. Otsuki and T. Hanya, "Production of dissolved organic matter from dead green algal cells. ii> anaerobic microbial decomposition," *Limonology and Oceanography*, vol. 17(2), pp. 258–264.

[186] X. Shen, E. A. Toorman, B. J. Lee, and M. Fettweis, "Biophysical flocculation of suspended particulate matters in Belgian coastal zones," *Journal of Hydrology*, vol. 567, no. October, pp. 238–252, 2018.

[187] J. Maerz and K. Wirtz, "Resolving physically and biologically driven suspended particulate matter dynamics in a tidal basin with a distribution-based model," *Estuarine, Coastal and Shelf Science*, vol. 84, no. 1, pp. 128–138, 2009.

[188] S. MacIntyre, A. L. Alldredge, and C. C. Gotschalk, "Accumulation of marines now at density discontinuities in the water column," *Limnology and Oceanography*, vol. 40, no. 3, pp. 449–468, 1995.

[189] B. J. Lee, E. Toorman, and M. Fettweis, "Multimodal particle size distributions of fine-grained sediments : mathematical modeling and field investigation," pp. 429–441, 2014.

[190] C. Guo, Q. He, B. C. van Prooijen, L. Guo, A. J. Manning, and S. Bass, "Investigation of flocculation dynamics under changing hydrodynamic forcing on an intertidal mudflat," *Marine Geology*, vol. 395, no. October 2017, pp. 120–132, 2018.

[191] D. Meunier, "PARTICLE DYNAMICS AND Skeletonema costatum," 2001.

[192] S. Balzando, Dianasarno, and W. Koostra, "Effects of salinity on the growth rate and morphology of ten skeletonema strains," *Journal of plankton Research*, vol. 33, pp. 937–945, 2011.

[193] A. Manning, C. Martens, T. de Mulder, J. Vanlede, J. C. Winterwerp, P. Ganderton, and G. Graham, "Mud floc observation in the tubidity maximum zone of the scheldt estuary during neap tides," *Journal of coastal Research*, vol. Special Issue 50, pp. 832–836, 2007.

[194] O. A. Mikkelsen, P. S. Hill, and T. G. Milligan, "Seasonal and spatial variation of floc size, settling velocity, and density on the inner Adriatic Shelf (Italy)," *Continental Shelf Research*, vol. 27, no. 3-4, pp. 417–430, 2007.

[195] F. Orvain, P. L. Hir, and P.-G. Sauriau, "A model of fluff layer erosion and subsequent bed erosion in the presence of the bioturbator, hydrobia ulvae," *Journal of Marine Research*, vol. 61, no. 6, pp. 821–849, 2003.

[196] L. C. Lund-Hansen, M. Laima, K. Mouritsen, N. N. Lam, and D. N. Hai, "Effects of benthic diatoms, fluff layer, and sediment conditions on critical shear stress in a non-tidal coastal environment," *Journal of the marine biological association of the United Kingdom*, vol. 82, no. 6, pp. 929–936, 2002.

[197] Y. Xu, "Approach to the erosion threshold of cohesive sediments," *Ocean Engineering*, vol. 172, pp. 183–190, jan 2019.

[198] J. Mcneil and W. Lick, "Erosion rates and bulk properties of sediments from the kalamazoo river," *Journal of Great Lakes Research*, vol. 30, no. 3, pp. 407–418, 2004.

[199] T. Soo, O. Joerdel, B. W. Flemming, and A. Bartholomä, "The role of particle aggregation / disaggregation in muddy sediment dynamics and seasonal sediment turnover in a back-barrier tidal basin , East Frisian Wadden Sea , southern North Sea," vol. 235, pp. 49–61, 2006.

[200] T. Van Kessel, H. Winterwerp, B. Van Prooijen, M. Van Ledden, and W. Borst, "Modelling the seasonal dynamics of SPM with a simple algorithm for the buffering of fines in a sandy seabed," *Continental Shelf Research*, vol. 31, no. 10 SUPPL., pp. S124–S134, 2011.

[201] M. Blaas, C. Dong, P. Marchesiello, J. C. McWilliams, and K. D. Stolzenbach, "Sediment-transport modeling on southern californian shelves: A roms case study," *Continental shelf research*, vol. 27, no. 6, pp. 832–853, 2007.

[202] M. Blaas, C. Dong, P. Marchesiello, J. C. McWilliams, and K. D. Stolzenbach, "Fine sediment deposits in gravel bed rivers: sensitivity analysis to particle properties using a 2d hydrodynamic and sediment model," *Conference paper*, vol. Published version, 2020.

[203] X. Shen, B. J. Lee, M. Fettweis, and E. A. Toorman, "A tri-modal flocculation model coupled with telemac for estuarine muds both in the laboratory and in the field," *Water research*, vol. 145, pp. 473–486, 2018.

[204] C. Chassagne, Z. Safar, Z. Deng, Q. He, and A. Manning, *Flocculation in Estuaries: Modeling, Laboratory and In-situ Studies*. IntechOpen, 2021.

[205] A. Horner-Divine, R. Hetland, and D. MacDonald, "Mixing and transport in coastal river plumes," *Annual review of fluid mechanics*, 2015.

[206] C. Chassagne, "Introduction to colloid science," *Delft academic Press*, 2020.

[207] J. C. Winterwerp, A. Manning, C. Martens, T. de Mulder, and J. Vanlede, "A heuristic formula for turbulence- induced flocculation of cohesive sediment," *Estuarine coastal and shelf science*, vol. 68, pp. 195–207, 2006.

[208] J.-F. Zhang and Q.-H. Zhang, "Lattice boltzmann simulation of the flocculation process of cohesive sediment due to differential settling," *Continental Shelf Research*, vol. 31, no. 10, pp. S94–S105, 2011.

[209] J.-F. Zhang, Q.-H. Zhang, J. P.-Y. Maa, and G.-Q. Qiao, "Lattice boltzmann simulation of turbulence-induced flocculation of cohesive sediment," *Ocean Dynamics*, vol. 63, no. 9-10, pp. 1123–1135, 2013.

[210] S. Rijnsburger, R. P. Flores, J. D. Pietrzak, A. R. Horner-Devine, A. J. Souza, and F. Zijl, "The evolution of plume fronts in the rhine region of freshwater influence," *Journal of Geophysical Research: Oceans*, vol. 126, no. 7, p. e2019JC015927, 2021.

[211] "Mos2-ii deterministic model calibration," 2013.

[212] G. Many, F. Borrin, X. Durrieu de madron, I. Pairaud, A. Gangloff, D. Doxaran, A. Ody, R. Verney, C. Menniti, D. Le Berre, and M. Jacquet, "Particle assemblage characterization in the rhone river rofi," *Journal of Marine Systems*, vol. 157, pp. 39–51, 2016.

[213] R. Kretzschmar, H. Holthoff, and H. Sticher, "Influence of ph and humic acid on coagulation kinetics of kaolinite: a dynamic light scattering study," *Journal of Colloid and Interface Science*, vol. 202, no. 1, pp. 95–103, 1998.

[214] C. Aurell and A. Wistrom, "Coagulation of kaolinite colloids in high carbonate strength water," *Colloids and Surfaces A: Physicochemical and Engineering Aspects*, vol. 168, no. 3, pp. 277–285, 2000.

[215] A. F. Blumberg, Z.-G. Ji, and C. K. Ziegler, "Modeling outfall plume behavior using far field circulation model," *Journal of hydraulic engineering*, vol. 122, no. 11, pp. 610–616, 1996.

[216] S. G. Pearson, R. Verney, B. C. van Prooijen, D. Tran, E. C. Hendriks, M. Jacquet, and Z. B. Wang, "Characterizing the composition of sand and mud suspensions in coastal and estuarine environments using combined optical and acoustic measurements," *Journal of Geophysical Research: Oceans*, vol. 126, no. 7, p. e2021JC017354, 2021.